

**TiO<sub>2</sub>: Application in Photocatalysis for the Degradation  
of Organic Pollutants and Aggregation  
Behavior in Aquatic Systems**

Zur Erlangung des akademischen Grades eines  
DOKTORS DER INGENIEURWISSENSCHAFTEN (Dr.-Ing.)

der Fakultät für Chemieingenieurwesen und Verfahrenstechnik des  
Karlsruher Instituts für Technologie (KIT)

genehmigte

DISSERTATION

von

M. Sc. Meijie Ren

Aus Yunnan, China

Referent: Prof. Dr. rer. nat. habil. Fritz H. Frimmel

Korreferent: Prof. Dr. Matthias Franzreb

Tag der mündlichen Prüfung: 29. Juni. 2015



*Treat the earth well:*

*It was not given to you by your parents,*

*It was loaned to you by your children.*

*We do not inherit the Earth from our ancestors,*

*We borrow it from our children.*

*Ancient Indian Proverb*



Die vorliegende Dissertation wurde am Engler-Bunte Institut des Karlsruhe Instituts für Technologie (KIT), Lehrstuhl für Wasserchemie und Wassertechnologie, im Zeitraum von September 2010 bis Dezember 2014 angefertigt.

Hiermit erkläre ich, dass ich die vorliegende Dissertation, abgesehen von der Benutzung der angegebenen Hilfsmittel, selbständig verfasst habe.

Alle Stellen, die gemäß Wortlaut oder Inhalt aus anderen Arbeiten entnommen sind, wurden durch Angabe der Quelle als Entlehnungen kenntlich gemacht.

Diese Dissertation liegt in gleicher oder ähnlicher Form keiner anderen Prüfungsbehörde vor.

Karlsruhe, den 11 March 2015

Meijie Ren



## Acknowledgments

First, I would like express my appreciation to my advisor Prof. Dr. Fritz H. Frimmel for his guidance and support throughout my PhD research. Prof. Frimmel allowed me the great freedom to my projects. I would like to thank Prof. Dr. Matthias Franzreb for his revision. I would like to extend my appreciation to Prof. Dr. Harald Horn and Mrs. Dr. Gudrun Abbt-Braun in the Chair of Water Chemistry and Water Technology in Engler-Bunte-Institute and staff members for their aid and support. With their supervision and encouragement, I could continuously improve my knowledge and skills on research.

I am also grateful to Mrs. Ursula Schafer and Mrs. Dr. Birgit Gordalla for their help preparing documents of research work and daily life, and to Mrs. Sylvia Heck who was always willing to lend a helping hand. I am grateful also to Mrs. Dr. Florencia Saravia, Mr. Dr. Markus Delay and Mr. Dr. Marios Drosos for their kind and comprehensive supervision and suggestion in research work and daily life, and to Mr. Axel Heidt, a facetious gentleman, who always gave me help at the first time whenever I got troubles.

I was very lucky to have the opportunity to work in a group that gathers so many good people in one place! At the beginning I was a little bit nervous, but when in Roma, do as Romans do. You taught me how to adapt myself soon and enjoy the working and life in a foreign country. I take many precious memories with me, our Normandy trip, our Christmas Party, our Barbecue evening, and many others. I enjoyed hard working and having fun with you!

I am very thankful to Ms. Dunja Haak for keeping the data safe and the computers running. I am also thankful to Mr. Rafael Peschke for HPLC measurement, thank you for your work and patient with my plenty of samples, and to Mrs. Elly Karle for IC analyzing, and to Mr. Matthias Weber for DOC measurement, and to Mr. Reinhard Sembritzki for your work of ICP measurement, and to Mr. Ulrich Reichert for AOX analyzing. I am also thankful to Ms. Stephanie West for organizing and ordering

## Acknowledgments

---

materials and reagents.

Everybody has difficult years, but a lot of times the difficult years end up being the greatest years of your whole entire life, if you survive them.

Living a place where is 8000 kilometers away from home, homesick is the most popular emotion. I am very thankful to my Chinese girls—Chunyan Li, Di Peng and Jueying Qian. Owing to the company of you, I overcame the difficult of work and life. We can discuss the academic questions; we can share the sad and happy; we can celebrate our festivals together. Many thanks to lovely you, you made my life brighter and more colorful.

I am very thankful and grateful to Mr. Norman Hack, Mr. Alexander Kondrakov, Ms. Elham Fatoorehchi, Ms. Eva Gilbert, Ms. Maria Pia Herrling, Mr. Shelesh Agrawal for nice academic atmosphere.

Lastly, I would like to thank my parents and my best Fan, who is a strong and nice man and always supports and encourages me to pursue my education. And the special thanks to my little Yiyang, who gives the sweetest life and hope.



## Contents

<b>Acknowledgments</b> .....	<b>I</b>
<b>Abstract</b> .....	<b>VI</b>
<b>Zusammenfassung</b> .....	<b>IX</b>
<b>1 Introduction</b> .....	<b>1</b>
1.1 Photocatalytic degradation of pharmaceutically active compounds by Pt/TiO <sub>2</sub> .....	1
1.2 Aggregation behavior of TiO <sub>2</sub> nanoparticles in aquatic solution: influence of different types of dissolved organic matter under different pH values and electrolytes.....	4
1.3 Multi-cycle photocatalytic degradation of bezafibrate by polyvinyl alcohol/TiO <sub>2</sub> (PVA/TiO <sub>2</sub> ) film.....	6
1.4 Aim of the dissertation.....	7
<b>2 Background</b> .....	<b>8</b>
2.1 TiO <sub>2</sub> in heterogeneous photocatalysis .....	8
2.2 Strategies for improving TiO <sub>2</sub> photocatalytic efficiency .....	9
2.3 Reaction kinetics and mechanisms in heterogeneous photocatalysis .....	14
2.3.1 Reaction kinetics.....	14
2.3.2 Reaction mechanisms .....	16
2.4 Fundamental parameters of photocatalytic degradation of organic pollutants in wastewater treatment .....	17
2.4.1 TiO <sub>2</sub> loading.....	18
2.4.2 pH value.....	18
2.4.3 Dissolved oxygen.....	19
2.4.4 Dissolved cation ions.....	19
2.4.5 Dissolved organic matter .....	20
2.5 Factorial design.....	21
2.6 Aggregation and stability of TiO <sub>2</sub> NPs in aquatic systems .....	23
2.6.1 DLVO theory .....	23
2.6.2 Influence of pH.....	24
2.6.3 Influence of ionic strength and specific electrolytes.....	25
2.6.4 Influence of NOM.....	25
2.7 Separation of TiO <sub>2</sub> from suspension .....	26
2.7.1 Membrane filtration .....	26
2.7.2 Immobilization of TiO <sub>2</sub> .....	27
<b>3 Materials and methods</b> .....	<b>28</b>
3.1 Reagents and materials .....	28
3.2 Analytical methods .....	30

3.2.1	Thermal chemical oxidation with carbon dioxide detection.....	30
3.2.2	Size exclusion chromatography with dissolved organic carbon and ultraviolet detection (SEC-DOC and SEC-UV).....	30
3.2.3	High performance liquid chromatography (HPLC).....	31
3.2.4	X-Ray diffraction (XRD).....	31
3.2.5	Scanning electron microscopy (SEM).....	31
3.2.6	Transmission electron microscopy (TEM) .....	31
3.2.7	Fourier transform infrared spectroscopy (FTIR) .....	32
3.2.8	Dynamic light scattering (DLS).....	32
3.2.9	Ion exchange chromatography (IC).....	33
3.2.10	Inductively Coupled Plasma—Optical Emission Spectroscopy (ICP-OES) .....	33
3.2.11	Adsorbed organic halogens (AOX) .....	33
3.2.12	Differential scanning calorimetry (DSC).....	33
3.3	Experimental equipment and procedure .....	34
3.3.1	For Chapter 4.....	34
3.3.2	For Chapter 5 .....	36
3.3.3	For Chapter 6.....	36
3.3.4	For Chapter 7.....	38

#### **4 Photocatalytic degradation of carbamazepine (CBZ) and clofibric acid (CA) using Pt/TiO<sub>2</sub> under environmentally relevant conditions 39**

4.1	Characterization of Pt/TiO <sub>2</sub> .....	39
4.2	Effect of process conditions and water matrices on the CBZ and CA photocatalytic degradation using a Solar light Simulator .....	42
4.3	Influence of oxygen concentration on the photocatalytic degradation of CBZ and CA in the presence of NOM .....	47
4.4	Photocatalytic degradation of NOM under different gas flow.....	49
4.5	Conclusions .....	53

#### **5 Photocatalytic elimination of diatrizoate (DA) and I<sup>-</sup> formation -- Influence of DO, metal ions and NOM..... 54**

5.1	Photocatalytic reaction kinetics of DA.....	55
5.2	Full factorial design and data analysis.....	56
5.3	Analyses for rate constants.....	57
5.4	Analyses for I <sup>-</sup> formation.....	61
5.5	Conclusions .....	65

#### **6 Aggregation behavior of TiO<sub>2</sub> nanoparticles in aqueous solution: influence of different types of DOM under different pH values and electrolytes ..... 66**

---

6.1	Determination of aggregation kinetics.....	66
6.2	Adsorption of DOM onto the surface of TiO <sub>2</sub> NPs.....	67
6.3	Material characterization .....	68
6.3.1	DOM characterization.....	68
6.3.2	TiO <sub>2</sub> NPs.....	69
6.4	Aggregation and stability of TiO <sub>2</sub> NPs as a function of pH value .....	70
6.5	TiO <sub>2</sub> NPs aggregation kinetics in the presence of monovalent cations.....	72
6.6	TiO <sub>2</sub> NPs aggregation kinetics in the presence of divalent cations.....	75
6.7	Image analysis .....	76
6.8	Conclusions.....	78
<b>7</b>	<b>Multi-cycle photocatalytic degradation of bezafibrate (BZF) by polyvinyl alcohol/TiO<sub>2</sub> (PVA/TiO<sub>2</sub>) film.....</b>	<b>80</b>
7.1	Characteristics.....	80
7.2	Stability of the PVA/TiO <sub>2</sub> film.....	84
7.3	Photocatalytic activity of the PVA/TiO <sub>2</sub> film.....	85
7.3.1	Effect of thickness.....	85
7.3.2	Effect of film age .....	86
7.3.3	Effect of pH .....	87
7.4	Comparison study of the immobilized TiO <sub>2</sub> for long term use .....	88
7.5	Application prospect of hybrid PVA/TiO <sub>2</sub> film .....	89
7.6	Conclusions.....	90
<b>8</b>	<b>Summary and outlook.....</b>	<b>91</b>
8.1	Photocatalytic degradation of pharmaceutically active compounds by Pt/TiO <sub>2</sub> under environmentally relevant conditions.....	91
8.2	Aggregation behavior of TiO <sub>2</sub> nanoparticles in aquatic solution: influence of different types of DOM under different pH values and electrolytes .....	93
8.3	Multi-cycle photocatalytic degradation of bezafibrate by polyvinyl alcohol/TiO <sub>2</sub> (PVA/TiO <sub>2</sub> ) film.....	94
8.4	Outlook .....	94
<b>9</b>	<b>References.....</b>	<b>96</b>
	<b>Abbreviation list.....</b>	<b>119</b>

## Abstract

Pharmaceutically active compounds (PhACs) are a class of emerging environmental contaminants that are extensively and increasingly being detected in aquatic systems. Photocatalysis based on  $\text{TiO}_2$  has achieved many successful applications for determination of organic pollutant in water. In this work the effects of environmental parameters such as pH, metal ions, and natural organic matter (NOM) content on the photocatalytic degradation rate constant of PhACs were investigated. Photocatalytic degradation of PhACs was strongly affected by the studied parameters and the character of the targeted compounds. The studied parameters can have different, even opposite, effects on the yield and kinetics of the photocatalytic degradation when comparing carbamazepine (CBZ) with clofibrac acid (CA) as indicators. Results demonstrate that the presence of NOM is the most restrictive parameter for the application of photocatalysis in wastewater treatment plants and in the environment. The presence of dissolved oxygen (DO) in the photocatalytic system can significantly eliminate the inhibitory NOM effect. Analytical size exclusion chromatography-organic carbon detection (SEC-OCD) results suggested that larger molecular sized fractions are predominant during the whole process in the absence of DO, while lower molecular sized fractions predominate after the first few minutes under air and  $\text{O}_2$  purging. The inhibitory effect of NOM is more dependent on the molecular size of NOM than on its concentration. High molecular sized NOM fractions with high aromaticity are more easily adsorbed onto the catalyst particles and act as an electron-hole scavenger and a light filter, reducing the photocatalytic degradation rate. In contrast, lower molecular sized NOM fractions cause less inhibition of the degradation reaction.

In addition, a simplified model concerning environmental conditions (such as DO, NOM and metal ions content) was developed to evaluate the effect of NOM and metal ions on the Pt/ $\text{TiO}_2$  photocatalytic degradation of diatrizoate (DA) and  $\text{I}^-$  formation in the presence of different DO levels. The results show that the increase of the DO

concentration and the decrease of the metal ions concentration led to the highest reaction rate. The DO concentration and the presence of NOM also severely affected the formation of  $I^-$ , and the simultaneous increase of both led to the highest  $I^-$  formation. The empirical models were developed for DA elimination and  $I^-$  formation, and the high  $R^2$  values of the model underline its reasonably good estimate of response for the system in the range studied.

The technically important aggregation behavior of  $TiO_2$  nanoparticles (NPs) was investigated at different pH values, electrolytes and in the presence of different types of dissolved organic matter (DOM) to simulate wastewater matrices: Hohloh Lake 10 fulvic acid (HO10FA), alginate, bovine serum albumin (BSA),  $\alpha$ -amylase and sodium dodecylbenzene sulfonate (SDS). The aggregation behavior of  $TiO_2$  NPs exhibited a DLVO-type interaction in the absence of DOM. Increasing electrolyte concentration and adding divalent calcium ions induced  $TiO_2$  NPs aggregation by shielding electrostatic charge and thereby suppressing electrostatic repulsion. The presence of BSA, HO10FA and alginate significantly retarded the aggregation rate of  $TiO_2$  NPs. BSA had the strongest effect with respect to slowing down the  $TiO_2$  NPs aggregation rate followed by alginate and HO10FA. The decrease of the aggregation rate of  $TiO_2$  NPs was primarily caused by the synergistic electrostatic effect and steric repulsive effect. It is interesting to note that there was no stabilization effect of SDS and  $\alpha$ -amylase. Calcium bridges were found in the presence of alginate and  $CaCl_2$  at the fast aggregation regime, which promoted to form large eye-catching and compact aggregations

With the aim of decreasing the release of  $TiO_2$  NPs via wastewater into the environment and increasing the recycle use of the  $TiO_2$  photocatalyst, a method for immobilization of  $TiO_2$  in polyvinyl alcohol (PVA) films (Ti-O-C bond formation) was developed. The simple and efficient method provides a highly active and recyclable photocatalyst for water purification without classical depth filtration. The photocatalytic tests for the degradation of bezafibrate (BZF) underlined the good photocatalytic activity of the PVA/ $TiO_2$  film. Since the photocatalytic degradation efficiency increased with the increase of reuse cycle, this points towards an economically and ecologically attractive

application of this hybrid photocatalyst. Technically the hybrid PVA/TiO<sub>2</sub> film was fairly stable under the long-term irradiation of the work: the weight loss rate of the hybrid film decreased with increase of irradiation time and no release of TiO<sub>2</sub> was observed. Comparing the photocatalytic activity with P25 particles suspension and other immobilized TiO<sub>2</sub> composite (pumice/TiO<sub>2</sub> and porous glass bead/TiO<sub>2</sub>), the PVA/TiO<sub>2</sub> hybrid film opens a door of a promising application of photocatalysis in wastewater treatment.

## Zusammenfassung

Die Auswirkungen von Umweltparametern wie pH-Wert, Metallionen und natürliche organische Materie (NOM) auf die photokatalytischen Abbaurate von pharmazeutisch aktiven Verbindungen (PhACs) wurden in wässrigen Lösungen untersucht. Der photokatalytische Abbau von PhACs wurde stark von den umweltrelevanten Bedingungen und dem Charakter der Zielverbindungen beeinflusst. Umweltparameter können verschiedene, Auswirkungen auf die Ausbeute und Kinetik des photokatalytischen Abbaus haben. Dies kann durch den Vergleich von Carbamazepin (CBZ) und Clofibrinsäure (CA) als Indikatoren verdeutlicht werden.

Die Ergebnisse zeigen, dass NOM die untersuchten Parameter beeinflusst und die Anwendung der Photokatalyse in Kläranlagen und in der Umwelt am meisten einschränkt. Der gelöste Sauerstoff (DO) in dem photokatalytischen System kann den inhibitorischen Effekt von NOM deutlich unterdrücken.

Die Ergebnisse der analytischen Größenausschlusschromatographie der organischen Kohlenstoffverbindungen legen nahe, dass hochmolekulare Fraktionen während des gesamten Verfahrens in Abwesenheit von DO dominieren, während niedermolekulare Fraktionen nach den ersten Minuten unter Luft und O<sub>2</sub>-Spülung dominieren. Die hemmende Wirkung von NOM ist somit stärker abhängig von der NOM Molekülgröße als von der NOM Konzentration.

Größere molekulare NOM Fraktionen mit hoher Aromatizität werden leichter auf den Katalysatorpartikeln sorbiert und wirken so als ein Elektronen-Loch-Scavenger und als ein Lichtfilter, wodurch die photokatalytische Abbaugeschwindigkeit reduziert wird. Umgekehrt verursachen kleinere molekulare NOM Fraktionen weniger Hemmung bei der Abbaureaktion.

Zusätzlich wurde ein vereinfachtes Modell zur Untersuchung von Umweltbedingungen entwickelt, um die Wirkung von NOM und Metallionen auf den

Pt/TiO<sub>2</sub> photokatalytischen Abbauprozess von Diatrizoat (DA) und die I<sup>-</sup> Bildung mit verschiedenen DO Niveaus zu beurteilen. Die Ergebnisse zeigen, dass die Erhöhung der Sauerstoffkonzentration und die Verringerung der Metall-Ionen-Konzentration zur höchsten Reaktionsgeschwindigkeit führten. Die Sauerstoff- und NOM Konzentration beeinflussen ebenfalls die Bildung von I<sup>-</sup>. Die simultane Zunahme von beiden führte zur höchsten I<sup>-</sup> Bildung. Empirische Modelle wurden für die DA-Eliminierung und I<sup>-</sup> Bildung entwickelt und die hohen  $R^2$ -Werte des Modells unterstreichen die gute Beschreibbarkeit der Reaktion im untersuchten Bereich .

Das Aggregationsverhalten von TiO<sub>2</sub> Nanopartikeln (NP), das für technische Prozesse wichtig ist, wurde bei unterschiedlichen pH-Werten, Elektrolyten und in Gegenwart von verschiedenen Typen gelöster organischer Materie (DOM) zur Nachbildung von Abwasser Matrices untersucht: Fulvimsäure (Hohlohsee, HO10FA), Alginat, Rinderserumalbumin (BSA),  $\alpha$ -Amylase und Natriumdodecylbenzolsulfonat (SDS). Das Aggregationsverhalten der TiO<sub>2</sub> NPs zeigte eine DLVO artige Wechselwirkung in Abwesenheit von DOM stattfindet. Die Erhöhung der Elektrolytkonzentration und die Zugabe von zweiwertigen Calciumionen induzierte die Aggregation von TiO<sub>2</sub> Nanopartikeln durch Abschirmung der elektrostatischen Ladung und damit wurde die elektrostatische Abstoßung unterdrückt. Die Anwesenheit von BSA, HO10FA und Alginat verzögerte deutlich die Aggregationsrate von TiO<sub>2</sub> Nanopartikeln. BSA hatte die stärkste Wirkung in Bezug auf die Verlangsamung der TiO<sub>2</sub> Nanopartikel Aggregationsrate, gefolgt von Alginat und HO10FA. Die Abnahme der Aggregationsrate von TiO<sub>2</sub> Nanopartikeln wurde in erster Linie durch die synergistisch, Effekte der elektrostatischen sowie sterischen Abstoßung verursacht. Es ist interessant festzustellen, dass keine Stabilisierungswirkung von SDS und  $\alpha$ -Amylase gab. Des Weiteren wurden Calcium Brücken in Gegenwart von Alginat und CaCl<sub>2</sub> in schnellen Aggregationsregimen gefunden, die zu auffällig großen und kompakten Aggregaten führten.

Mit dem Ziel der Herabsetzung der Freisetzung von TiO<sub>2</sub> NPs im Abwasser und damit in die Umwelt und der Erhöhung der Rückführung von verwendeten



TiO<sub>2</sub>-Photokatalysatoren wurde ein Verfahren zur Immobilisierung von TiO<sub>2</sub> in Polyvinylalkohol(PVA)-Filmen (Ti-O-C-Bindung) entwickelt. Die einfache und effiziente Methode separiert hochaktive und wiederverwendbare Photokatalysatoren zur Wasseraufbereitung ohne die klassische Tiefenfiltration. Die Ergebnisse der photokatalytischen Untersuchungen zum Abbau von Bezafibrat (BZF) unterstreichen die gute photokatalytische Aktivität des PVA/TiO<sub>2</sub>-Films. Da die photokatalytische Abbauleistung mit jedem Wiederverwendungszyklus erhöht wird, handelt es sich um eine ökonomisch und ökologisch attraktive Anwendung des Photokatalysators. Der PVA/TiO<sub>2</sub>-Film zeigte unter Langzeitbestrahlung eine hohe Stabilität: es fand eine Gewichtsabnahme des Films mit Zunahme der Bestrahlungszeit statt ohne erhebliche Freisetzung von TiO<sub>2</sub>. Vergleicht man die photokatalytische Aktivität von der P25 Teilchensuspension mit der andere, immobilisierter TiO<sub>2</sub> Komposite (Bimsstein/TiO<sub>2</sub> und porösen Glasperlen/TiO<sub>2</sub>), bietet der untersuchte PVA/TiO<sub>2</sub> Film die vielversprechende Möglichkeit für Anwendungen in der Photokatalyse zur Abwasserbehandlung.



## 1 Introduction

Titanium dioxide (TiO<sub>2</sub>) is applied in a wide variety of technological applications where surface properties play a role. It is used in heterogeneous catalysis; as photocatalyst; in solar cells for the production of hydrogen and electric energy; as white pigment; in cosmetics; as corrosion-protective or optical coating; as spacer material in magnetic spin-value systems; and it is important in earth sciences (Diebold 2003b).

By far, the most actively pursued applied research on TiO<sub>2</sub> is its use for photo-assisted degradation of organic molecules. TiO<sub>2</sub> is a semiconductor and the electron-hole pair, which is created upon irradiation with sunlight, may separate and the resulting charge carriers might migrate to the surface where they react with adsorbed water and oxygen to produce radical species. They attack any adsorbed organic molecule and can, ultimately, lead to complete decomposition into CO<sub>2</sub> and H<sub>2</sub>O (Diebold 2003a). The photocatalytic properties of TiO<sub>2</sub> have been investigated extensively (Nakata and Fujishima 2012) and established for many successful applications, such as water splitting (Maeda 2011), reduction of CO<sub>2</sub> into gaseous hydrocarbons (Tan et al. 2006), disinfection and decontamination of water and air (Crittenden et al. 1997, Peral et al. 1997), surfaces self-cleaning (Nishimoto and Bhushan 2013), and antimicrobial biomedical materials (Rupp et al. 2010).

### 1.1 Photocatalytic degradation of pharmaceutically active compounds by Pt/TiO<sub>2</sub>

Photocatalysis based on TiO<sub>2</sub> has been intensively investigated in order to achieve better photocatalytic efficiency for different applications such as decomposition of various organic pollutants in water (Axelsson and Dunne 2001). Studies on introducing non-metal and metal ions into TiO<sub>2</sub> have become attractive in the area of photocatalysis (Bazzo and Urakawa 2013, Chong et al. 2010). Pt modified TiO<sub>2</sub> (Pt/TiO<sub>2</sub>) as

representative new photocatalyst due to its obviously higher photocatalytic activity (Lee and Choi 2004, Miller et al. 2010) and its easy availability (Nomikos et al. 2014) has been frequently used.

The photocatalytic efficiency for the degradation of pollutants is strongly dependent on the reaction conditions, e.g. temperature, pH value, and the presence of oxygen, organic matter, inorganic elements and dissolved metal ions (Asahi 2001, Brezova et al. 1995, Chong et al. 2010, Schwegmann et al. 2013, Valencia et al. 2012). At this point questions arise: Is photocatalysis a suitable technique for wastewater treatment concerning the influence of technically and environmentally relevant conditions? Is there any restrictive parameter for the application of photocatalysis in the real wastewater treatment plant? Can inhibition effects be eliminated?

Studies have partially shown, conflicting or non-easily comparable information, either because they used different target compounds, and different model compounds as natural organic matter (NOM). Furthermore, type of photocatalyst (which, in turn, affects the activity), ionic strength or NOM concentrations and different photocatalytic reactors used are too different to gain results which can be directly compared (Asahi 2001, Brezova et al. 1995, Chong et al. 2010, Schwegmann et al. 2013, Valencia et al. 2012).

A family of pollutants that has come into focus in recent years is the pharmaceutically active compounds (PhACs) which made their way into the aquatic environment worldwide (Sanderson et al. 2004). Many of the PhACs are applied in human and/or in veterinary medical care and a great part of them gets unchanged or slightly transformed into the wastewater via excretion (Heberer 2002). There, some of them are recalcitrant to microbiological attack and hence are not removed during conventional biological wastewater treatment or in membrane bioreactors (Clara et al. 2004, Joss et al. 2005, Miao and Metcalfe 2003, Radjenovic et al. 2007). PhACs have also been detected in pharmaceutical plant effluents, hospital effluents, secondary treated effluents, in ground water and even in drinking water in concentration ranges from  $\text{ng L}^{-1}$  to  $\text{mg L}^{-1}$  (Doll and Frimmel 2003a, Kohler et al. 2012, Lacey et al. 2008, Laera et al. 2011, Phillips et al. 2010, Prasse et al. 2010, Sacher et al. 2001). Among the PhACs

which have been commonly found in natural waters are antiphlogistics (e.g. diclofenac, ibuprofen, ketoprofen and naproxen), lipid regulators (e.g. bezafibrate, gemfibrozil, clofibric acid) and antiepileptic drugs (carbamazepine) (Comoretto and Chiron 2005). Another broadly identified pharmaceutical product often found in natural water sources is iodinated x-ray contrast media (ICM), substances used for various diagnostic imaging approaches. Worldwide use of ICM has been estimated to be on the order of  $3.5 \times 10^6$  kg yr<sup>-1</sup> (Putschew et al. 2000). Due to the resistance to human metabolism, the good water solubility and the high polarity, ICM and its metabolic products are well reflected in adsorbable organohalogenes (AOX) in wastewater treatment plants, in their effluents and finally in the natural aquatic systems. Elevated concentrations of ICM and AOI have been detected especially in hospital and domestic wastewater, in treated wastewater effluents, surface water, groundwater, and even in finished drinking water (Kuemmere et al. 1998, Sacher et al. 2001, Seitz et al. 2006). These PhACs are environmental pollutants due to their persistency and environment risk (Mehinto 2010). Hence, degradation of PhACs has become a hot topic and it is necessary to develop and assess water treatment processes with regard to their potentials for the elimination of pharmaceutical.

In this dissertation, four PhACs: carbamazepine (CBZ), bezafibrate (BZF), clofibric acid (CA) and diatrizoate (DA) were chosen as targets compounds for photocatalytic degradation. The antiepileptic drug CBZ is a top compound in the research list due to its high detection frequency in natural waters, and at higher concentrations, than most of the other PhACs (Cunningham et al. 2010). It has been proven to possess acute aquatic toxicity for representing bacteria (Kim et al. 2007). On the contrary, little work exists on the investigation of the photocatalytic degradation of CA and BZF (the lipid-lowering agents) under environmentally relevant conditions in spite of its toxic effect and environmental risk which have been already reported (Cleuvers 2003, Weston et al. 2009). DA, an ionic ICM, rarely removed when passing through the municipal sewage treatment plant, is found in ground water frequently, where it obviously persists for a long time without any removal (Ternes et al. 2007).

Chapter 4 and 5 provide 1) a complete characterization of the photocatalytic

degradation of the selected PhACs under environmentally relevant conditions, investigating the influence of pH values, NOM, metal ions and etc.; 2) to evaluate the application of photocatalysis in pharmaceutical wastewater treatment.

### **1.2 Aggregation behavior of TiO<sub>2</sub> nanoparticles in aquatic solution: influence of different types of dissolved organic matter under different pH values and electrolytes**

The increasing application of TiO<sub>2</sub> nanoparticles (NPs) has led to increased concerns about potential environmental and health impacts of NPs (Gottschalk et al. 2009, Ju-Nam and Lead 2008). The first investigative step is to assess their transport, fate, and behavior in the environment. The environmental transportation and transformation, as well as the toxicity against organism, of TiO<sub>2</sub> NPs in the aquatic environments might be strongly dependent on their sizes, surface properties and interactions with other substances in water (Battin et al. 2009). The aggregation of TiO<sub>2</sub> NPs seems to be a critical factor affecting most of the other NPs properties in the aquatic environment.

The interactions between NPs become more complicated in the presence of natural organic matter (NOM). Three categories (fractions) represent the most important part of NOM in surface waters: humic substances, polysaccharides and proteins with highly different molecular properties (Philippe and Schaumann 2014). Humic acids (HAs), which are abundant in the environment, can react with NPs and significantly increase the stability of NPs in the aquatic environment (Abe et al. 2011, Yang et al. 2009, Zhu et al. 2014). HA adsorbed on the surface of NPs can contribute more negative surface charges and increase the electrostatic double layer (EDL). Repulsive energy leads to the stabilization of NPs with smaller particle size (Domingos et al. 2009b). Additionally, NPs can be stabilized by HAs through complexation between acidic functional groups (mainly carboxylic acid) in HAs and the surface of NPs (Hajdu et al. 2009). Similarly, alginate, a linear polysaccharide block copolymer extracted from the cell walls of brown seaweed, was reported to stabilize NPs by neutralization effects (Abe et al. 2011,

Huangfu et al. 2013, Loosli et al. 2013, Ostermeyer et al. 2013). Protein, an important biopolymer which was reported to account for approximately 15% of dissolved organic matter (DOM) in several water samples (Imai et al. 2002, Li et al. 2014), could stabilize NPs primarily by increase of steric repulsion as well (Huangfu et al. 2013, Ostermeyer et al. 2013).

Additionally, the most important distribution pathway for NPs into the environment is thought the effluent coming from wastewater treatment plants (WWTPs). It is reported that there are some DOM sources resulting from human activities — anthropogenic DOM sources in wastewater treatment effluent in addition to NOM (Li et al. 2014). One important fraction is hydrophobic neutral and includes hydrocarbons, pesticides and carbonyl compound. Synthetic detergents such as linear alkylbenzene sulfonates (LAS) also play a major role (Imai et al. 2002, Li et al. 2014). Sodium dodecylbenzene sulfonates (SDS) are the most frequently used anionic surfactants in the world, and its application in laundry and household cleaning represents approximately 80% of its market use (Crey-Desbiolles et al. 2009). Thus, during the use and disposal of these products, surfactants are likely to be co-released with NPs, which could facilitate or reduce the environmental transport of NPs.

A substantial amount of studies on the aggregation and dispersion of TiO<sub>2</sub> NPs under different conditions (e.g. changing of pH values, ionic strengths, salt valences, and surface charges) have been reported (Romanello and de Cortalezzi 2013, Sajjadi et al. 2013). The results indicate that TiO<sub>2</sub> NPs aggregate at pH near the point of zero charge but are stable at other pH values. Moreover high ionic strength and presence of divalent salts (e.g. Ca<sup>2+</sup>) facilitate obviously aggregate formation (Romanello and de Cortalezzi 2013, Sajjadi et al. 2013). However, research of aggregation kinetics of TiO<sub>2</sub> NPs was limited to consider the influence of humic substances. The interaction between TiO<sub>2</sub> NPs and other DOM sources (e.g. polysaccharides, proteins and anthropogenic DOM) under different pH values and electrolytes in aquatic system has been rarely investigated.

The main goal of Chapter 6 is the investigation of the characteristics, dispersions and stabilities of TiO<sub>2</sub> NPs as a function of pH value and ionic strength (NaCl and CaCl<sub>2</sub>

solutions) in the presence of five different DOM sources: Hohloh Lake 10 fulvic acid (HO10FA), alginate, bovine serum albumin (BSA),  $\alpha$ -amylase and SDS at realistic DOC environmental concentrations.

### **1.3 Multi-cycle photocatalytic degradation of bezafibrate by polyvinyl alcohol/TiO<sub>2</sub> (PVA/TiO<sub>2</sub>) film**

Owing to the risk of released TiO<sub>2</sub> NPs (Dankovic et al. 2007), several novel technological approaches have been developed with the aim of decreasing the discharge of TiO<sub>2</sub> NPs into the environment. Two attempts seem to be most promising: membrane filtration and immobilization (Augugliaro et al. 2005, Azrague et al. 2007, Benotti et al. 2009, Fang et al. 2011, He and Gong 2003). Microfiltration and nanofiltration have been extensively used for elimination and recycling TiO<sub>2</sub> particles from suspension. However, high running costs and induced secondary pollution have become the limitations for practical application (Jung et al. 2008, Mozia 2010). In addition, the TiO<sub>2</sub> deduced abrasion on membrane materials turned out to be problematic (Ziegmann et al. 2010). Some efforts have been reported on the immobilization of TiO<sub>2</sub> nanoparticles on a variety of matrices, such as glass, pumice beads, stainless steel plates, and polymers (Hou et al. 2014, Liu et al. 2014b, Pastrana-Martinez et al. 2013, Wang et al. 2013a). The adherences between matrix and TiO<sub>2</sub> particles have been deduced from physical adsorption (Hosseini et al. 2007), electrostatic interaction (Matsuzawa et al. 2008), hydrogen bond formation (Zhang et al. 2011) and chemical bond interactions (Huang et al. 2006). Among these interactions, chemical bonding between polymer and TiO<sub>2</sub> nanoparticles is considered to be the most efficient technique. For instance, polyvinyl alcohol/TiO<sub>2</sub> (PVA/TiO<sub>2</sub>) composition has been reported to possess good photocatalytic properties in wastewater treatment (Song et al. 2014, Zhang et al. 2013b). Therefore the photocatalytic activity and mechanisms of PVA/TiO<sub>2</sub> hybrid film in photocatalysis under different reaction conditions are worth to be highly considered.

The aim of Chapter 7 was to: (1) immobilize TiO<sub>2</sub> nanoparticles in PVA films for



photocatalysis; (2) investigate major influences, such as pH value, reaction time, thickness of the film and multi-use of the film; (3) compare the applicability of PVA/TiO<sub>2</sub> hybrid films with TiO<sub>2</sub> suspension and other TiO<sub>2</sub> immobilized composites (pumice/TiO<sub>2</sub> and porous glass bead/TiO<sub>2</sub>) for long term use.

#### **1.4 Aim of the dissertation**

The work done in this dissertation aimed to:

- (1) achieve a better understanding of the application of TiO<sub>2</sub> based NPs in photocatalytic processes for the degradation of selected pharmaceuticals under environmentally relevant conditions (Chapter 4 and 5);
- (2) study the aggregation behavior of the TiO<sub>2</sub> in aquatic systems (Chapter 6);
- (3) develop a novel immobilization method of TiO<sub>2</sub> for technical application in water treatment (Chapter 7).

## 2 Background

### 2.1 TiO<sub>2</sub> in heterogeneous photocatalysis

TiO<sub>2</sub> exists in three crystalline forms: anatase, rutile and brookite. Anatase and rutile are the most used forms in photocatalysis, while brookite has been rarely employed for experimental investigation owing to its synthesis limitation (Carp et al. 2004, Kandiel et al. 2010). TiO<sub>2</sub> is classified as a semiconductor according to the energy difference between the highest occupied molecular orbital, valence band (VB) which is filled with electrons, and the lowest unoccupied molecular orbital, conduction band (CB) which is partly filled or empty. The band gap of anatase and rutile are 3.2 and 3.0 eV, respectively (Fujishima 1999).

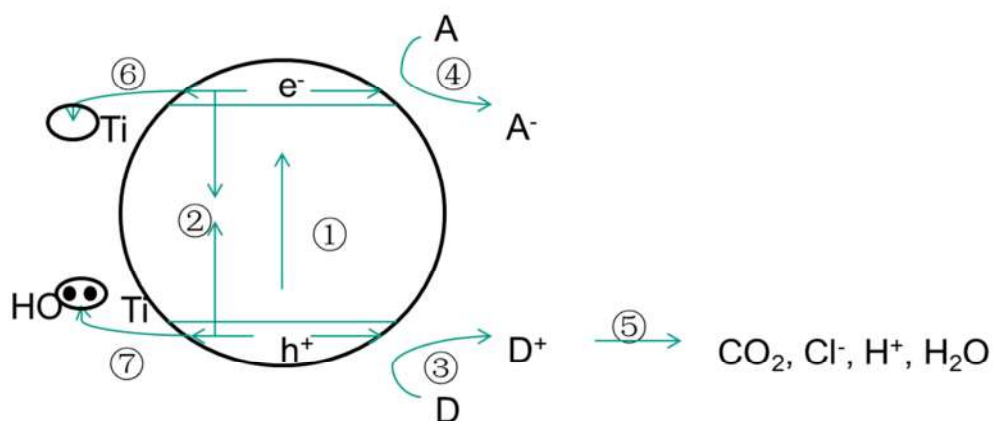
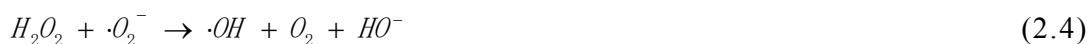
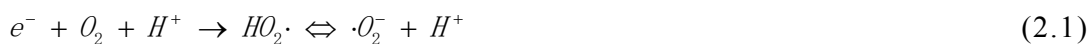


**Fig. 2.1 Primary steps in the photoelectrochemical mechanism (Hoffmann et al. 1995): (1) formation of charge carriers by a photon; (2) charge carrier recombination to liberate heat; (3) initiation of an oxidative pathway by a valence band hole; (4) initiation of an reductive pathway by a valence band electron; (5) further thermal (e.g. hydrolysis or reaction with active oxygen species) and photocatalytic reactions to yield mineralization products; (6) trapping of a conduction band electron in a dangling surficial bond to yield Ti(III); (7) trapping of a valence band hole at a surficial titanol group.**

When TiO<sub>2</sub> is impacted by a photon of energy  $h\nu$  matching or exceeding the band gap energy, an electron is promoted from the VB into the CB to form the photogenerated

holes and electrons. The excited electrons in the CB and the VB holes can either recombine, get trapped in metastable surface states, or react with electron donors or acceptors at or in the immediate vicinity of the semiconductor surface. This ability to donate and accept electrons, can initiate redox processes at a surface and is the basis of heterogeneous photocatalysis (Fig. 2.1) (Hoffmann et al. 1995).

After generation, the electrons and holes rapidly transfer to the TiO<sub>2</sub> surface, where they are trapped and can initiate various kinds of redox reactions at the ambient conditions. Because of trapping and consuming by reactions, the recombination of electrons and holes is avoided to a large extent (Hoffmann et al. 1995, Kabra et al. 2004, Linsebigler et al. 1995). In most experiments, the electrons are transferred to O<sub>2</sub>, which act as a primary electron acceptor and decrease the electron-hole recombination (Eqs. 2.1 to 2.3). Reactive oxygen species (ROS) such as superoxide radical anions ( $\cdot O_2^-$ ), hydroperoxyl radicals (HO<sub>2</sub> $\cdot$ ), hydrogen peroxide (H<sub>2</sub>O<sub>2</sub>) and singlet molecular oxygen (<sup>1</sup>O<sub>2</sub>) are formed (Daimon and Nosaka 2007, Gerischer and Heller 1991, Ishibashi et al. 2000, Tsuruta et al. 2008). In addition, superoxide radicals ( $\cdot O_2^-$ ) and hydrogen peroxide (H<sub>2</sub>O<sub>2</sub>) can lead to additional formation of  $\cdot OH$  and participate in oxidation reactions (Eqs. 2.4 to 2.6) (Guo et al. 2011, Wang et al. 2011).



## 2.2 Strategies for improving TiO<sub>2</sub> photocatalytic efficiency

In contrast to many merits of TiO<sub>2</sub> such as low toxicity, chemical stability and relatively high photocatalytic activity (Chiang et al. 2004), there is a poor overlap between its electronic structure, the band gap, and the solar spectrum which results in a low efficiency (the component of UV/near UV light in sunlight amounts to only 3 to 5%)

of the solar energy utilization and therefore limits its technological applications (Kivrak et al. 2009, Shifu et al. 2007, Wang et al. 2009, Wu et al. 2007). Furthermore, electron-hole recombination was shown to occur within a few hundred picoseconds of their formation in colloidal TiO<sub>2</sub> (Rothenberger et al. 1985). In order to enhance the photocatalytic activity of TiO<sub>2</sub>, much attention has been paid for suppressing the recombination of electron-hole pairs and enriching properties in terms of light absorption. Selecting the right physical characteristics of TiO<sub>2</sub> including particle size (Liu et al. 2014a), morphology (Lakshminarasimhan et al. 2007), crystallinity (Tanaka et al. 1991) and crystal facet (Kiatkittipong et al. 2011) can enhance the photocatalytic activity by photocurrent generation and photoluminescence. Furthermore, doping or deposition with either noble metals (Au, Ag, Pt, Pd) (Bumajdad et al. 2014, Kozlova et al. 2011, Ma et al. 2010, Mateos-Pedrero et al. 2013, Tapin et al. 2013, Tsuru et al. 2006), transition metals (Fe, Mo, Cu, V) (Cui et al. 2009, Lin and Yang 2014, Wang et al. 2013c, Zhang et al. 2013a), non-metals (C, N, S) (Hamadianian et al. 2013, Petkovich et al. 2014, Wang et al. 2014a), metalloids (B, Si, Sb) (Chen et al. 2012, Liang et al. 2012, Moon et al. 2001) or configuring composites, like SnO<sub>2</sub>-, CeO<sub>2</sub>- and WO<sub>3</sub>-TiO<sub>2</sub> (Iliev et al. 2010, Kusior et al. 2013, Munoz-Batista et al. 2014) also opens the door for successful developing high efficient photocatalysts. Compared with neat TiO<sub>2</sub>, modified TiO<sub>2</sub> can significantly improve processes like light absorption, interfacial charge transfer kinetics and organic adsorption, leading to enhance photocatalytic activity.

Incorporation of a metal has been expected to lead to a promotion of the photocatalytic activity of TiO<sub>2</sub> (Li et al. 2007, Ma et al. 2008). Electrically neutral and isolated from each other, the metal and the TiO<sub>2</sub> have different Fermi level positions, and the former has a higher work function ( $\phi_m$ ) than the TiO<sub>2</sub> ( $\phi_s$ ). When the two materials are connected electrically, electron migration from the TiO<sub>2</sub> to the metal occurs until the two Fermi levels are aligned. The electrical contact has formed a space charge layer. The surface of the metal acquires an excess negative charge while the TiO<sub>2</sub> exhibits an excess positive charge as a result of electron migration away from the barrier region. The bands of the TiO<sub>2</sub> bend upward toward the surface. The barrier formed at the metal-TiO<sub>2</sub>

interface is called the Schottky barrier (Fig. 2.2). The height of the barrier is given by Eq. 2.7. This barrier serves as an efficient electron trap preventing electron-holes recombination (Linsebigler et al. 1995). Under UV light irradiation, the photogenerated electrons in TiO<sub>2</sub> migrate to the metal particles which function as the catalytic sites for reduction reactions and the holes are free to diffuse to the TiO<sub>2</sub> surface where oxidation of organic species can occur (Fig. 2.3 left) (Qu and Duan 2013). Furthermore, the newly generated Fermi level in the TiO<sub>2</sub> and the metal system with a lower band gap energy, which can produce electron-hole pairs excitable by even visible light irradiation (Falch and Kriek 2013, Kutty and Avudaitai 1989). Diffusion reflection spectroscopy results have proven that metal doped TiO<sub>2</sub> shows the ability of visible light adsorption comparing to bare TiO<sub>2</sub> (Bessekhouad et al. 2012, Inturi et al. 2014, Liu et al. 2013, Mohamed and Aazam 2013, Wantala et al. 2010).

$$\phi_b = \phi_m - E_x \quad (2.7)$$

In addition, the metallic nanoclusters can function as effective cocatalysts to reduce the over potential for surface electrochemical reactions. For instance, the presence of Pt nanoclusters on the surface of anatase TiO<sub>2</sub> photocatalysts can greatly improve the efficiency of hydrogen evolution processes for water splitting reactions (Qu and Duan 2013). Under visible light excitation, the electrons from the excited metal plasmonic band are injected into the conduction band of TiO<sub>2</sub>, where reduction reaction occurs. At the same time, the transfer of electrons into TiO<sub>2</sub> leaves unbalanced holes in the metal particles, which can be used for oxidation (Fig. 2.3 right).

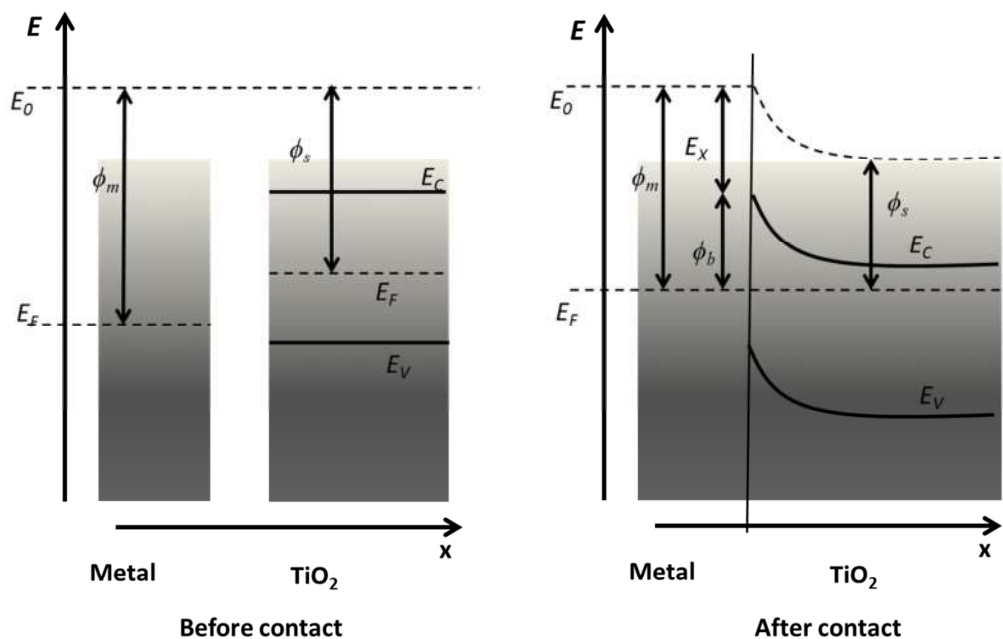


**Fig. 2.2** Schematic of Schottky barrier.  $E_F$ : Fermi level,  $E_V$ : valence band,  $E_C$ : conduction band,  $E_0$ : vacuum level,  $E_X$ : electron affinity,  $\phi_m$ : work function of metal,  $\phi_s$ : work function of  $\text{TiO}_2$ ,  $\phi_b$ : height of the barrier.

The different Fermi levels of metals and  $\text{TiO}_2$  (work functions) can partly govern the extent of which metal deposits attract electrons from  $\text{TiO}_2$ . The IUPAC defined the work function of a metal, to be the minimum energy required to remove an electron from the highest occupied level of a metal (Fermi level) across a surface carrying no net charge (IUPAC 2012). Hence, a greater electron trapping on the metal surface is promoted by a higher difference of work functions between the metal and  $\text{TiO}_2$ . Work function values of  $\text{TiO}_2$  and selected metals are shown in Table 2.1. The values are only to be used as a guide to illustrate the tendency of each metal to attract electrons from  $\text{TiO}_2$ . The values are for bulk clean metals and do not take into account several factors which are of influence such as crystal facet (Imanishi et al. 2007), metal- $\text{TiO}_2$  interfacial area (Sasahara et al. 2006), metal atom size (Kim et al. 2010), metal capping layer (Li et al. 2008), metal deposition method (Kampen et al. 2004), oxygen diffusion (Mulyukov 2006), temperature (Ibragimov and Korol'kov 2001) and the presence of water (Musumeci and Pollack 2012). According to Table 2.1, Pt exhibits the highest work function among the selected metals. Research works have already proven that Pt modified  $\text{TiO}_2$  (Pt/ $\text{TiO}_2$ ) possessed a greater capability for trapping the photogenerated electrons with the more effective electron-hole pairs separation, and accelerates the

photocatalytic degradation rate of the target pollutants (Bazzo and Urakawa 2013, Cui and Lu 2013, Kamegawa et al. 2013, Kim et al. 2013, Miller et al. 2010, Nomikos et al. 2014, Song et al. 2013, Zhang et al. 2013c).

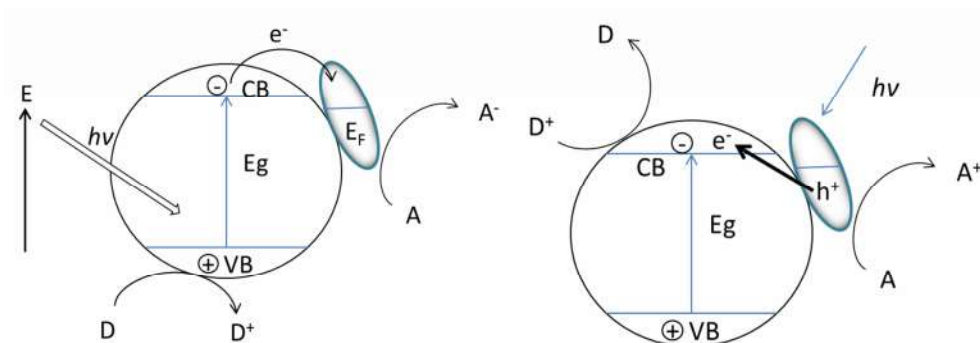


**Fig. 2.3 Schematic illustration of organic matter degradation from metal/TiO<sub>2</sub> photocatalysts under UV light irradiation**

The addition of Pt to a semiconductor also changes the photocatalytic process by changing the semiconductor surface properties. Thus the deposited Pt changes the resultant catalytic activity (Egerton and Mattinson 2010). Pt can improve the adsorption of organic compounds on the catalyst's surface as well (Denny et al. 2007). Compared with neat TiO<sub>2</sub>, Pt/TiO<sub>2</sub> surface acidity increases significantly, and its isoelectric point decreases with the increase of Pt depositing. The increased acidic character assists adsorption and reaction of molecules with polarized functional groups such as carboxylic acids or amino acids with affinities for the acidic surface (Kozlov and Bicelli 2000, Tran et al. 2006). The active oxygen species generated on the irradiated Pt/TiO<sub>2</sub> surface are stable enough to survive for several minutes even in the dark, and take part in a successive photo-oxidation reaction (Hwang et al. 2003). It has been found that Pt deposited on TiO<sub>2</sub> stabilized the photoformed  $\cdot\text{O}_2^-$  and  $\text{O}_3^-$  species which can take part in the oxidation reaction in the dark (Einaga et al. 2001). In addition, Pt could also alter the reaction mechanism and improve the reaction kinetics (Lee and Choi 2004).

Table 2.1 Work functions of TiO<sub>2</sub> and metals

TiO <sub>2</sub> or metal	Work function (eV)	Reference
TiO <sub>2</sub>	4.46 ~ 4.65	(Gutmann et al. 2010)
Ag	4.74	(Trasatti 1971)
Ru	4.71	(Trasatti 1971)
Au	5.10 ~ 5.47	(Trasatti 1971)
Pd	5.22 ~ 5.55	(Trasatti 1971)
Pt	6.74 ~ 6.97	(Skriver and Rosengaard 1992)
Al	4.25	(Kiejna and Wojciechowski 1981)
Cu	4.40	(Kiejna and Wojciechowski 1981)
Fe	5.16 ~ 5.54	(Skriver and Rosengaard 1992)

## 2.3 Reaction kinetics and mechanisms in heterogeneous photocatalysis

### 2.3.1 Reaction kinetics

The Langmuir–Hinshelwood (L–H) kinetics model is based on the Langmuir isotherm for monolayer adsorption of molecules on the active sites of a solid material. This model has mostly been used to explain the kinetics of the heterogeneous photocatalytic degradation of organic matters. It is given by:

$$r = -\frac{dc}{dt} = \frac{k_r K_s c}{1 + K_s c} \quad (2.8)$$



where  $dc/dt$  is the degradation rate ( $r$ ),  $k_r$  is the apparent reaction rate constant,  $K_s$  is the equilibrium constant for adsorption of the substance on the catalyst, and  $c$  is the reactant concentration. In case the concentrations of substances exceed the saturation coverage of the catalyst surface, Eq. 2.8 (i.e.  $K_s c \gg 1$ ) simplifies to a zero order rate equation.

$$r = -\frac{dc}{dt} = k \quad (2.9)$$

For very low concentrations (i.e.  $K_s c \ll 1$ ), the L–H equation simplifies to a pseudo-first-order kinetics law (Eq. 2.10) where  $k_{app}$  is the pseudo first order rate constant.

$$r = -\frac{dc}{dt} = k_{app}c \quad \text{or} \quad c_t = c_0 e^{-k_{app}t} \quad (2.10)$$

While widely cited in photocatalysis, flaws have been found with this model. Because the continued displacement of the adsorbed reactants caused by active species such as electrons, holes,  $\bullet$ OH and organic compounds under irradiation, adsorption/desorption equilibriums are not established. Ollis (Ollis 2005) developed a pseudo-steady state (PSS) model beyond adsorption/desorption equilibrium assumption (Eq. 2.11).

$$r = \frac{k_r c}{1 + K_d c} \quad (2.11)$$

where  $K_d$  is a desorption equilibrium constant.

It has also been observed that  $k_r$  and  $1/K_s$  varied with light intensity to the same exponent, which could be 1.0 or 0.5 with very low intensity or high intensity respectively (Emeline et al. 2000, Turchi and Ollis 1990). Du et al. (Du et al. 2009) proposed a modified L–H kinetic model (Eqs. 2.12 and 2.13) to account for the light intensity ( $I$ ) contribution during photocatalytic reactions (Du et al. 2009).

$$\frac{1}{k_r} = \frac{\alpha}{I^{1/2}} + \beta \quad (2.12)$$

$$K_s = \frac{\omega}{I^{1/2}} + \psi \quad (2.13)$$

where  $\alpha$ ,  $\beta$ ,  $\omega$  and  $\psi$  are constants determined by elementary reactions and catalyst

properties.

### 2.3.2 Reaction mechanisms

Photocatalysis is the mostly used as pretreatment technology in wastewater treatment process owing to the high cost of irradiation (Chen et al. 2013, Sarria et al. 2001). In practical application, the irradiation time should be shortened for economic reasons. This way cause incomplete degradation of pollutants and may form some more harmful intermediates. Therefore, qualitatively and quantitatively clarifying characteristics of intermediates promote a great interest for identifying the products and degradation pathway(s). Substantial efforts have been made for identifying the major degradation pathways, for evaluating the toxicity of the intermediates (Khataee et al. 2013, Kondrakov et al. 2014) and for recognizing the reaction limiting steps.

During photocatalysis, the organic compounds are degraded to numerous intermediates primarily as a consequence of the non-selective reaction of  $\bullet\text{OH}$  and the participation of the other photogenerated radicals. Many of these transformation products have aromatic rings, heteroatoms, and other chromophore groups with phenolic, nitro, and naphthoxyl structure (Boreen et al. 2003). Hydroxylation of the isopropyl and methoxy groups has been identified as the main reaction pathway (Eqs. 2.14 and 2.15) (Antonopoulou and Konstantinou 2015). The breakdown also involves hydroxylation of the aromatic ring by an electrophilic attack of  $\bullet\text{OH}$  radicals, cleavage of C-O, C-N or S-N bonds and cleavage of  $\alpha$ -position in aromatic moieties and rings opening (Fatta-Kassinos et al. 2011). In some cases the transformation products can be more toxic and persistent than the parent compounds. One example is the photocatalytic degradation of sulfamethoxazole by solar photo-Fenton in distilled water and in seawater (Trovo et al. 2009). Degradation and mineralization of sulfamethoxazole decreased significantly in seawater compared to distilled water. In spite of 45% mineralization in seawater, toxicity in *V. fischeri* bioassays increased from 16% to 86%, which indicates that the different degradation pathway in seawater is different from those in distilled water. Kondrakov et al. (Kondrakov et al. 2014) also reported different breakdown pathways when compared

photolysis and photocatalysis by using bisphenol A as a model compound. A hazardous DNA-binding agent, bisphenol A 3,4-quinone, was detected during photocatalytic degradation.



The overall photocatalysis reaction is divided into five independent steps (Fogler 1999, Herrmann et al. 1999),

1. Mass transfer of the organic matter(s) in the bulk fluid to the TiO<sub>2</sub> surface.
2. Adsorption of the organic matter(s) onto the photon activated TiO<sub>2</sub> surface (i.e. surface activation by photon energy occurs simultaneously in this step).
3. Photocatalysis reaction of the adsorbed phase on the TiO<sub>2</sub> surface.
4. Desorption of the intermediate(s) from the TiO<sub>2</sub> surface.
5. Mass transfer of the intermediate(s) from the interface region to the bulk fluid.

In the term of rate determination, the limiting step is the slowest step. If the mass transfer steps are much faster than the reaction steps, the molecules adsorption or surface contact with the catalyst plays a key role during the photocatalytic degradation. If the mass transfer steps are much slower than the reaction steps, changing the flow circumstances at the TiO<sub>2</sub> surface may alter the overall photocatalytic reaction rate.

## 2.4 Fundamental parameters of photocatalytic degradation of organic pollutants in wastewater treatment

It has been demonstrated that the oxidation rates and efficiency of the photocatalytic

system not only depend on loading and catalyst properties (such as crystalline phase, specific surface area, and porosity) (Kozlova and Vorontsov 2010), initial concentration of target compound (Doll and Frimmel 2004b), light intensity and wavelength (Dionysiou et al. 2008), but also on O<sub>2</sub> concentration (Muzyka and Fox 1991), pH (Piscopo et al. 2001), and the presence of organic (Yang et al. 2010) and inorganic matter (Vamathevan et al. 2001, Zhao et al. 2012) in the solution.

### **2.4.1 TiO<sub>2</sub> loading**

Catalyst loading affects the overall photocatalysis reaction rate in a heterogeneous catalytic regime. Generally, photocatalytic oxidation rates increase with the increase of catalyst loading owing to a higher contact area between catalyst and target compounds. A linear dependency was proposed to describe the influence of catalyst loading on photocatalytic oxidation rate in liquid phase (Gaya and Abdullah 2008). With the further increase of catalyst loading, the light photon absorption coefficient usually decreases, and the photocatalytic oxidation rates decrease consequently.

Plenty of studies have reported the effect of TiO<sub>2</sub> loadings on the process efficiency (Ji et al. 2013, Nomikos et al. 2014, Rammohan and Nadagouda 2013, Zhang et al. 2013c). The optimum TiO<sub>2</sub> loading varied, and mainly depends on reactor geometry, UV irradiation characteristics (power, wavelength) and the type of organic substances being degraded.

### **2.4.2 pH value**

The pH value is an important parameter in photocatalysis which affects the ionization states of organic compounds, the surface charges and aggregation size of the catalyst as well as the formation rate of •OH and other active radicals in the reaction solution (Haroune et al. 2014, Schwegmann et al. 2013). For some weakly acidic organic substances, the decrease of pH leads to an increased photocatalytic oxidation rate due to increased adsorption. On the contrary, for some alkaline organic substances, the photocatalytic degradation rate increases at higher pH values (Haroune et al. 2014, Ji et

al. 2013). The point of zero charge (PZC) of TiO<sub>2</sub> is also considered to impact the photocatalytic oxidation performance. The PZC of TiO<sub>2</sub> is reported to be in the pH range of 4.5 to 7.0, depending on the catalyst used (Chong et al. 2010). At the pH of PZC, the interaction between TiO<sub>2</sub> particles and organic contaminants is negligible because of the lack of any electrostatic force. When the pH < PZC, TiO<sub>2</sub> nanoparticles exhibit a positive charge and exert an electrostatic attraction force towards the negatively charged compounds, which can intensify the adsorption onto the photon activated TiO<sub>2</sub> surface for subsequent photocatalytic reactions (Gogniat et al. 2006). At pH > PZC, TiO<sub>2</sub> nanoparticles exhibit negative charge and repulse the anionic compounds in water, and the photocatalytic degradation decreases accordingly.

### 2.4.3 Dissolved oxygen

Dissolved oxygen (DO) plays several important roles in the photocatalytic process. It is considered to be a highly efficient electron scavenger in photocatalysis to form superoxide radicals  $\bullet\text{O}_2^-$ , thereby reducing charge recombination and promote reactions with organic radical cations (Youn et al. 2010). Furthermore,  $\bullet\text{O}_2^-$  and hydrogen peroxide which are produced by the reaction of DO and electrons can lead to additional formation of  $\bullet\text{OH}$ , which explains the observed oxidizability (Guo et al. 2011, Wang et al. 2011).

The absence of DO can alter the pathway for the photocatalytic degradation of certain organics. It has been reported (Axelsson and Dunne 2001) that photocatalytic oxidation of 3,4-dichlorophenol occurred with a different reaction mechanism when O<sub>2</sub> was absent. In the presence of O<sub>2</sub>,  $\bullet\text{OH}$  addition to the 3,4-dichlorophenol molecule was observed, while partial dechlorination of the organic compound was noticed due to electron transfer from the Ti<sup>3+</sup> site to the aromatic ring in the absence of O<sub>2</sub>.

### 2.4.4 Dissolved cation ions

Cations either enhance or degrade the rate of reaction depending on the mechanism of reaction. To date, the effects of inorganic cations (i.e. Na<sup>+</sup>, K<sup>+</sup>, Ca<sup>2+</sup>, Cu<sup>2+</sup>, Mn<sup>2+</sup>, Mg<sup>2+</sup>, Ni<sup>2+</sup>, Fe<sup>2+</sup>, Zn<sup>2+</sup> and Al<sup>3+</sup>) on the photocatalytic water treatment have been investigated

(Habibi et al. 2005, Leng et al. 2000, Ozkan et al. 2004, Rincon and Pulgarin 2004, Schmelling et al. 1997, Wong and Chu 2003). A general consensus from these studies concludes that  $\text{Cu}^{2+}$ ,  $\text{Fe}^{2+}$  and  $\text{Al}^{3+}$ , at certain levels may decrease photo-mineralization reaction rates while  $\text{Ca}^{2+}$ ,  $\text{Mg}^{2+}$  and  $\text{Zn}^{2+}$  may have negligible effects because they are at their maximum oxidation states resulting in their inability to inhibit the photocatalytic reaction. And  $\text{Fe}^{3+}$  is considered as an efficient electron scavenger which can increase the photocatalytic reaction rate by trapping and transferring electrons (Brezova et al. 1995, Vamathevan et al. 2001, Wan et al. 2013). Transition metals such as  $\text{Cu}^{2+}$  and  $\text{Fe}^{3+}$  decrease the reduction of  $\cdot\text{O}_2^-$  by the conduction electrons, subsequently block the formation of ROSs ( $\cdot\text{O}_2^-$  and  $\cdot\text{OH}$ ), and depresses the degradation of organic matters during photocatalysis (Chen et al. 2002). However, exceptions exist everywhere according to different light sources, targets, catalysts and reaction conditions.  $\text{Ni}^{2+}$  and  $\text{Cu}^{2+}$  were found to work as electron scavenger to improve the degradation ability of the chitosan- $\text{TiO}_2$  complex for methyl orange (Zhao et al. 2012). The enhancement of  $\text{Cu}^{2+}$  was also observed in the case of phenol degradation by  $\text{TiO}_2$  and  $\text{WO}_3$  (Wan et al. 2013).

### 2.4.5 Dissolved organic matter

The presence of dissolved organic matter (NOM) and other organic substances retarded the photocatalysis of a specific persistent substance by the combination of radiation attenuation, competition for active sites and surface deactivation of the catalyst by adsorption. In case of photocatalytic degradation of carbamazepine, the first-order rate constant  $k$  of carbamazepine degradation was reduced for ca. 40% in the presence of NOM at a quite low DOC concentration ( $\rho_0(\text{DOC}) = 0.5 \text{ mg L}^{-1}$ ) which was explained by the synergy of these three effects (Doll and Frimmel 2005). A stronger inhibition effect for NOM was observed with the increase of pH and initial DOC concentration (Pelaez et al. 2011).

Additionally, NOM in soils and aquatic systems is recognized to strongly affect the environmental distribution of organic compounds, and by this affect the fate of pollutants in the environment. Water associated with NOM may have a significant impact on

NOM–organic compound interactions such as carbamazepine–NOM interactions which can be enhanced by one to two orders of magnitude when NOM became fully hydrated (Borisover et al. 2011). This complex interaction also occurs between NOM and metal ions. In case of removal arsenic by photocatalysis, the presence of NOM can significantly reduce the amount of arsenic adsorbed at the steady-state by occupying some available binding sites for arsenic adsorption on the TiO<sub>2</sub> surface (Liu et al. 2008).

## 2.5 Factorial design

In the case of processes influenced by multiple variables, factorial design has been shown to be a powerful tool for determining the effects of operational factors and their interactions. This technique has been used widely in chemical industry. The factorial design can cover the main effects and interaction effects of the parameters within a whole range of selected parameters. According to the sparsity of effects principle in factorial design, it is most likely that main (single factor) effects and two-factor interactions are the most significant effects, and the higher order interactions (three-factor interactions) are negligible. The most common type of factorial design is that carried out at two levels (coded  $\pm 1$ ), and can include all possible combinations of the two levels for each factor and thus require  $2^k$  experimental runs, where  $k$  is the number of factors to be studied (Box et al. 2005). Two-level full factorial designs for  $k = 2$ , and 3 are presented in Table 2.2.

The factorial design can cover the main and interaction effects of the parameters within the whole range of selected parameters. According to the sparsity of effects principle in factorial design, it is most likely that main (single factor) effects and two-factor interactions are the most significant effects, and the higher order interactions (three-factor interactions) are negligible. Considering the general function expressing the interaction between the independent and dependent variables a second order model was employed (Eq. 2.16):

$$Y = \beta_0 + \sum_{i=A}^C \beta_i X_i + \sum_{i=A}^C \sum_{j=B \neq i}^C \beta_{ij} X_i X_j + \varepsilon \quad (2.16)$$

Where  $Y$  is the predicted response,  $x_i$  are levels of the factors,  $\beta_0$  is mean response,  $\beta_i$  are the main effect coefficients for each factor and  $\beta_{ij}$  are the interaction effect coefficients (Box et al. 2005). The observed response is fitted in terms of deviations from the mean response owing to changes in the variables of interest ( $x_i$ , scaled and centered,  $\pm 1$ ). Estimation of the regression coefficients ( $\beta$ ) can be easily carried out by the least squares method. Notice that the coefficients obtained in this way are independent of each other as a consequence of the orthogonality of the full factorial design (Box et al. 2005).

When doing factorial design, there are two classes of effect: main effect and interaction effect. A main effect is an outcome that is a consistent difference between levels of a factor. An interaction effect occurs when the effect of one independent variable on the dependent variable changes depending on the level of another independent variable. The determination of main effects and interaction effects are calculated by the difference between averages response of the high “+1” and low “-1” setting for each factor (Box et al. 2005).

**Table 2.2a Experimental matrix for a  $2^2$  full factorial design**

$x_1$	$x_2$
+1	+1
+1	-1
-1	+1
-1	-1

**Table 2.2b Experimental matrix for a  $2^3$  full factorial design**

$x_1$	$x_2$	$x_3$
-1	-1	-1
-1	-1	+1
-1	+1	-1
-1	+1	+1
+1	-1	-1
+1	-1	+1
+1	+1	-1
+1	+1	+1



## 2.6 Aggregation and stability of TiO<sub>2</sub> NPs in aquatic systems

It is generally accepted that the electrophoretic mobility of TiO<sub>2</sub> NPs in aquatic environments is strongly dependent on their aggregation. The aggregation process is well described by the traditional DLVO theory, and determined by the total interaction energy ( $V_{TOTAL}$ ) between particles when they approach each other (Thio et al. 2010). There is a dependence on pH and ionic strength, which control the surface charge of the NPs and the thickness of the electric double layer surrounding the particles (Thio et al. 2011). Recent studies have made use of various analytical techniques and experiments to describe and understand the behavior of TiO<sub>2</sub> NPs under different conditions (e.g. pH value, ionic strength and kind of water) (Domingos et al. 2009b, Romanello and de Cortalezzi 2013). Results have indicated that the behavior, transport, and fate of NPs in aqueous systems are controlled both by their surface properties and by the chemistry of the aqueous system (Battin et al. 2009).

### 2.6.1 DLVO theory

The DLVO theory is named after Derjaguin and Landau, Verwey and Overbeek. This theory is used to explain the aggregation of colloid particles and describe the force between charged surfaces interacting through a liquid medium. According to this theory, the stability of colloidal particles in aqueous environments is determined by the total interaction energy ( $V_{TOTAL}$ ), which is the sum of the attractive energy — Van der Waals interactions ( $V_{vdw}$ ) and the repulsive energy — electrical double layer interactions ( $V_{EDL}$ ).

Van der Waals interactions were calculated according to Eq. 2.17 without retardation,

$$V_{vdw}^{attr.} = -\frac{A \cdot a}{12d} \quad (2.17)$$

where  $a$  is the primary aggregate radius,  $d$  is the minimum distance between particles, and  $A$  is the Hamaker constant. This equation is only valid for  $d$  much smaller than  $a$ .

$V_{EDL}$  was calculated according to the linear super position approximation, a useful compromise between constant number and constant-charge assumptions (Romanello and de Cortalezzi 2013), according to Eq. 2.18.

$$V_{EDL}^{rep.} = \frac{a \cdot n_{\infty} \cdot k \cdot T \cdot G^2}{K^2} \exp(-K \cdot d) \quad (2.18)$$

$$n_{\infty} = 1000 \cdot N_A \cdot c_i \quad (2.19)$$

$$G = \tan d \left( \frac{z \cdot e \cdot P}{4 \cdot k \cdot T} \right) \quad (2.20)$$

$$K = 2.32 \times 10^9 \cdot \left( \sum c_i \cdot z_i^2 \right)^{1/2} \quad (2.21)$$

where  $n_{\infty}$  is the bulk number concentration which is calculated according to Eq. 2.19, where  $c_i$  is the ion molar concentration,  $k$  is the Boltzmann constant,  $T$  is the temperature. The parameter  $G$  is calculated as shown in Eq. 2.20, where  $z$  is the charge of the ions,  $e$  is the electron charge and  $P$  is the experimentally determined zeta potential. The inverse Debye length ( $K$ ) is calculated according to Eq. 2.21,  $z_i$  is the charge of the ion. Eq. 2.18 is only valid for  $K \times d \gg 1$ , and for symmetric electrolytes.

### 2.6.2 Influence of pH

The surface charge of TiO<sub>2</sub> NPs is strongly affected by the pH value, and the PZC of TiO<sub>2</sub> NPs was reported to be between pH 4.5 and pH 7 (Frimmel and Niessner 2010, Romanello and de Cortalezzi 2013). Bare TiO<sub>2</sub> surfaces can be negatively or positively charged in aquatic systems. Below the PZC, the oxygen atoms in the surface of TiO<sub>2</sub> NPs would accept protons contributing to a positive zeta potential, and above the PZC hydrogen ions would be lost from the surface of the nanoparticles, contributing to a negative zeta potential (Stumm et al. 1992). At the PZC-pH, there is a significant decrease in the electrostatic repulsion between NPs or between a NP and the surrounding solid surfaces, resulting in a faster rate of aggregation, increasing aggregate size and rate of deposition onto soil and sediment particles (Thio et al. 2011). The adsorption capacity of the NPs is related to the pH as well. For example, the adsorption of NOM on the NPs' surface which is via electrostatic adsorption and ligand exchange (mainly hydroxyl and

carboxyl groups) is dependent on the pH value (Zhu et al. 2014). Generally, the investigation of the influence of pH value is also related to other parameters like ionic strength or NOM.

### 2.6.3 Influence of ionic strength and specific electrolytes

Many of studies have reported the destabilization effect of electrolytes on the aggregation of NPs in aqueous environments (French et al. 2009, Li and Sun 2011). Romanello et al. (Romanello and de Cortalezzi 2013) pointed out that the TiO<sub>2</sub> NPs aggregation was only observed at and around pH of PZC in indifferent electrolyte solutions (i.e. Na<sup>+</sup>, 0.9 mM). However, divalent cations (i.e. Ca<sup>2+</sup>, Mg<sup>2+</sup>, 0.3 mM) may cause aggregation at pHs above the PZC due to specific adsorption which avoids the surface charge to acquire sufficient negative values to create a potential barrier for aggregation, while their effect is negligible at pH values below the PZC. At any given pH, an increase of ionic strength results in a thinner electric double layer surrounding the NPs, thus increasing the aggregation rate, the aggregates size, and the rate of deposition onto mineral surfaces. Furthermore, plenty of the previous work focused on the effect of monovalent cations (i.e. Na<sup>+</sup>) and divalent cations (i.e. Ca<sup>2+</sup>, Mg<sup>2+</sup>) as background ions in the presence of NOM (Erhayem and Sohn 2014, Thio et al. 2011, Zhu et al. 2014).

### 2.6.4 Influence of NOM

Adsorption is the most important interaction occurring between NOM and TiO<sub>2</sub> NPs, which is influenced by several parameters like the kind of NOM, and the medium characteristics (Philippe and Schaumann 2014). The adsorption of NOM decreases with the increase of pH and the decrease of ionic strength (Erhayem and Sohn 2014). Evidences from UV and IR spectroscopy indicate that phenol groups and carboxyl groups of smaller molecules can form complexes with the surface of TiO<sub>2</sub> NPs (Pettibone et al. 2008, Yang et al. 2009). Humic substances (HS), comprise the major organic constituents (up to 30 ~ 50%) in aquatic environments (Reemtsma et al. 2008), represent an active and important fraction of NOM and have been studied extensively. It is well known that the adsorbed HS have a stabilizing effect on the TiO<sub>2</sub> NPs through adsorption

of the negatively charged compounds. Under highly acidic conditions, however, HS promote the surface charge of TiO<sub>2</sub> NPs neutralization and cause the aggregation of NPs (Bolyard et al. 2013, Erhayem and Sohn 2014, Romanello and de Cortalezzi 2013, Zhu et al. 2014). By further increasing HS concentrations charge inversion and stabilization of TiO<sub>2</sub> NPs are obtained (Loosli et al. 2013). Furthermore, Loosli et al. observed that addition of alginate and Suwannee River humic acids leads to a partial fragmentation of the previously formed TiO<sub>2</sub> aggregates (at pH equal to PZC) by adsorbing on the free surface and increasing the negative charges on the surface (Loosli et al. 2013).

### **2.7 Separation of TiO<sub>2</sub> from suspension**

There are two problems: removal and reuse, which limit the industrial application of TiO<sub>2</sub> suspensions. In order to deal with these problems and spread the use of TiO<sub>2</sub>, several novel technologies have been developed. Two attempts seem to be most promising: membrane filtration and immobilization.

#### **2.7.1 Membrane filtration**

In recent years, hybrid processes based on membranes (reverse osmosis, nanofiltration, ultrafiltration and microfiltration) and photocatalysis have been extensively used to elimination and recycle the powder TiO<sub>2</sub> (Jiang et al. 2010, Mozia 2010, Mozia et al. 2010). When the catalyst NPs are in suspension, however, membrane fouling is observed in case of microfiltration and ultrafiltration membranes. Moreover, the catalyst NPs can abrade and easily pass through the membranes, and thus decrease the permeate quality (Ziegmann et al. 2010). In contrast to the traditional pressure-driven membrane techniques, Mozia (Mozia et al. 2005) described a novel possibility of coupling photocatalysis and membrane distillation for the degradation of organic pollutants in aquatic solution, which reduced fouling significantly. It was also found that the addition of TiO<sub>2</sub> did not affect the distillate flux, regardless of the catalyst concentration applied.

### 2.7.2 Immobilization of TiO<sub>2</sub>

Simultaneously, some efforts have been devoted to immobilizing TiO<sub>2</sub> NPs on a variety of matrices, such as glass (Daneshvar et al. 2005), pumice beads (Hosseini et al. 2007, Rao et al. 2003), stainless steel plate (Chen and Dionysiou 2005), and polymers (Liu et al. 2010a).

For industrial applications, the catalyst is always expected to be efficient and recyclable for long term use. Although, the immobilized TiO<sub>2</sub> showed good mechanical stabilities with efficient long-term stabilities, the photocatalytic activity is far away from that of a TiO<sub>2</sub> suspension (Doll and Frimmel 2004a, Kwon et al. 2006).

The adherences between matrix and TiO<sub>2</sub> particles are focused on physical adsorption (Hosseini et al. 2007) and electrostatic interaction (Matsuzawa et al. 2008), hydrogen bond interaction (Zhang et al. 2011) and chemical bond interaction (Huang et al. 2006). Among these interactions, chemical bond formation is considered to be the best way to fasten the TiO<sub>2</sub> nanoparticles onto the matrix. Therefore, effective immobilization of TiO<sub>2</sub> nanoparticles through chemical bond formation and keeping high photocatalytic activity in practical use has become an exciting and imperative challenge.

PVA, a hydrophilic polymer with good film-forming ability at low cost, possesses hydroxyl groups or carboxyl groups on the molecular chains and has been used to form chemical bonds with the hydroxyl groups on the surface of inorganic nanoparticles like nano SiO<sub>2</sub> and nano TiO<sub>2</sub> (Yang et al. 2008). This can be attributed to the Ti-O-C chemical bonds between TiO<sub>2</sub> nanoparticles and the PVA matrix, which make it difficult for the TiO<sub>2</sub> NPs to lose from the hybrid films (Lei et al. 2012). The PVA/TiO<sub>2</sub> composite is mostly used in film science and food package science (Ahmadpoor et al. 2013, Liu et al. 2012). Nowadays, this novel immobilization technology of TiO<sub>2</sub> NPs in a PVA matrix is reported to be a promising method with high photocatalytic activity for multi-cycle use. Some tentative investigations have been done and the results have opened a door of the application of TiO<sub>2</sub> catalysts in wastewater treatment industry (Abd El-Rehim et al. 2012, Song et al. 2014, Wang et al. 2009).

### 3 Materials and methods

#### 3.1 Reagents and materials

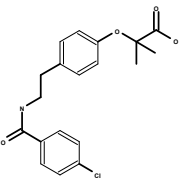
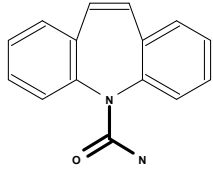
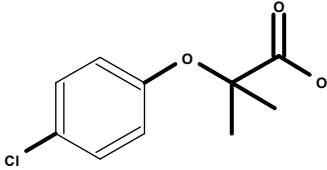
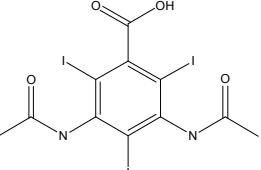
All chemicals used were analytical grade, and they were used without further purification (Table 3.1 and 3.2).

**Table 3.1 Chemical list**

Chemical	Formula	Grade	Source
Alginic acid sodium	$(C_6H_8O_6)_n$	p.a.	Sigma-Aldrich
Bezafibrate	$C_{19}H_{20}ClNO_4$	p.a.	Sigma-Aldrich
Bovine serum albumin	--	$\geq 98\%$	Sigma-Aldrich
Calcium chloride	$CaCl_2$	$>94\%$	Carl Roth
Carbamazepine	$C_{15}H_{12}N_2O$	p.a.	Sigma-Aldrich
Chloroplatinic Acid Hexahydrate	$H_2PtCl_6 \cdot 6H_2O$	p.a.	Alfa Aesar
Clofibric acid	$C_{10}H_{11}ClO_3$	p.a.	Sigma-Aldrich
Copper chloride	$CuCl_2 \cdot 2H_2O$	p.a.	Merck
Diatrizoate	$C_{11}H_9I_3N_2O_4$	99%	Sigma-Aldrich
Ferric chloride	$FeCl_3$	98%	Sigma-Aldrich
Hydrogen chloride	HCl	40%	Merck
P25	$TiO_2$		Degussa
Polyvinyl alcohol	$(C_2H_4O)_x$	98%	Sigma-Aldrich
Potassium chloride	KCl	p.a.	Merck
Porous glass beads		4 mm	Carl Roth
Pumice beads		2 ~ 5 mm	Sigma-Aldrich
Silver nitrate	$AgNO_3$	98%	Merck
Sodium chloride	NaCl	p.a.	Carl Roth
Sodium dodecylbenzene sulfonate	$C_{18}H_{29}NaO_3S$	97%	Sigma-Aldrich
Sodium hydrogen carbonate	$NaHCO_3$	98%	Sigma-Aldrich

Sodium hydroxide	NaOH	p.a.	Merck
Zinc chloride	ZnCl <sub>2</sub>	97%	Sigma-Aldrich
$\alpha$ -amylase	--	21 mg mL <sup>-1</sup>	Sigma-Aldrich

Table 3.2 Chemical structure of the pharmaceutically active compounds

Compound	Formula	Chemical structure
Bezafibrate	C <sub>19</sub> H <sub>20</sub> ClNO <sub>4</sub>	
Carbamazepine	C <sub>15</sub> H <sub>12</sub> N <sub>2</sub> O	
Clofibric acid	C <sub>10</sub> H <sub>11</sub> ClO <sub>3</sub>	
Diatrizoate	C <sub>11</sub> H <sub>9</sub> I <sub>3</sub> N <sub>2</sub> O <sub>4</sub>	

NOM source, HO24 (Hohloh Lake, 24<sup>th</sup> sampling,  $\rho_0(\text{DOC}) = 16.5 \text{ mg L}^{-1}$ ), was taken as humic-rich water from a bog lake (Hohloh Lake, Black Forest, Germany). This bog lake water has been extensively used as a reference material to study the characteristics and behavior of aquatic NOM (Frimmel 2002). All the solutions and suspensions were made up by ultrapure water (Milli-Q water, 18.2 M $\Omega$  cm). Hohloh Lake fulvic acid (HO10FA) was isolated by using XAD-8 material and a cation exchange resin (Abbt-Braun et al. 1991).

## **3.2 Analytical methods**

### **3.2.1 Thermal chemical oxidation with carbon dioxide detection**

Quantification of dissolved organic carbon (DOC) was performed by a thermal chemical method using a Total Organic Carbon (TOC) Shimadzu TOC-V CSE analyzer. Briefly, the samples were filtered through previously rinsed 0.45  $\mu\text{m}$  membrane filters and injected into the TOC analyzer using an automatic sampler. In the TOC analyzer, the samples are first acidified with phosphoric acid to shift the equilibrium for inorganic carbon from  $\text{CO}_3^{2-}$  and  $\text{HCO}_3^-$  to  $\text{CO}_2$ , which is removed by vacuum. Then the samples are UV-irradiated (185 and 254 nm) in the presence of an oxidizing agent ( $(\text{NH}_4)_2\text{S}_2\text{O}_8$ ) to fully oxidize the DOC to carbon dioxide, water and inorganic acids. The formed  $\text{CO}_2$  is quantified through electrical conductivity after separation with a semipermeable membrane.

### **3.2.2 Size exclusion chromatography with dissolved organic carbon and ultraviolet detection (SEC-DOC and SEC-UV)**

Size exclusion chromatograms (SEC-DOC and SEC-UV<sub>254</sub> system) were used according to Huber and Frimmel (Huber and Frimmel 1991). The chromatographic retention times were inversely correlated to the molecular size of the organic matter which was detected with a flow through cell and an online  $\text{CO}_2$  detector for UV-photolysed OC. The chromatographic column (manufacturer Grom.) was packed with Toyopearl HW 50S resin (Tosoh Corp., Japan) and a phosphate eluent ( $1.5 \text{ g L}^{-1} \text{ Na}_2\text{HPO}_4 \cdot 2\text{H}_2\text{O} + 2.5 \text{ g L}^{-1} \text{ KH}_2\text{PO}_4$ ; flow rate of  $1 \text{ mL min}^{-1}$ ) was used as mobile phase. The column length was 250 mm and 20 mm inner diameter (Novogrom columns, Alltech Grom, Germany). Samples were diluted 1:5 prior to analysis. The injection volume was 1 mL and the DOC of each sample was calculated on the basis of an external calibration using potassium hydrogen phthalate.



### 3.2.3 High performance liquid chromatography (HPLC)

The concentration of BZF, CBZ, CA and DA were measured by high performance liquid chromatography (HPLC) using an HP 1100 HPLC system (column RP 18e, 5 $\mu$ m; mobile phase acetonitrile : water of 60 : 40;  $\dot{V} = 1 \text{ mL min}^{-1}$ ) with detection at  $\lambda = 230 \text{ nm}$ , 280 nm and 254 nm by a UV detector for CBZ, CA, BZF and DA respectively. The samples were filtered through 0.45  $\mu$ m polycarbonate membrane filters (Millipore, Ireland) prior to analysis.

### 3.2.4 X-Ray diffraction (XRD)

To examine the structural characteristics of the prepared Pt/TiO<sub>2</sub> samples, the crystallinities of the particles were analyzed by XRD analyses using a Bruker AXS D8 diffractometer using Cu-K $\alpha$  radiation (1.5418 $\text{\AA}$  wavelength), a beam voltage of 45 kV and a current of 40 mA. The sample scans were done with a diffraction angle range  $2\theta = 20$  to 80 $^\circ$ . (The measurement was performed in the Institute of Functional Interfaces, KIT).

### 3.2.5 Scanning electron microscopy (SEM)

Scanning electron microscope (SEM, JSM-7001) was used to characterize the original PVA film, PVA/TiO<sub>2</sub> film and irradiated PVA/TiO<sub>2</sub> film. For the irradiated PVA/TiO<sub>2</sub> film, the prepared film was immersed into ultrapure water and irradiated by using a Solar UV Simulator (Oriel Corp., Stratfort, CT, USA) with additional WG 295 filters (6 mm, Schott Glaswerke, Germany) for 24 h. All film samples were dry and sputtered with a thin layer of platinum for SEM analysis. (The measurement was performed in the Laboratory for Electron Microscopy, KIT).

### 3.2.6 Transmission electron microscopy (TEM)

The morphology of bare TiO<sub>2</sub>, Pt/TiO<sub>2</sub> and TiO<sub>2</sub> aggregation were investigated by

Transmission electron microscopy (TEM) and scanning transmission electron microscopy (STEM). TEM and STEM analyses were performed using a Philips CM200 FEG/ST and an FEI Titan<sup>3</sup> 80 – 300 microscope operated at 200 and 300 keV, respectively. High-angle annular dark-field (HAADF) STEM images were taken to directly visualize different phase regions by exploiting the chemical sensitivity (atomic-number contrast<sup>30 – 32</sup>) of this imaging mode. (The measurement was performed in the Laboratory for Electron Microscopy, KIT).

#### **3.2.7 Fourier transform infrared spectroscopy (FTIR)**

The chemical structure and interaction of PVA and TiO<sub>2</sub> nanoparticles were confirmed by using attenuated total reflection Fourier transform infrared spectroscopy (ATR-FTIR). FTIR spectra of samples were obtained by a Bruker Tensor 27 Fourier transform IR spectrometer (Bruker Optik GmbH, Ettlingen, Germany) with a Bruker Platinum ATR cell. The cell was equipped with an ATR crystal made from diamond, onto which the samples were pressed directly. A total of 32 scans in the 4000 to 400 cm<sup>-1</sup> spectral range were recorded with a scan velocity of 10 kHz and a spectral resolution of 4 cm<sup>-1</sup>. The reference spectra were acquired with the unloaded diamond crystal. (The measurement was performed in the Institute of Functional Interfaces, KIT).

#### **3.2.8 Dynamic light scattering (DLS)**

A Zetasizer Nano ZS (Malvern Instruments Ltd.) was used to determine the zeta potential as well as the size distribution of NPs at a suspension concentration of 20 mg L<sup>-1</sup> by dynamic light scattering (DLS).

For the size distribution measurement, a 1.5 mL sample was introduced into an acrylic disposable cuvette (SARSTEDT AG & Co., Germany) for DLS measurement as soon as the samples were prepared. All DLS measurements were conducted at 25 °C. Zeta potential determination for each sample was measured 3 times after size distribution measurement. The pH values were adjusted by adding HCl (0.1 M) and NaOH (0.1 M).

### **3.2.9 Ion exchange chromatography (IC)**

Ion chromatography (IC) (790 Personal IC, Metrohm, Switzerland) analyses were performed using a Metrosep A Supp 5 (100 × 4.0mm, 5µm packing material) analytical column and an electronic conductivity detector.

### **3.2.10 Inductively Coupled Plasma—Optical Emission Spectroscopy (ICP-OES)**

Measurements of total metal concentrations were performed by means of inductively coupled plasma optical emission spectroscopy (ICP-OES) using a Vista-Pro CCD simultaneous ICP-OES spectrometer (Varian). The wavelength used for Ti was 336.122 nm.

### **3.2.11 Adsorbed organic halogens (AOX)**

The AOX measurements were done by an ECS 1200 (Euroglas Analytical Instrument). For the determination of AOX 50 mg activated carbon were added to each sample according to DIN 38409-14 (1985). After shaking for 1 h the samples were filtered. The covered filters containing the loaded activated carbon were inserted into the AOX-furnace. The AOX concentration was measured by using a pyrolytic microcoulometer according to DIN 38409-14 (1985). The relative standard deviation of the concentration values was <8%.

### **3.2.12 Differential scanning calorimetry (DSC)**

Differential scanning calorimetry (DSC) spectra of PVA and hybrid PVA/TiO<sub>2</sub> film have been obtained using a Q200 set up (TA instruments, Eschborn, Germany) instrument. Measurements were performed over the temperature range of 25 to 250°C at the heating rate of 10 °C/min. (The measurement was performed in the Institute for Technical Chemistry and Polymer Chemistry, KIT).

### **3.3 Experimental equipment and procedure**

#### **3.3.1 For Chapter 4**

##### **3.3.1.1 Catalyst preparation**

Pt modified TiO<sub>2</sub> (Pt/TiO<sub>2</sub>) was prepared by using photodeposition. A calculated volume (1.1 mL) of an aqueous solution of hexachloroplatinic (IV) acid hexahydrate (c (H<sub>2</sub>PtCl<sub>6</sub>·6H<sub>2</sub>O) = 40 mM) was added to an aqueous suspension of TiO<sub>2</sub> (5 weight% (wt.%)), followed by addition of methanol (at a 500:1 methanol to metal molar ratio). The suspension was irradiated with a 1000 W Xe short-arc lamp for 6 h under continuous stirring. Afterwards, the solutions were filtered and the solid samples were washed twice with deionized water, centrifuged, calcined at a temperature of 450 °C for 2 h and grinded carefully.

##### **3.3.1.2 Sample preparation**

All the samples were prepared by dissolving CBZ and CA in ultrapure water. The samples were stirred for several hours and placed in an ultrasonic bath for 15 min to ensure complete dissolution. For the irradiation experiments the catalyst suspension was freshly prepared by suspending Pt/TiO<sub>2</sub> in ultrapure water and ultrasonification for 5 min. In order to investigate the influence of oxygen addition on the PhAC degradation, pure O<sub>2</sub>, air and N<sub>2</sub> were purged for 20 min prior to the photocatalytic reactions. The gas flow was adjusted to 0.3 L min<sup>-1</sup> and remained constant in all the experiments. The oxygen concentrations of each solution were stable during the whole reaction process by continuously purging of the respective gases. The DO concentrations were checked by a DO meter (WTW, HQ30D) during the reactions to confirm a constant oxygen concentration.

##### **3.3.1.3 Irradiation experiments**

Two reactors were used to compare the influences of reactor geometry and operation

conditions. The samples used for photocatalytic degradation, shown in Section 4.2, were irradiated by using a Solar UV Simulator (Oriel Corp., Stratfort, CT, USA) with additional WG 295 filters (6 mm, Schott Glaswerke, Germany). The scheme and a detailed description of the solar simulator used are given by Doll et al. (Doll and Frimmel 2003b). The radiation source was a 1000-W Xe short-arc lamp, which was turned on at least 30 min prior to start of the irradiation experiments in order to insure a constant photon flux. The photon flow in the UV range ( $290 < \lambda < 400$  nm) of the solar UV simulator estimated by this method was  $0.1 \mu\text{E s}^{-1}$ . All the samples were stirred, open to the atmosphere and irradiated simultaneously from above by a homogenous light field. The individual sample volume was 25 mL, and the catalyst concentration was  $1 \text{ g L}^{-1}$ . During the photoreaction, samples for analysis were taken at different time intervals. Before irradiation, adsorption was allowed to take place for at least 30 min.

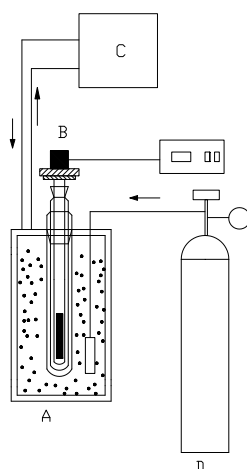


**Fig. 3.1 Schematic of irradiation reactor: A, reactor; B, UV lamp; C, cooling system; D, air/O<sub>2</sub>/N<sub>2</sub>.**

The samples used for photocatalytic degradation, shown in Section 4.3, were irradiated using a lab-batch scale glass cylinder (Fig. 3.1). The radiation source was a low-pressure mercury ozone free lamp (15 W, Katadyn GmbH, Germany), equipped with the doped quartz to cut off the VUV irradiation, had monochromatic spectrum at  $\lambda = 254$  nm and  $4 \mu\text{E s}^{-1}$  irradiance. The lamp was turned on at least 30 min prior to start of the irradiation reaction in order to insure a constant photon flux. The irradiated

sample volume was 130 mL, and the catalyst concentration was  $0.1 \text{ g L}^{-1}$ . During the photoreaction, samples ( $V = 3 \text{ mL}$ ) were collected at different time intervals for analysis. Before irradiation, adsorption was allowed to take place for at least 30 min in the dark.

## **3.3.2 For Chapter 5**

### **3.3.2.1 Sample preparation**

All the samples were prepared by dissolving DA in ultrapure water. The samples were stirred for several hours and placed in an ultrasonic bath for 15 min to ensure complete dissolution. For the irradiation experiments the catalyst suspension was freshly prepared by suspending Pt/TiO<sub>2</sub> in ultrapure water and ultrasonification for 5 min. In order to investigate the effect of DO on the DA degradation, high ( $32 \text{ mg L}^{-1}$ ), medium ( $8 \text{ mg L}^{-1}$ ) and low ( $< 0.4 \text{ mg L}^{-1}$ ) DO level solutions were prepared by purging pure O<sub>2</sub>, air and N<sub>2</sub> for 20 min prior to the photocatalytic reactions. The oxygen concentrations of each solution were maintained during the whole reaction process by continuously purging of the respective gases. The DO concentrations were checked by a DO meter during the reactions to confirm a constant oxygen concentration.

### **3.3.2.2 Irradiation Experiments**

The irradiation procedure as well as a lab-batch scale glass cylinder (Fig. 3.1) are described in Section 3.3.1.3.

## **3.3.3 For Chapter 6**

### **3.3.3.1 Sample preparation**

TiO<sub>2</sub> NPs stock suspensions of  $1 \text{ g L}^{-1}$  were prepared by dispersing TiO<sub>2</sub> NPs in ultrapure water (Milli-Q water,  $18.2 \text{ M}\Omega \text{ cm}$ ) through sonication for 1 h at 250 W. The stock suspension was freshly prepared every day.

The TiO<sub>2</sub> NPs suspensions in different water matrices were prepared according to

the following steps. 4.9 mL DOM sample was placed into a glass cuvette, 0.1 mL dispersed stock solution was quickly transferred into the cuvette by using a pipette. The final concentration of nanomaterial dispersed in synthetic wastewater was 20 mg L<sup>-1</sup>. The DOC concentration in each sample was fixed at 1 mg L<sup>-1</sup>. Then the pH values were adjusted by adding HCl (0.1 M, Merck) and NaOH (0.1 M, Merck).

### 3.3.3.2 Determination of aggregation kinetics

Kinetic size measurement was carried out immediately after the suspensions were prepared. Each measurement lasted for 100 s. Each sample was measured continuously for 30 runs. The aggregation rates are expressed as the slope  $\Delta D/\Delta t$  (nm s<sup>-1</sup>), where  $\Delta D$  means the increase in the TiO<sub>2</sub> NPs diameters (nm) and  $\Delta t$  denotes the time range (s). All the size data were number mean value according to the literature (Li and Sun 2011, Romanello and de Cortalezzi 2013). Final hydrodynamic diameter was estimated as an average of the last 6 measurements taken.

### 3.3.3.3 Adsorption experiment

A batch adsorption test was performed to estimate adsorption of different DOM on the TiO<sub>2</sub> NPs' surface. An aluminum paper covered Erlenmeyer flask contained 20 mg TiO<sub>2</sub> NPs sorbent was introduced, where DOC concentration range from each DOM resource was from 2 to 80 mg L<sup>-1</sup>. The sample was shaken for 24 h at 300 rpm in the room temperature. The pH of all samples was adjusted to  $8.6 \pm 0.1$ . DOC analysis was performed using a Shimadzu TOC-V CSE analyzer with inorganic carbon remover and automatic sampler. The samples were filtered through 0.45  $\mu$ m polycarbonate membrane filters (Millipore, Ireland) prior to analysis.

### **3.3.4 For Chapter 7**

#### **3.3.4.1 3.3.4.1 Preparation of PVA/TiO<sub>2</sub> hybrid films, pumice/TiO<sub>2</sub> and porous glass bead/TiO<sub>2</sub> composites**

PVA was added to ultrapure water, followed by ultrasonic treatment at 90°C for 3 h. TiO<sub>2</sub> nanoparticles were dispersed in ultrapure water and ultrasonification for 1 h. The two solutions were mixed under ultrasonic agitation at room temperature for 1 h. Subsequently, the solution mixture was cast onto clean glass plates to give 0.5 to 2 cm thick layers. The solution was evaporated overnight at 60°C. Then, the hybrid films were heat-treated under vacuum at 120°C for 2 h. The weight ratio of PVA to TiO<sub>2</sub> was 9:1.

The pumice/TiO<sub>2</sub> composites and porous glass bead/TiO<sub>2</sub> composites were prepared by a doping method (Rao et al. 2003). The pumice and porous glass beads were calcined at 450°C for 2 h. Then, the pumice and porous glass beads were impregnated with a sonicated suspension of TiO<sub>2</sub> (100 g L<sup>-1</sup>), dried, washed to eliminate the excess of TiO<sub>2</sub>. The generated composites were calcined at 450°C for 2 h. The weight of TiO<sub>2</sub> retained was 50 to 70 g m<sup>-2</sup>.

#### **3.3.4.2 Sample preparation**

All the samples for photocatalytic treatment were prepared by dissolving BZF in ultrapure water. The samples were stirred for several hours and placed in an ultrasonic bath for 15 min to ensure complete dissolution. The concentration of BZF solution was 10 mg L<sup>-1</sup>. For the irradiation experiments the PVA/TiO<sub>2</sub> film was cut into small pieces (3 to 4 mm<sup>2</sup>) to increase the mobility.

#### **3.3.4.3 Irradiation experiments**

The irradiation procedure as well as a Solar UV Simulator (Oriel Corp., Stratford, CT, USA) with additional WG 295 filters (6 mm, Schott Glaswerke, Germany) are described in Section 3.3.1.3.



## **4 Photocatalytic degradation of carbamazepine (CBZ) and clofibric acid (CA) using Pt/TiO<sub>2</sub> under environmentally relevant conditions**

Photocatalysis is an efficient and green advanced oxidation process (AOP). It has been introduced to water and wastewater treatment for decades (Chong and Jin 2012, Katsumata et al. 2009, Miranda-García et al. 2011). However, the efficiency for the degradation of pollutants is strongly dependent on the reaction conditions, e.g. oxygen content, temperature, pH value, organic matter, inorganic elements and dissolved metal ions (Asahi 2001, Brezova et al. 1995, Chong et al. 2010, Schwegmann et al. 2013, Valencia et al. 2012).

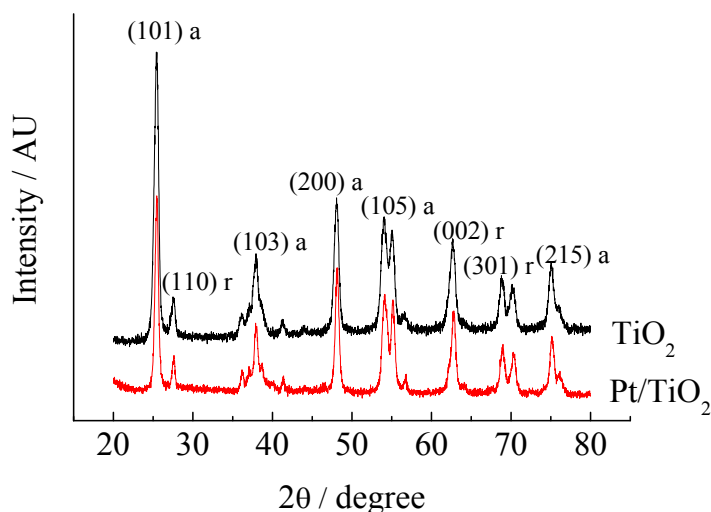
In this Chapter, we provided a characterization of the photocatalytic degradation of PhACs under environmentally relevant conditions, investigating the influence of pH values, NOM, metal ions etc. The applicability of photocatalysis in pharmaceutical wastewater treatment was evaluated as well.

Two PhACs, carbamazepine (CBZ) and clofibric acid (CA), were chosen as model compounds due to their persistency, environmental risk and research frequency. Pt modified TiO<sub>2</sub> (Pt/TiO<sub>2</sub>) was used in this work, as a representative new photocatalyst due to its obviously higher photocatalytic activity (Lee and Choi 2004, Miller et al. 2010) and easy availability (Nomikos et al. 2014).

### **4.1 Characterization of Pt/TiO<sub>2</sub>**

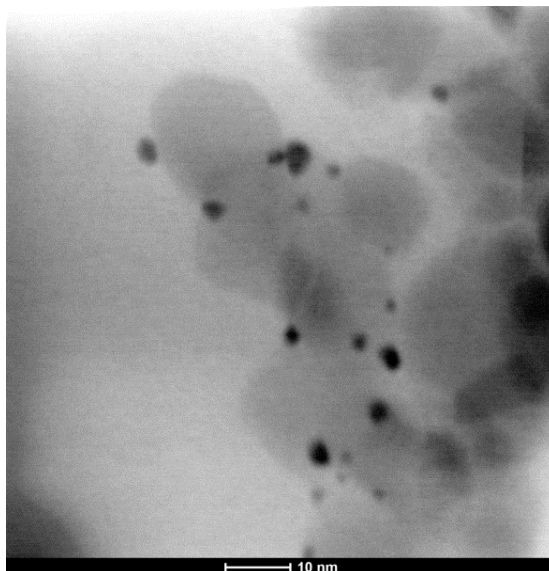
The X-ray diffraction patterns of TiO<sub>2</sub> and Pt/TiO<sub>2</sub> are shown in Fig. 4.1. The major phase of the TiO<sub>2</sub> is anatase (a) with typical diffraction peaks at 25.4°, 37.8°, 48.1°, 53.9° and 75.1° (2θ), whereas rutile (r) exists as the minor phase with diffraction peaks at 27.7°, 62.7° and 69.1° (2θ). The diffraction patterns of Pt/TiO<sub>2</sub> samples were almost the same as that of

the TiO<sub>2</sub>, indicating that the crystallite of the TiO<sub>2</sub> were not changed by the modification process. For the Pt/TiO<sub>2</sub> sample, no significant peaks related to the presence of Pt were detected. This was expected due to the high dispersion of the relatively low amount of fine Pt nanoparticles on the TiO<sub>2</sub> surface (Zielinska-Jurek and Zaleska 2014). However, the Pt nanodeposits were obviously observed in TEM micrographs (Fig. 4.2). It distributed uniformly on the TiO<sub>2</sub> surface with the Pt diameter predominantly around 2 nm.



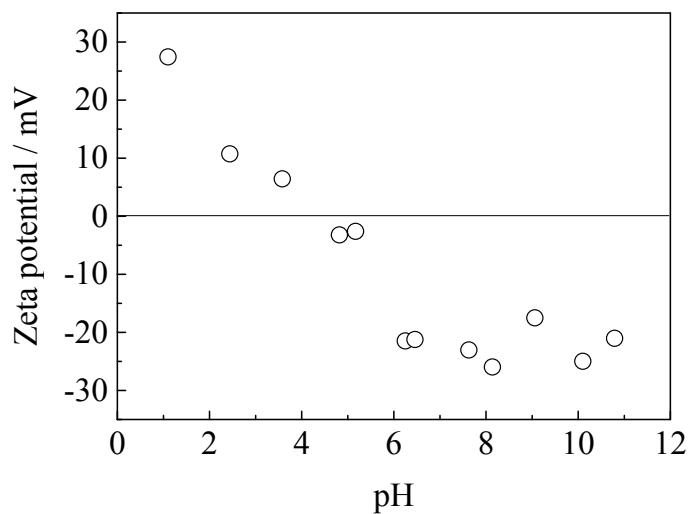
**Fig. 4.1** XRD patterns of TiO<sub>2</sub> and Pt/TiO<sub>2</sub>.

Fig. 4.3 displays the zeta potentials of the Pt/TiO<sub>2</sub> as a function of the solution pH value. The Pt/TiO<sub>2</sub> particles exhibit an isoelectric point (PZC) around pH 4 in KCl solution (10 mM) which is much lower than the reported value for pure TiO<sub>2</sub> that shows an isoelectric point at 6 < pH < 6.5 (Schwegmann et al. 2013). Shifting of pH to a lower value would be caused by the introduction of Pt which results in the change of the electronic environment of the titanium lattice and the presence of hydroxyl groups on the surface of the TiO<sub>2</sub> nanoparticles (Hu et al. 2003). The obtained results indicate that the Pt/TiO<sub>2</sub> nanoparticles dispersed well in the solution at the experimental pH value (pH = 6.9).



**Fig. 4.2** TEM image of Pt/TiO<sub>2</sub>.

The photocatalytic activity of Pt/TiO<sub>2</sub> in aqueous solution with UV irradiation is shown in Table 4.1. As expected, the pseudo first order rate constants of CBZ and CA in the presence of the Pt/TiO<sub>2</sub> were higher than those for pure TiO<sub>2</sub>, owing to the lower recombination rate of photogenerated electrons (e<sup>-</sup>) and holes (h<sup>+</sup>) in Pt/TiO<sub>2</sub>. It is also attractive to assume that this is supported by the good dispersion of Pt/TiO<sub>2</sub> nanoparticles under the experiment conditions.



**Fig. 4.3** Zeta potential of Pt/TiO<sub>2</sub> at different pH values in KCl solution (10 mM).

4 Photocatalytic degradation of carbamazepine (CBZ) and clofibric acid (CA) using Pt/TiO<sub>2</sub> under environmentally relevant conditions

**Table 4.1 Pseudo first order photocatalytic reaction rate constant (*k*) for the photodegradation of CBZ and CA under different reaction conditions ( $\rho(\text{TiO}_2) = 1 \text{ g L}^{-1}$ ,  $(\text{Pt/TiO}_2) = 1 \text{ g L}^{-1}$ ,  $\text{pH} = 6.9$ )**

Catalyst	Carbamazepine	Clofibric acid
	<i>k</i> (min <sup>-1</sup> )	<i>k</i> (min <sup>-1</sup> )
No catalyst	0	0.001
TiO <sub>2</sub>	0.016	0.036
Pt/TiO <sub>2</sub>	0.028	0.077

## 4.2 Effect of process conditions and water matrices on the CBZ and CA photocatalytic degradation using a Solar light Simulator

Further batch experiments under different process conditions (i.e., solution pH and dissolved ions) were performed for the purpose of a systematic study and the obtained overall results are summarized in Table 4.2a and 4.2b. Our results assume the photocatalytic degradation of CBZ and CA under different operation conditions are expressed as pseudo-first-order kinetics.

**Table 4.2a Photocatalytic degradation rate constants (*k*) of CBZ in different water matrices**

Photocatalyst loading g L <sup>-1</sup>	pH	HCO <sub>3</sub> <sup>-</sup> μM	Fe(III) μM	Zn <sup>2+</sup> μM	Ca <sup>2+</sup> μM	NOM (DOC) mg L <sup>-1</sup>	<i>k</i> min <sup>-1</sup>	<i>R</i> <sup>2</sup>
1 Effect of pH								
1	2.5	0	0	0	0	0	0.014	0.991
1	6.9	0	0	0	0	0	0.028	0.989
1	12.7	0	0	0	0	0	0.035	0.998
2 Effect of HCO <sub>3</sub> <sup>-</sup>								
1	6.9	0	0	0	0	0	0.028	0.989
1	6.9	10	0	0	0	0	0.012	0.997
1	6.9	100	0	0	0	0	0.007	0.998
3 Effect of Fe(III)								
1	6.9	0	0	0	0	0	0.030	0.989
1	6.9	0	10	0	0	0	0.029	0.997
1	6.9	0	50	0	0	0	0.018	0.998
1	6.9	0	100	0	0	0	0.015	0.991

4 Photocatalytic degradation of carbamazepine (CBZ) and clofibric acid (CA) using Pt/TiO<sub>2</sub> under environmentally relevant conditions

4 Effect of Zn <sup>2+</sup>									
1	6.9	0	0	0	0	0	0.030	0.989	
1	6.9	0	0	10	0	0	0.029	0.969	
1	6.9	0	0	50	0	0	0.018	0.991	
1	6.9	0	0	100	0	0	0.016	0.996	
5 Effect of Ca <sup>2+</sup>									
1	6.9	0	0	0	0	0	0.030	0.989	
1	6.9	0	0	0	10	0	0.023	0.997	
1	6.9	0	0	0	50	0	0.017	0.966	
1	6.9	0	0	0	100	0	0.011	0.931	
6 Effect of NOM									
1	6.9	0	0	0	0	0	0.030	0.989	
1	6.9	0	0	0	0	0.4	0.012	0.998	
1	6.9	0	0	0	0	0.8	0.013	0.972	
1	6.9	0	0	0	0	1.7	0.012	0.998	
1	6.9	0	0	0	0	6.6	0.007	0.913	
1	6.9	0	0	0	0	16.5	0.002	0.904	
7 Effect of NOM and metal ions combination									
1	6.9	0	10	0	0	1.7	0.016	0.981	
1	6.9	0	0	10	0	1.7	0.017	0.992	
1	6.9	0	0	0	10	1.7	0.020	0.869	
1	6.9	0	10	0	0	16.5	0.006	0.892	
1	6.9	0	0	10	0	16.5	0.006	0.895	
1	6.9	0	0	0	10	16.5	0.004	0.819	

Table 4.2b Photocatalytic degradation rate constants (*k*) of the CA in different water matrices

Photocatalyst loading g L <sup>-1</sup>	pH	HCO <sub>3</sub> <sup>-</sup> μM	Fe(III) μM	Zn <sup>2+</sup> μM	Ca <sup>2+</sup> μM	NOM (DOC) mg L <sup>-1</sup>	<i>k</i> min <sup>-1</sup>	<i>R</i> <sup>2</sup>
1 Effect of pH								
1	2.5	0	0	0	0	0	0.089	0.981
1	6.9	0	0	0	0	0	0.077	0.996
1	12.7	0	0	0	0	0	0.071	0.998
2 Effect of HCO <sub>3</sub> <sup>-</sup>								
1	6.9	0	0	0	0	0	0.077	0.996
1	6.9	10	0	0	0	0	0.054	0.997
1	6.9	100	0	0	0	0	0.029	0.978
3 Effect of Fe(III)								
1	6.9	0	0	0	0	0	0.077	0.996
1	6.9	0	10	0	0	0	0.095	0.999
1	6.9	0	50	0	0	0	0.104	0.978
1	6.9	0	100	0	0	0	0.168	0.997
4 Effect of Zn <sup>2+</sup>								
1	6.9	0	0	0	0	0	0.077	0.996

4 Photocatalytic degradation of carbamazepine (CBZ) and clofibric acid (CA) using Pt/TiO<sub>2</sub> under environmentally relevant conditions

1	6.9	0	0	10	0	0	0.142	0.969
1	6.9	0	0	50	0	0	0.210	0.981
1	6.9	0	0	100	0	0	0.256	0.996
5 Effect of Ca <sup>2+</sup>								
1	6.9	0	0	0	0	0	0.077	0.996
1	6.9	0	0	0	10	0	0.147	0.987
1	6.9	0	0	0	50	0	0.059	0.966
1	6.9	0	0	0	100	0	0.031	0.961
6 Effect of NOM								
1	6.9	0	0	0	0	0	0.077	0.996
1	6.9	0	0	0	0	0.4	0.051	0.998
1	6.9	0	0	0	0	0.8	0.038	0.952
1	6.9	0	0	0	0	1.7	0.025	0.979
1	6.9	0	0	0	0	6.6	0.017	0.963
1	6.9	0	0	0	0	16.5	0.008	0.974
7 Effect of NOM and metal ions combination								
1	6.9	0	10	0	0	1.7	0.068	0.995
1	6.9	0	0	10	0	1.7	0.036	0.978
1	6.9	0	0	0	10	1.7	0.040	0.992
1	6.9	0	10	0	0	16.5	0.008	0.915
1	6.9	0	0	10	0	16.5	0.004	0.923
1	6.9	0	0	0	10	16.5	0.006	0.929

pH value is a complex parameter in photocatalysis which affects the ionization states of organic compounds and the surface charge of the catalyst as well as the formation rate of •OH and other active radicals in the reaction solution (Haroune et al. 2014, Schwegmann et al. 2013). The tested range of pH ( $2.5 \leq \text{pH} \leq 12.7$ ) covers most wastewaters and natural waters. The photocatalytic degradation of CBZ ( $\text{pK}_a = 13.9$ ), a neutral compound, is highly pH dependent. The degradation rate constant significantly increased with the increase of the pH value. At alkaline conditions, high level of hydroxide ions (OH<sup>-</sup>) induced the generation of •OH, which came from the photo-oxidation by holes forming on the Pt/TiO<sub>2</sub> surface. In case of CA, the pH value didn't contribute significantly on its photocatalytic degradation. The rate constant decreased slightly with increase of pH. At pH 6.9 and 12.7, the lower photo-degradation rate constant was most likely due to the antagonism of the higher electrostatic repulsive interaction between Pt/TiO<sub>2</sub> and the anionic CA ( $\text{pK}_a = 3.3$ ), and the excessive radical formation.

#### 4 Photocatalytic degradation of carbamazepine (CBZ) and clofibric acid (CA) using Pt/TiO<sub>2</sub> under environmentally relevant conditions

---

The dissolved metal ions present in natural and waste waters can significantly modify the photocatalytic process (Brezova et al. 1995). Fe(III), Zn<sup>2+</sup> and Ca<sup>2+</sup> were chosen to investigate their influences on the photocatalytic degradation of CBZ and CA for their high concentration in natural water (Obiefuna and Orazulike 2010) and their irregular influences in photocatalysis (Tachikawa et al. 2004). Table 4.2b shows that the photocatalytic degradation rate constant of CA exhibited an obvious increase by adding Fe(III) and Zn<sup>2+</sup> ions. The effect of adding Ca<sup>2+</sup> ions showed a more complex behavior, which increased the rate constant at low concentration slightly and lowered significantly the rate constant at high concentrations under the given condition. The enhancement of CBZ degradation due to dissolved metal ions was observed only for 10 μM Fe(III). Otherwise, the rate constant decreased in a different extent. It is known that dissolved metal ions are decent electron scavengers and can increase the photocatalytic degradation (Brezova et al. 1995). However, from the results so far it can be deduced that the contribution of organic pollutants is higher. It is suggested that metal ions will combine electron/hole pairs with different behaviors according to the charge of the targeted compounds: CA carries anionic charges that help the connection of the metal ions and the electron/hole pairs due to their complementary charges, while the neutral CBZ has a competitive connection with the metal ions. The significant decrease of the rate constant in the presence of Ca<sup>2+</sup> might result from the aggregation of the catalyst caused by dissolved Ca<sup>2+</sup> (Romanello and de Cortalezzi 2013), and consequently the decrease of the surface area and the active sites.

Bicarbonate, a common ionic constituent of natural waters, inhibited the photocatalytic degradation of CBZ and CA. The addition of 10 mM and 100 mM HCO<sub>3</sub><sup>-</sup> lowered the observed rate constants by 57% and 75% for CBZ and 30% and 62% for CA, respectively. These results are consistent with previous reports that the dissolved carbonate species act as •OH scavengers in natural waters (Sugihara et al. 2013). A part of the observed inhibition may also be due to the competitive inhibition of CBZ as well as CA by dissolved carbonate species adsorption.

NOM is ubiquitous in natural water and plays a fundamental role in the function of

#### 4 Photocatalytic degradation of carbamazepine (CBZ) and clofibric acid (CA) using Pt/TiO<sub>2</sub> under environmentally relevant conditions

the aquatic environment. The rate constant decreased rapidly when the DOC concentration (from NOM) is up to 1.7 mg L<sup>-1</sup>, and then followed by a slight decrease (Fig. 4.4). It is evident that the presence of NOM in such concentrations suppressed the photocatalytic degradation of both target compounds due to their possible •OH scavenger behavior (Haroune et al. 2014, Sugihara et al. 2013). It suggested that when the DOC concentration (from NOM) is lower than 1.7 mg L<sup>-1</sup> all the NOM molecules were adsorbed onto the Pt/TiO<sub>2</sub> surface. With the increase of the DOC concentration (from NOM), no more NOM molecule was adsorbed onto the already totally covered Pt/TiO<sub>2</sub> surface, and therefore the deactivation rate decreased.

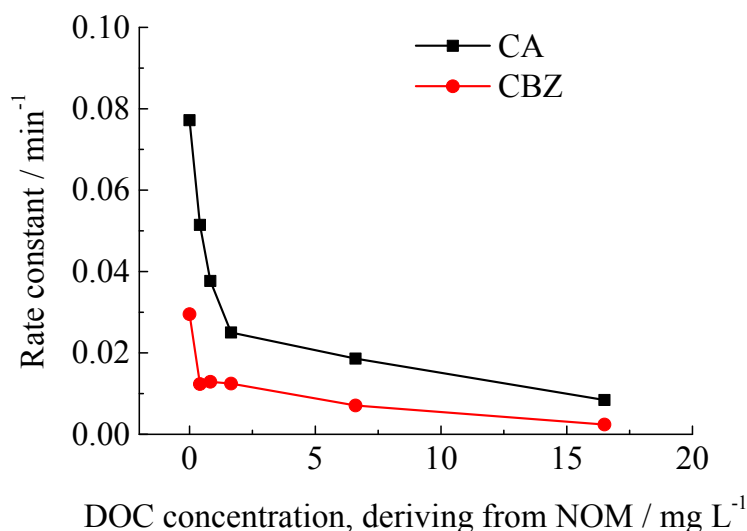


**Fig. 4.4** Photocatalytic degradation rate constant of CBZ and CA as a function of NOM (DOC) concentration in the presence of Pt/TiO<sub>2</sub> ( $\rho_0$  (PhACs) = 10 mg L<sup>-1</sup>;  $\rho$ (Pt/TiO<sub>2</sub>) = 1 g L<sup>-1</sup>; pH = 6.9).

The results demonstrate a significant inhibitory effect of adsorbed NOM, which will be critical to the design of practical treatment systems. We have already shown that NOM could vary the effect of photocatalyst according to its NOM/TiO<sub>2</sub> ratio (Drosos et al. 2015). Thus, future work examining these effects in greater detail in combination with other water quality variables (e.g. metal ions, oxygen content) are needed to develop predictive treatment models applicable to diverse natural waters.

It is evident that the NOM-metal complex can control the chemistry, fate, toxicity, and mobility of both NOM and metal ions (Borrok et al. 2007), and affect the redox



reactions subsequently. We therefore decided to test whether metal cations could affect the inhibitory effect of NOM in photocatalysis. 1.7 mg L<sup>-1</sup> and 16.5 mg L<sup>-1</sup> of DOC (from NOM) and 10 μM of metal ions were used. In case of lower DOC concentrations (from NOM), the results showed an enhancement of the photocatalytic degradation rate constant for both CBZ and CA in relation to what was observed with NOM and no cations. These results suggest that by absorption of sunlight, aqueous metal complexes can undergo a ligand to metal charge transfer, that leads to the formation of •OH radicals, which are capable of oxidizing NOM or any other organic pollutant subsequently (Brinkmann et al. 2003). In the presence of higher DOC concentration (from NOM), the added metal ions did not show any significant enhancement to balance the inhibition effect of NOM, which is mainly due to the strong deactivation effect by the adsorbed NOM.

Dissolved oxygen (DO) content is also an important parameter in natural water systems. If oxygen occurs in solution, the superoxide anion is formed on the catalyst surface with the participation of oxygen in the photocatalytic process. This ion can react with organic molecules to induce its destructive oxidation. It is already reported that the high partial pressure of oxygen strongly increases the photocatalytic degradation of pollutants (Shibuya et al. 2013). Hence, the increase of oxygen in the complex photocatalytic system is expected to react with the adsorbed NOM and lower its inhibition effect.

To test this hypothesis, we investigated the photocatalytic degradation of CBZ and CA in the presence of different DO and NOM concentrations. A new cylinder reactor (Fig. 3.1 in Section 3.3.1.3) was introduced in the following sections, and the schematics and detail information are discussed in Section 4.3.

### **4.3 Influence of oxygen concentration on the photocatalytic degradation of CBZ and CA in the presence of NOM**

Table 4.3a and 4.3b show that the degradations of CBZ and CA by direct photolysis

4 Photocatalytic degradation of carbamazepine (CBZ) and clofibric acid (CA) using Pt/TiO<sub>2</sub> under environmentally relevant conditions

(UV-C 254 nm) were inefficient compared to the photocatalytic reactions. However, the overall rate constants using the cylinder reactor (Fig. 3.1 in Section 3.3.1.3) were much higher than those obtained by the solar simulator. The increased rate constant under UV-C photolysis or photocatalysis occurs because of the higher quantum yields, the high photon adsorption (CA) at  $\lambda = 254$  nm, and the stronger absorption of titanium dioxide below 300 nm (Sun and Bolton 1996).

**Table 4.3a Photocatalytic degradation rate constants (*k*) for CBZ in the presence of various NOM (DOC) and DO concentrations**

photocatalyst loading g L <sup>-1</sup>	pH	O <sub>2</sub> mg L <sup>-1</sup>	NOM (DOC) mg L <sup>-1</sup>	<i>k</i> min <sup>-1</sup>	<i>R</i> <sup>2</sup>
0	6.9	8 (air)	0	0.004	0.931
0.1	6.9	< 0.4 (N <sub>2</sub> )	0	0.030	0.993
0.1	6.9	< 0.4 (N <sub>2</sub> )	1.7	0.009	0.977
0.1	6.9	8 (air)	0	0.047	0.999
0.1	6.9	8 (air)	1.7	0.038	0.993
0.1	6.9	32 (O <sub>2</sub> )	0	0.074	1.000
0.1	6.9	32 (O <sub>2</sub> )	1.7	0.070	0.994

**Table 4.3b Photocatalytic degradation rate constants (*k*) for CA in the presence of various NOM (DOC) and DO concentrations**

photocatalyst loading g L <sup>-1</sup>	pH	O <sub>2</sub> mg L <sup>-1</sup>	NOM (DOC) mg L <sup>-1</sup>	<i>k</i> min <sup>-1</sup>	<i>R</i> <sup>2</sup>
0	6.9	8 (air)	0	0.231	0.998
0.1	6.9	< 0.4 (N <sub>2</sub> )	0	0.431	0.998
0.1	6.9	< 0.4 (N <sub>2</sub> )	1.7	0.184	0.994
0.1	6.9	8 (air)	0	0.599	0.999
0.1	6.9	8 (air)	1.7	0.634	0.979
0.1	6.9	32 (O <sub>2</sub> )	0	0.722	0.999
0.1	6.9	32 (O <sub>2</sub> )	1.7	0.759	0.985

The degradation of CBZ and CA mixed with NOM in the presence of different DO concentrations were carried out under the different gas flow (Table 4.3a and 4.3b). The addition of NOM declined the degradation rate constant of CBZ, especially under N<sub>2</sub> purging. The rate constant decreased by 70%. However, the inhibition diminished with the increase of DO concentration. The photocatalytic degradation rate decreasing only 5%

#### 4 Photocatalytic degradation of carbamazepine (CBZ) and clofibric acid (CA) using Pt/TiO<sub>2</sub> under environmentally relevant conditions

under O<sub>2</sub> purging. A significant inhibition of NOM on the degradation of CA was only observed under N<sub>2</sub> purging (decline rate: 57%). Under air and O<sub>2</sub> purging, NOM showed a slightly enhanced degradation.

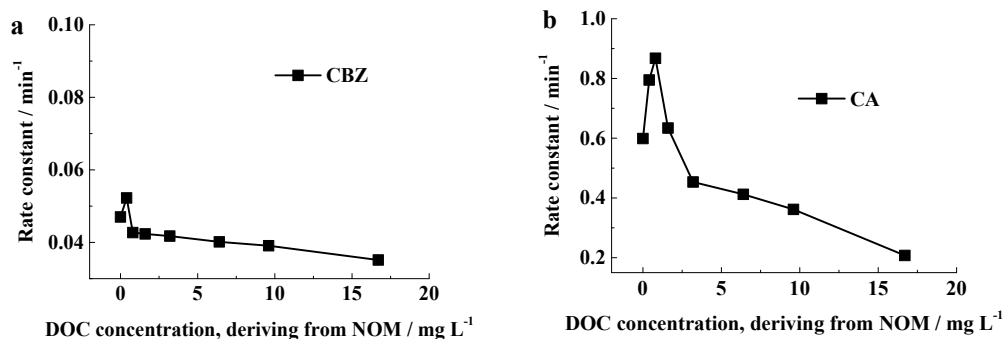


**Fig. 4.5 Photocatalytic degradation rate constant of CBZ (a) and CA (b) in the presence of various NOM (DOC) concentrations under air flow.**

Fig.4.5a and 4.5b show the rate constants for CBZ and CA in the presence of different DOC concentrations (from NOM) under air flow. With the increase of DOC concentration, the rate constants increased and then were followed by a rapid decrease until the DOC concentration was up to 1.7 mg L<sup>-1</sup>. Ultimately the rate constant reached a constant value. This behavior was also previously reported by Drosos et al. (Drosos et al. 2015). In order to characterize qualitatively the behavior of NOM during the photocatalytic process, SEC-DOC chromatograms of NOM ( $\rho_0$  (DOC) = 1.7 mg L<sup>-1</sup>) for different irradiation times under different gas flow were run (Fig. 4.6).

#### 4.4 Photocatalytic degradation of NOM under different gas flow

The SEC retention times (*tr*) were roughly assigned to three fractions (F1, F2 and F3) for the larger molecular sized humic substances, aromatic organic acids and smaller aliphatic molecules respectively (Valencia et al. 2012).

The chromatogram of NOM adsorption onto the catalyst under N<sub>2</sub> purging (Fig. 4.6a) in the dark showed the removal of entire fractions without any peak shift, but the adsorption decreased with the increase of the *tr* value according to smaller molecular size. The larger molecular sized fractions of NOM were preferentially degraded over the

#### 4 Photocatalytic degradation of carbamazepine (CBZ) and clofibric acid (CA) using Pt/TiO<sub>2</sub> under environmentally relevant conditions

irradiation time, and the main peak around  $t_r = 45$  min in F1 shifted continuously towards longer retention times. After 15 min of irradiation, there was an obvious degradation of F1-matter, accompanied by a slight increase in the F2- and F3- fraction for which the formation exceeded the rate of degradation. After 30 min of irradiation, the main peak in the F1 fraction shifted to  $t_r = 45$  min, and the F2 and F3 had reached their maximum. After 60 min of irradiation, the F2- and F3- fractions continuously decreased.

Under air purging (Fig. 4.6b), there was a lower adsorption of NOM onto the catalyst in the dark possibly because of the competition of NOM and oxygen on the adsorption sites of Pt/TiO<sub>2</sub> surface. However, the degradation rate of the larger molecular sized fractions of NOM increased significantly compared to those under the N<sub>2</sub> purging attributed to the oxidation of the radicals caused by the oxygen. Under air purging most of the F1 fraction was degraded within 10 min, and two small fractions remained in F2 and F3 (around  $t_r = 50$  min and 56 min respectively). After 30 min of irradiation, most of the higher molecular size NOM fractions were removed due to mineralization.

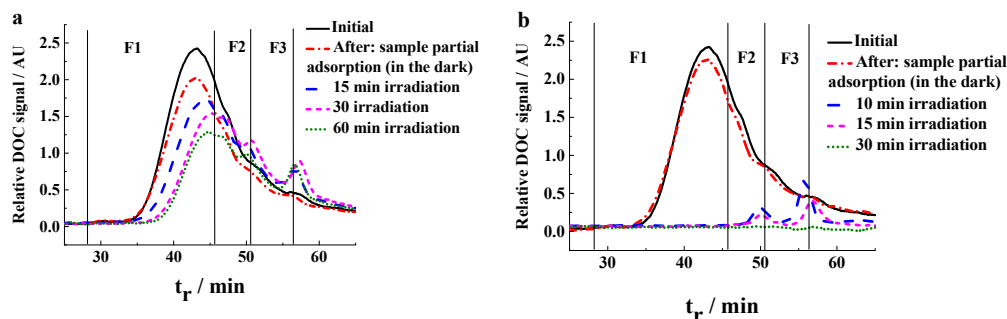


**Fig. 4.6** SEC-DOC chromatograms of NOM (HO<sub>24</sub>;  $\rho_0$  (DOC) = 16.5 mg L<sup>-1</sup>) for different photocatalytic reaction times ( $\rho(\text{Pt}/\text{TiO}_2) = 0.1$  g L<sup>-1</sup>) under different gas flow (a: N<sub>2</sub>; b: air).

Fig. 4.7a and 4.7b show the SEC-UV<sub>254</sub> chromatograms for the photocatalytic degradation of NOM under different gas flow. The SEC-UV<sub>254</sub> results are qualitatively similar to those of SEC-DOC. However, the removal rate of UV<sub>254</sub> absorption is faster than that of DOC. Under N<sub>2</sub> purging, the adsorption of NOM onto the catalyst is higher without any peak shift in the dark. After irradiation, the absorption decreased and shifted to larger chromatographic retention times (lower molecular size). Under air purging,

#### 4 Photocatalytic degradation of carbamazepine (CBZ) and clofibric acid (CA) using Pt/TiO<sub>2</sub> under environmentally relevant conditions

there is again a slighter adsorption of NOM onto the catalyst. After 10 min of irradiation, no UV<sub>254</sub> signal was observed in the entire chromatograph range with the exception of a small fraction around *t<sub>r</sub>* of 30 min.

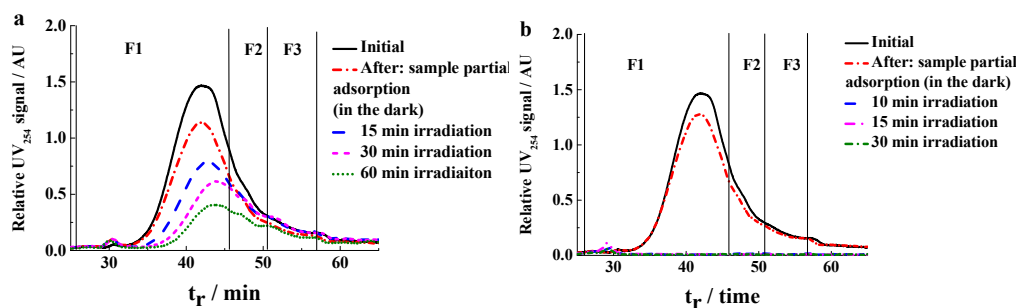


**Fig. 4.7** SEC-UV<sub>254</sub> chromatograms of NOM (HO24;  $\rho_0$  (DOC) = 16.5 mg L<sup>-1</sup>) for different photocatalytic reaction times ( $\rho$ (Pt/TiO<sub>2</sub>) = 0.1 g L<sup>-1</sup>) under different gas flow (a: N<sub>2</sub>; b: air).

The degradation processes under both conditions implies that oxygen shows a significant influence on the photocatalytic degradation and mineralization of the larger molecular sized fractions of NOM. Adsorbed oxygen acts as a highly efficient carrier, transferring electrons from the catalyst to NOM.

Fig. 4.8 shows SEC-DOC chromatograms of NOM ( $\rho_0$  (DOC) = 1.7 mg L<sup>-1</sup>) and CA (10 mg L<sup>-1</sup>) for different irradiation times under air purging ( $\rho_0$  (DO) = 8 mgL<sup>-1</sup>). The CA molecules show a peak at  $t_r \leq 120$  min and the unresolved NOM molecules at max  $t_r \approx 42$  min (Fig. 4.8a). Under the defined experimented conditions in the mixture, most of the initial NOM and less than 5% of CA were adsorbed onto the catalyst in the dark (Fig. 4.8b). After 1 min of irradiation, CA degraded rapidly, while two new peaks appeared around  $t_r \approx 50$  and 55.6 min, which highly resulted from the degradation of the adsorbed NOM (Fig. 4.8c). After 5 min of irradiation, more than 95% of the CA was removed, while the emerging NOM fractions had reached their maximum. After 10 min of irradiation, CA was completely eliminated, and NOM fractions continuously formed smaller molecular sized fractions due to partial mineralization and/or disaggregation.

#### 4 Photocatalytic degradation of carbamazepine (CBZ) and clofibric acid (CA) using Pt/TiO<sub>2</sub> under environmentally relevant conditions

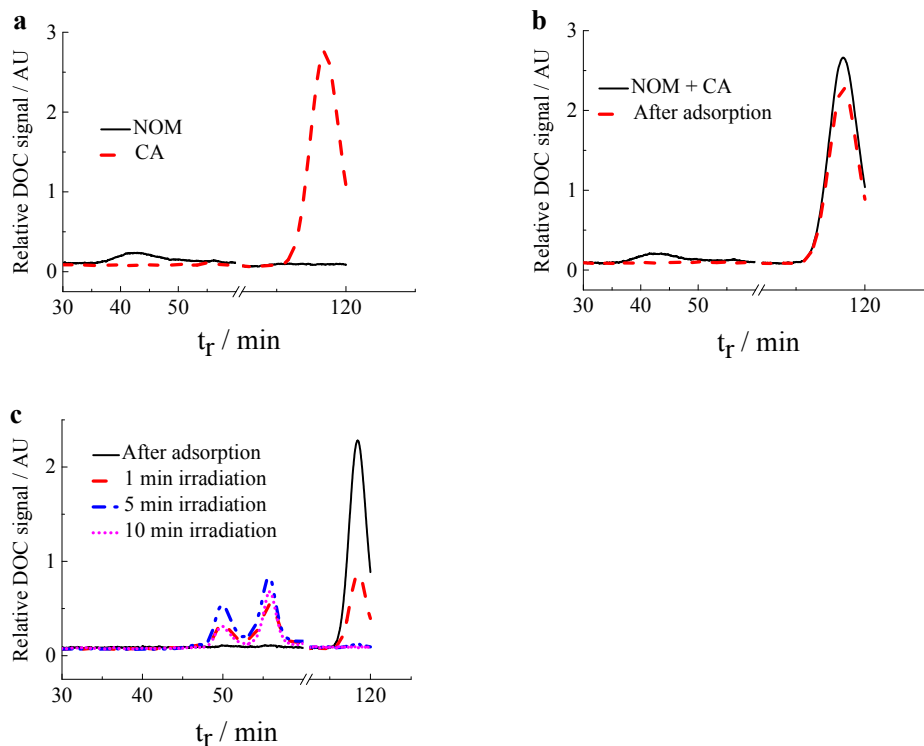


**Fig. 4.8** SEC-DOC chromatograms of NOM (HO24;  $\rho_0$  (DOC) = 1.7 mg L<sup>-1</sup>) and CA (10 mg L<sup>-1</sup>) under air flow ( $\rho$  (DO) = 8 mg L<sup>-1</sup>). (a[control data]: individual matter, no catalyst; b: dark adsorption experiment,  $\rho$ (Pt/TiO<sub>2</sub>) = 0.1 g L<sup>-1</sup>; c: irradiation experiment,  $\rho$ (Pt/TiO<sub>2</sub>) = 0.1 g L<sup>-1</sup>).

Again, larger molecular sized fractions of NOM were preferentially degraded during irradiation time to form lower molecular sized fractions. The degradation rate decreased dramatically with the decrease of DO concentration. Under N<sub>2</sub> purging, larger molecular sized fractions are predominant during the whole process, while lower molecular sized fractions predominate after the first few minutes under air and O<sub>2</sub> purging. The degradation processes indicated that the inhibition influence of NOM on the photocatalytic degradation of PhACs is more dependent on the molecular size of NOM than on its concentration. High molecular sized NOM fractions with high aromaticity are more easily adsorbed onto the catalyst particles and act as an electron-hole scavenger and a light filter, reducing the photocatalytic degradation rate. Conversely, the lower molecular sized NOM fractions cause less inhibition of the degradation reaction. They even can assist the electron transfer by forming triplet excited states followed by the formation of other reactive species, including <sup>1</sup>O<sub>2</sub>, HO<sub>2</sub>•, and •O<sub>2</sub><sup>-</sup> (Frimmel et al. 1987).

## 4.5 Conclusions

Photocatalytic degradation of CBZ and CA was strongly affected by the environmentally relevant conditions and the character of the targeted compounds. Environmental parameters can have different, even opposite, effects on the yield and kinetics of the photocatalytic degradation when comparing CBZ with CA. Among these parameters, NOM showed the largest deactivation effect caused by adsorption. On the catalyst which is critical for the design of practical treatment systems. However, the addition of oxygen can significantly eliminate this inhibitory NOM effect. Results demonstrate that the presence of NOM is the most restrictive parameter for the application of photocatalysis in wastewater treatment plant and in the environment. Further research of introducing new agents or developing new catalysts are required in order to reduce the inhibitory effect of NOM in high concentrations.

## 5 Photocatalytic elimination of diatrizoate (DA) and I<sup>-</sup> formation -- Influence of DO, metal ions and NOM

In Chapter 4 it was demonstrated that the presence of NOM is the most restrictive for the application of photocatalysis in wastewater treatment and in the environment. The addition of metal ions and DO can partly eliminate this inhibitory NOM effect. Therefore, a simplified model of environmental conditions was used to identify the photocatalytic degradation of PhAC in the presence of different concentration of DO, metal ions (Fe(III), Zn<sup>2+</sup> and Ca<sup>2+</sup>) and NOM. In the case of processes influenced by multiple variables, a statistical experimental design is a powerful tool for determining the effects of operational factors and their interactions. This technique has been used widely in chemical industry. In order to systematically explore the experimental region, a full factorial design (see 2.5) was used for 3 variables in 2 levels (2<sup>3</sup> experimental runs), which comprises all possible combinations of the +1 and -1 levels shown in Table 5.1. The selected levels of the variables were based on the results of Chapter 4 not on the wastewater.

**Table 5.1 Experimental factors for the interaction of major water constituents**

Factors	Coded variable	Levels	
		-1	+1
O <sub>2</sub> (mg L <sup>-1</sup> )	$x_A$	0	8
Me <sup>n+</sup> (μM)	$x_B$	0	10
DOC (mg L <sup>-1</sup> )	$x_C$	0	1.6

Diatrizoate (DA), an ionic ICM, was chosen as a model compound in this Chapter. It was rarely removed when passing through the municipal sewage treatment plant, was found in ground water frequently and persisted for a long time without any removal



(Ternes et al. 2007).

## 5.1 Photocatalytic reaction kinetics of DA

The experimental results (Fig. 5.1) demonstrate that the photocatalytic activity of Pt/TiO<sub>2</sub> was somewhat higher than the one of pure TiO<sub>2</sub>, owing to the lower recombination of photogenerated electrons (e<sup>-</sup>) and holes (h<sup>+</sup>) in Pt/TiO<sub>2</sub>.

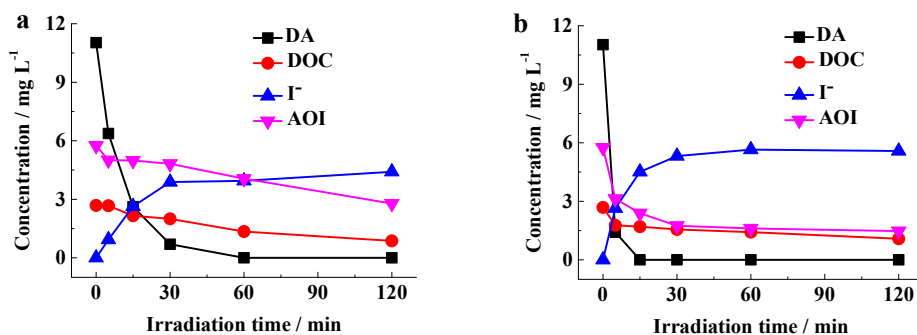


**Fig. 5.1** Concentrations profiles for DA, DOC, AOI and I<sup>-</sup> as a function of irradiation time in the presence of two different catalyst (a:  $\rho_0$  (TiO<sub>2</sub>) = 0.1 mg L<sup>-1</sup>; b:  $\rho_0$  (Pt/TiO<sub>2</sub>) = 0.1 mg L<sup>-1</sup>).

In the presence of Pt/TiO<sub>2</sub>, total photocatalytic degradation of DA was reached within 20 min under the given conditions, while no significant loss of DOC occurred. The missing mineralization indicates that DA is recalcitrant. During the irradiation of the DA the concentration of I<sup>-</sup> increased and the concentration of AOI decreased accordingly. After photocatalytic irradiation of 30 min, the elimination of the DA concentration was 17.97  $\mu$ M, and the formed I<sup>-</sup> concentration was about 42  $\mu$ M. Based on the assumption that each degraded DA molecule loses 3 I<sup>-</sup> ions, this equals to 14  $\mu$ M. The eliminated DA was theoretically de-iodinated for 77.6% which is consistent with the elimination rate of adsorbable organic iodine (AOI) (74.4%). The increasing I<sup>-</sup> concentration and the decreasing AOI concentration over the irradiation time indicates the stepwise de-iodination of the tri-iodinated contrast media DA and also the formation of partially iodinated intermediates during the photocatalytic degradation.

## 5.2 Full factorial design and data analysis

Table 5.2 Factorial design matrix with experimental responses

(a) Factorial design matrix with experimental degradation rate constants (*k*) for DA

Run	Coded values of independent variables			<i>k</i> (min <sup>-1</sup> )		
	<i>x<sub>A</sub></i>	<i>x<sub>B</sub></i>	<i>x<sub>C</sub></i>	*	**	***
1	-1	-1	-1	0.508	0.508	0.508
2	+1	-1	-1	0.529	0.529	0.529
3	-1	+1	-1	0.408	0.385	0.305
4	+1	+1	-1	0.498	0.427	0.503
5	-1	-1	+1	0.544	0.544	0.544
6	+1	-1	+1	0.579	0.579	0.579
7	-1	+1	+1	0.372	0.331	0.286
8	+1	+1	+1	0.641	0.575	0.549

(b) Factorial design matrix with experimental formed I<sup>-</sup> concentration

Run	Coded values of independent variables			I <sup>-</sup> (mg L <sup>-1</sup> )		
	<i>x<sub>A</sub></i>	<i>x<sub>B</sub></i>	<i>x<sub>C</sub></i>	*	**	***
1	-1	-1	-1	3.05	3.05	3.05
2	+1	-1	-1	3.05	3.05	3.05
3	-1	+1	-1	2.72	2.40	2.39
4	+1	+1	-1	2.57	2.72	3.26
5	-1	-1	+1	2.74	2.74	2.74
6	+1	-1	+1	3.79	3.79	3.79
7	-1	+1	+1	2.45	2.25	1.87
8	+1	+1	+1	3.81	4.29	4.02

*x<sub>A</sub>*: O<sub>2</sub>; *x<sub>B</sub>*: metal ions; *x<sub>C</sub>*: DOC. \*: in the case of Fe(III); \*\*: in the case of Zn<sup>2+</sup>; \*\*\*: in the case of Ca<sup>2+</sup>

Table 5.2a and 5.2b show the design matrix used in the 2<sup>3</sup> full factorial design, along with the reaction rate constants and the formed I<sup>-</sup> concentrations in each run. The effects of the studied factors and interaction effect between factors on the DA photocatalytic degradation rate constants and the formed I<sup>-</sup> concentrations are presented comparatively in Fig. 5.2. Analysis of the effect of principal factors showed that in the considered range of parameters, DO and metal ions are the most intense single factors and the interaction between them is the most significant variable in achieving maximum rate constants for the photocatalytic degradation of DA. According to the positive effect of DO, increasing in oxygen concentration enhanced the rate constant and the formed I<sup>-</sup> concentration. In

comparison, the presence of metal ions decreased the rate constant. DO and metal ions have the opposite tendency for I<sup>-</sup> formation, while Ca<sup>2+</sup> plays a more negative role than Fe(III) and Zn<sup>2+</sup>. The interaction between DO and NOM is the most intense one for I<sup>-</sup> formation. In this analysis, the interaction effect between metal ions and NOM (BC) was very low for DA degradation rate constant and I<sup>-</sup> formation, and therefore it can be neglected. The interaction effect oxygen and metal ions (AB) can also be neglected for I<sup>-</sup> formation due to its low effect.

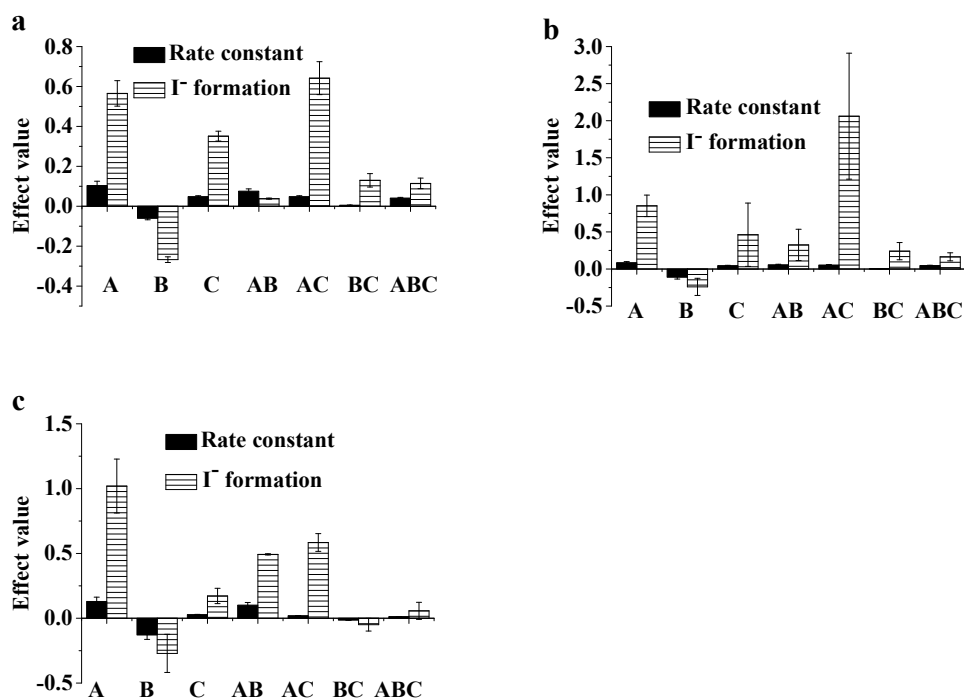


Fig. 5.2 Estimated effects of different factors on the photocatalytic degradation rate constant of DA and on the I<sup>-</sup> formation using fractional factorial design (present metal: a: Fe(III); b: Zn<sup>2+</sup>; c: Ca<sup>2+</sup>; A, B and C see Table 5.1).

### 5.3 Analyses for rate constants

The estimates of main effects of the factors and their interactions on the rate constant were also examined from the interaction plot. The effect of DO was investigated by addition of various amounts of metal ions and NOM (Fig. 5.3). It can be seen, that the rate constant increased with increasing DO concentration caused by the increased amount of

5 Photocatalytic elimination of diatrizoate (DA) and I<sup>-</sup> formation – influence of DO, metal ions and NOM

<sup>1</sup>O<sub>2</sub> and •HO<sub>2</sub><sup>-</sup>, and •O<sub>2</sub> formed by DO in the photocatalysis process (Canario et al. 2013).

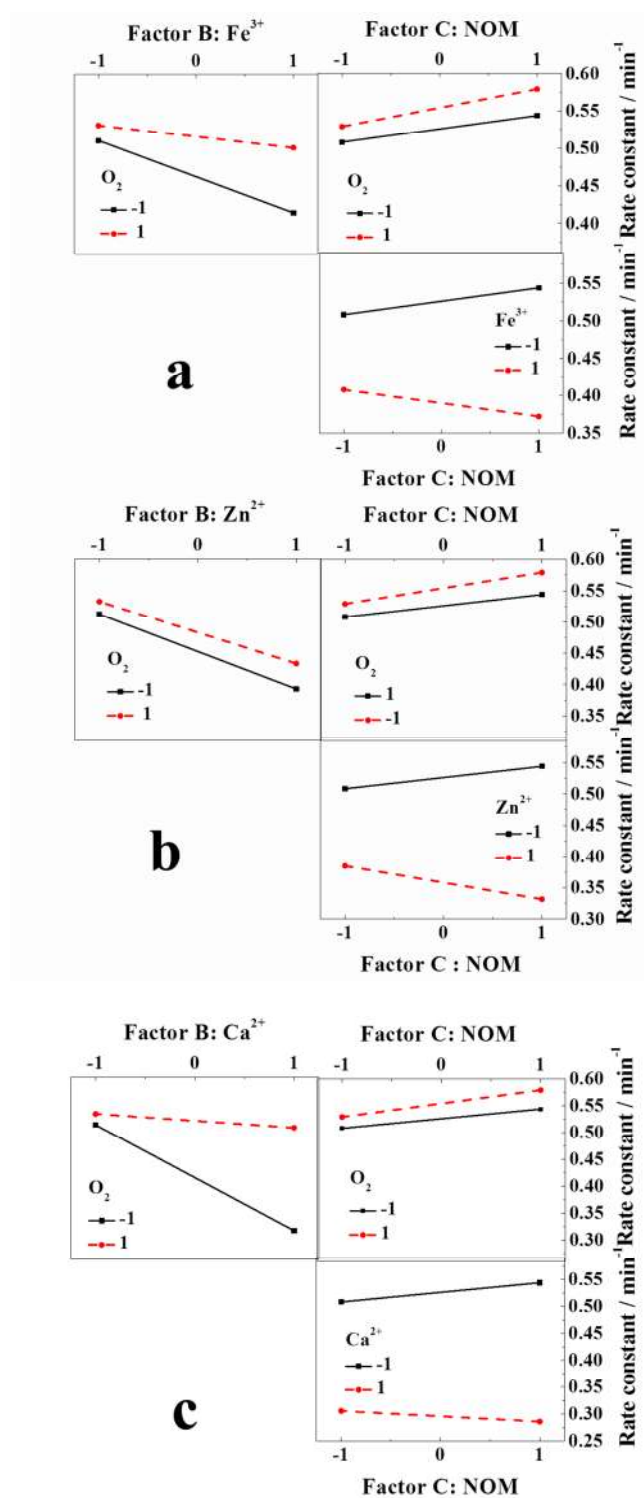
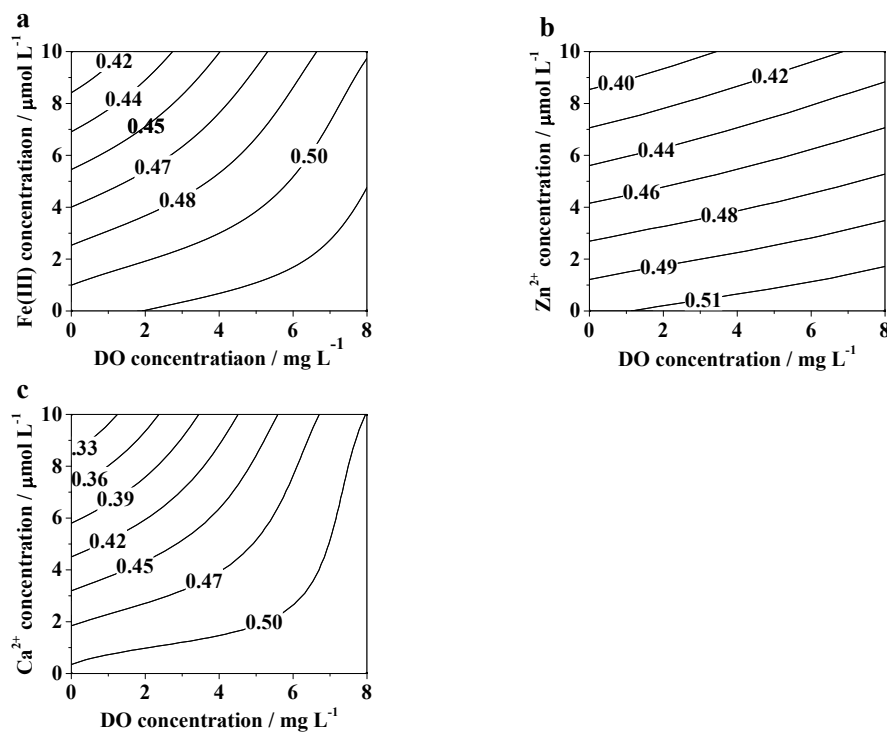


Fig. 5.3 Interaction effect between parameters in the photocatalytic degradation rate constant of DA (Based on the rate constant of Table 5.2a. Present metal: a: Fe(III); b: Zn<sup>2+</sup>; c: Ca<sup>2+</sup>).

It was also found that all the selected metal ions ( $Fe(III)$ ,  $Zn^{2+}$  and  $Ca^{2+}$ ) decreased the rate constant. At low DO concentration, metal ions significantly influenced the removal of DA, especially  $Ca^{2+}$ . With the increase of the DO concentration, the influence of metal ions decreased gradually. It is attributed that the presence of metal ions inhibits the formation of superoxide anion-radicals, radical intermediates and peroxy titanium species by the competitive reaction of photogenerated electrons with metal ions (Brezova et al. 1995).



**Fig. 5.4** Influence of the second-order interactions on the photocatalytic degradation rate constant ( $\text{min}^{-1}$ ) of DA: (a) DO and  $Fe(III)$ , (b) DO and  $Zn^{2+}$  and (c) DO and  $Ca^{2+}$ . (Based on the rate constant of Table 5.2a).

The best way to visualize the effect of the independent variables on the dependent ones is to draw 2D contour curves response lots of the model, which were done by varying two variables within the experimental range and holding the other constant (Box et al. 2005). Fig. 5.4 shows the 2D contour curves of the interactions between DO and metal ions on the rate constants. It was observed that increasing of the DO concentration as well as decreasing of the concentration of metal ions leads to better results of photocatalytic degradation of DA.

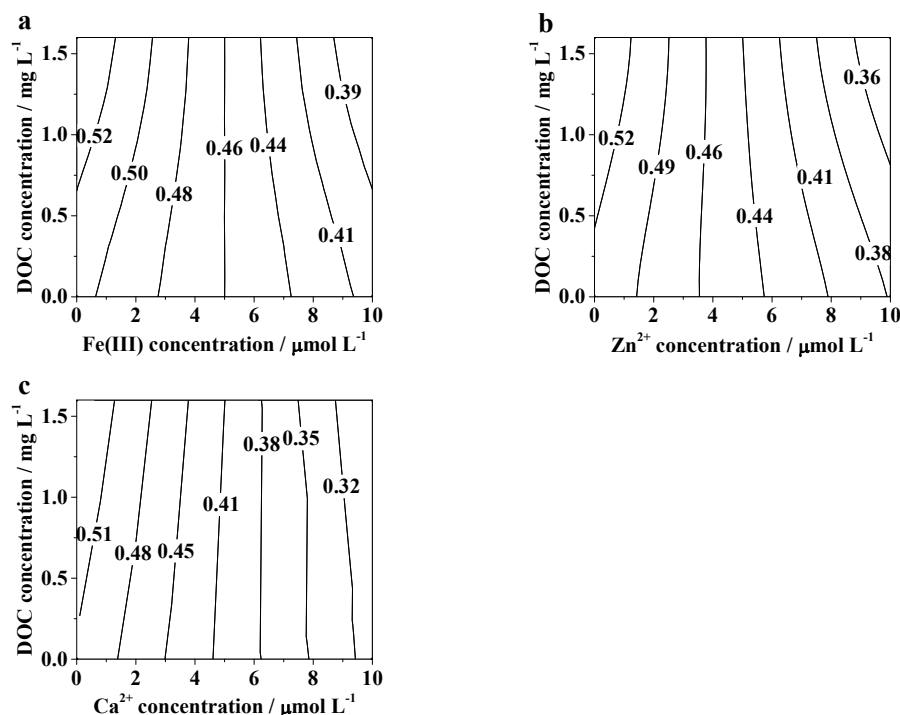


**Fig. 5.5 Influence of the second-order interactions on the photocatalytic degradation rate constant (min<sup>-1</sup>) of DA: (a) NOM and Fe(III), (b) NOM and Zn<sup>2+</sup> and (c) NOM and Ca<sup>2+</sup>. (Based on the rate constant of Table 5.2a)**

The rate constants were also enhanced by NOM. It is attractive to assume the formation of triplet excite states formed by NOM under UV irradiation(Frimmel et al. 1987). No obvious interaction between DO and NOM was observed. In comparison, NOM decreased the rate constants in the presence of metal ions (Fig. 5.5). The contour curves are nearly perpendicular to the metal ions axis, which shows that the metal ions have a more pronounced influence than the NOM. To more formally examine the trends in rate constant, we used the model shown in Eq. (2.16) to fit the experimental data in the table 5.2 (note the use of the coded variables instead of the real variables) (Espinoza et al. 2009).The resulting model can be presented by Eqs. 5.2 to 5.4:

$$Y_k = 0.51 + 0.052x_A - 0.03x_{B(Fe(III))} + 0.024x_C + 0.038x_Ax_{B(Fe(III))} + 0.024x_Ax_C \quad (5.2)$$

$$Y_k = 0.485 + 0.043x_A - 0.055x_{B(Zn^{2+})} + 0.023x_C + 0.029x_Ax_{B(Zn^{2+})} + 0.027x_Ax_C \quad (5.3)$$

$$Y_k = 0.475 + 0.065x_A - 0.065x_{B(Ca^{2+})} + 0.014x_C + 0.051x_Ax_{B(Ca^{2+})} \quad (5.4)$$

The predicted data from the model were also compared with the experimental data

measured (Fig. 5.6). The high  $R^2$  (0.93, 0.92 and 0.98 for Fe<sup>3+</sup>, Zn<sup>2+</sup> and Ca<sup>2+</sup>, respectively) values signify that the model is able to give a reasonably good estimate of response for the system in the range studied.

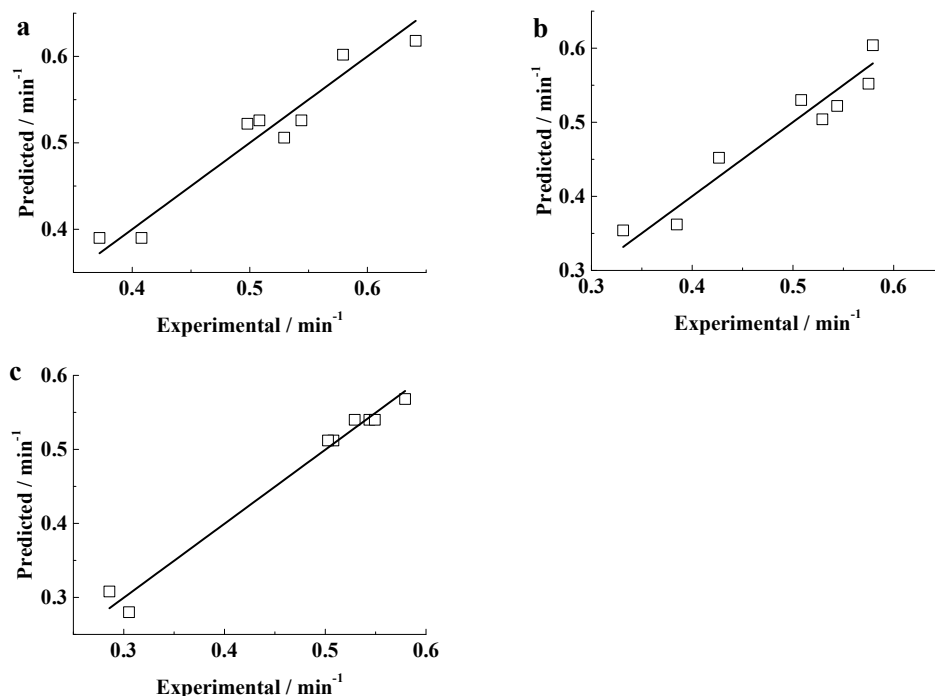


**Fig. 5.6** Comparison of experimental (data in table 5.2) and predicted (calculated data according to Eqs. 5.2 to 5.4) photocatalytic degradation rate constant of DA (present metal: a: Fe(III); b: Zn<sup>2+</sup>; c: Ca<sup>2+</sup>).

## 5.4 Analyses for I<sup>-</sup> formation

The effects of DO, metal ions and NOM on I<sup>-</sup> formation are shown in Fig. 5.7. In contrast to the rate constants, no effect of DO on the final I<sup>-</sup> concentration in the system was observed. While, the de-iodination rate of DA obviously increased with the increase of oxygen concentration (Fig. 5.8). The identical final I<sup>-</sup> concentration might result from the consumption of I<sup>-</sup> in the presence of high DO concentration (Eq. 5.5).



5 Photocatalytic elimination of diatrizoate (DA) and I<sup>-</sup> formation – influence of DO, metal ions and NOM

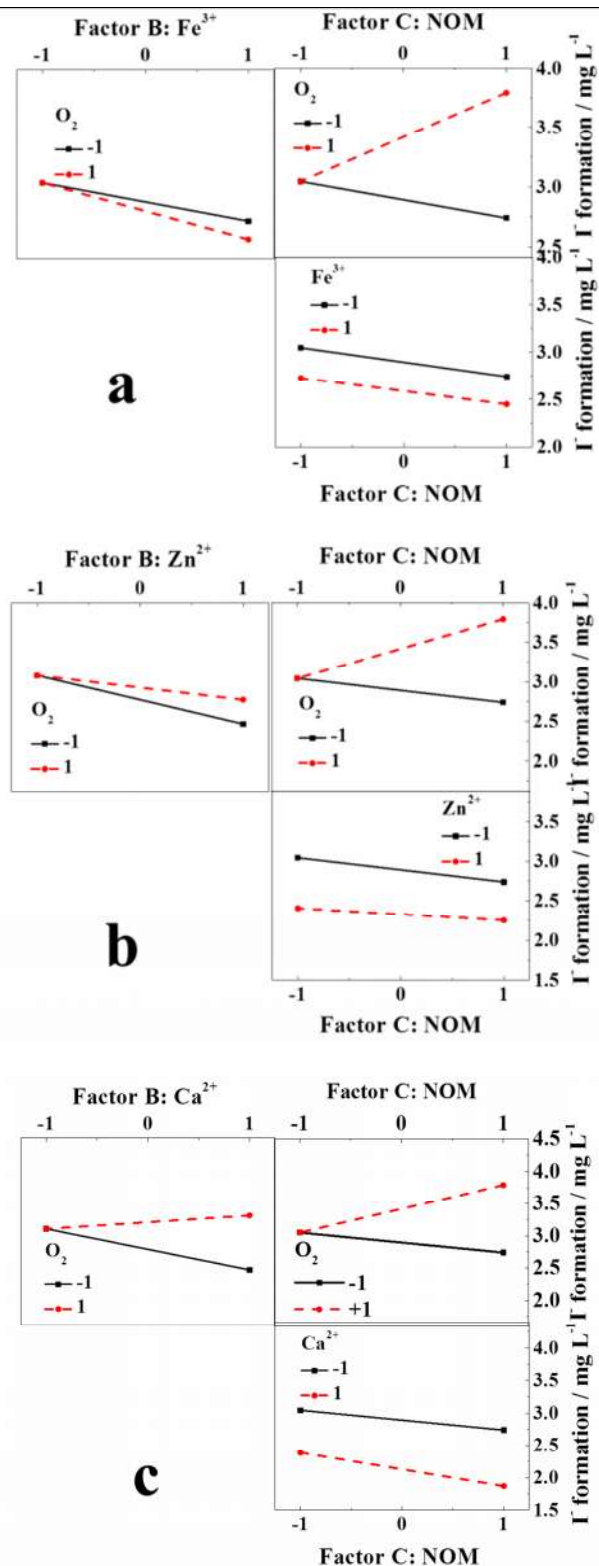


Fig. 5.7 Interaction effect between parameters in I<sup>-</sup> formation (Based on the rate constant of Table 5.2b. Present metal: a: Fe<sup>3+</sup>; b: Zn<sup>2+</sup>; c: Ca<sup>2+</sup>).

Similar with the rate constant, it was also found that all the selected metal ions (Fe(III),



5 Photocatalytic elimination of diatrizoate (DA) and  $I^-$  formation – influence of DO, metal ions and NOM

$Zn^{2+}$  and  $Ca^{2+}$ ) decreased the  $I^-$  formation in the low DO concentration. With the increase of the DO concentration, the effect of metal ions varied. Notably, in the presence of Fe(III),  $I^-$  concentration in solution decreased with the increase of oxygen concentration, which might be caused by the oxidation consumption of  $I^-$  (Eq. 5.6 and 5.7). The inhibiting effects of  $Zn^{2+}$  and especially  $Ca^{2+}$  decreased with increase of oxygen. The  $I^-$  concentration increased by adding  $Ca^{2+}$  in the presence of high DO concentration, which implied that the inhibition effect of  $Ca^{2+}$  was completely covered by the enhanced influence of DO.

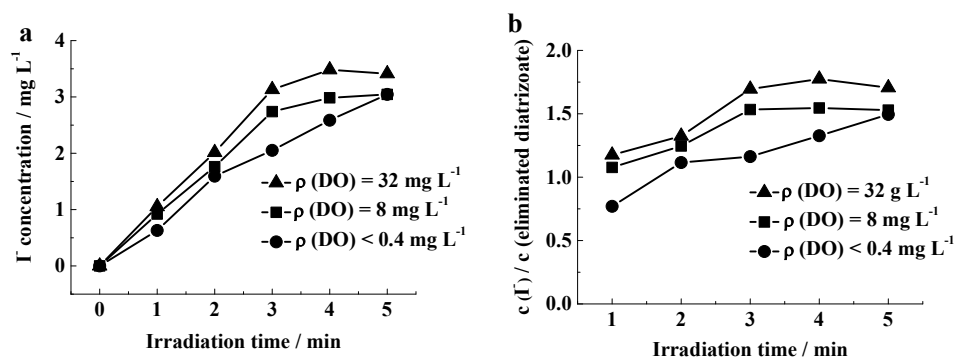


**Fig. 5.8 (a)  $I^-$  concentration as a function of irradiation time in the presence of different DO levels; (b) the ratio of  $I^-$  concentration and eliminated DA in the presence of different DO levels.**

In the presence of NOM the final  $I^-$  concentration decreased significantly at low DO concentration, while in the high DO level, the  $I^-$  concentration obviously increased. As discussed, the interaction between DO and NOM is the most intense for  $I^-$  formation, and the 2D contour curved (Fig. 5.9) of the interaction between NOM and DO revealed that the simultaneous increase of both factors lead to the largest  $I^-$  formation. And there is a synergistic effect between NOM and DO which means the influence of NOM increased with the increase of DO concentration.

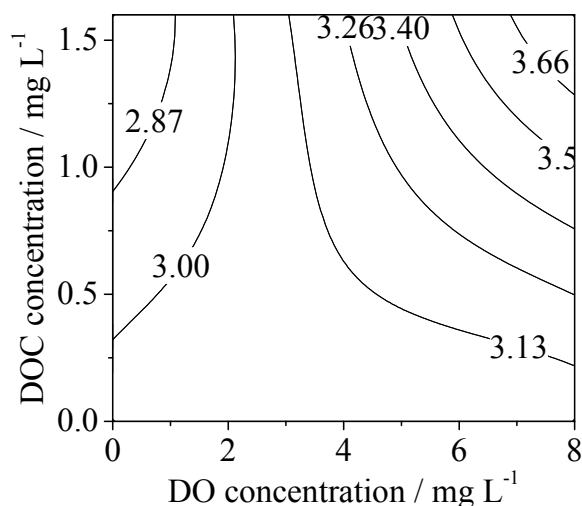


**Fig. 5.9 Influence of the second-order interactions of DO and NOM on I<sup>-</sup> formation (mg L<sup>-1</sup>).**

The trend in I<sup>-</sup> formation concentration were determined by using the Eq. 2.16 to fit the data in the Table 5.2b and the resulting model can be presented by Eqs. 5.8 to 5.10.

$$Y_{I^-} = 3.02 + 0.28x_A - 0.13x_{B(Fe(III))} + 0.18x_C + 0.32x_Ax_C \quad (5.8)$$

$$Y_{I^-} = 3.04 + 0.43x_A - 0.12x_{B(Zn^{2+})} + 0.23x_C + 0.16x_Ax_{B(Zn^{2+})} + 0.35x_Ax_C \quad (5.9)$$

$$Y_{I^-} = 3.02 + 0.51x_A - 0.14x_{B(Ca^{2+})} + 0.09x_C + 0.25x_Ax_{B(Ca^{2+})} + 0.29x_Ax_C \quad (5.10)$$

The predicted data from the model were also compared with the experimental data measured (Fig. 5.10). Using all coefficients in Eqs. 5.8 to 5.10 results in an almost perfect fit of the data ( $R^2$  of 0.97, 0.95 and 0.98 for Fe(III), Zn<sup>2+</sup> and Ca<sup>2+</sup>, respectively).

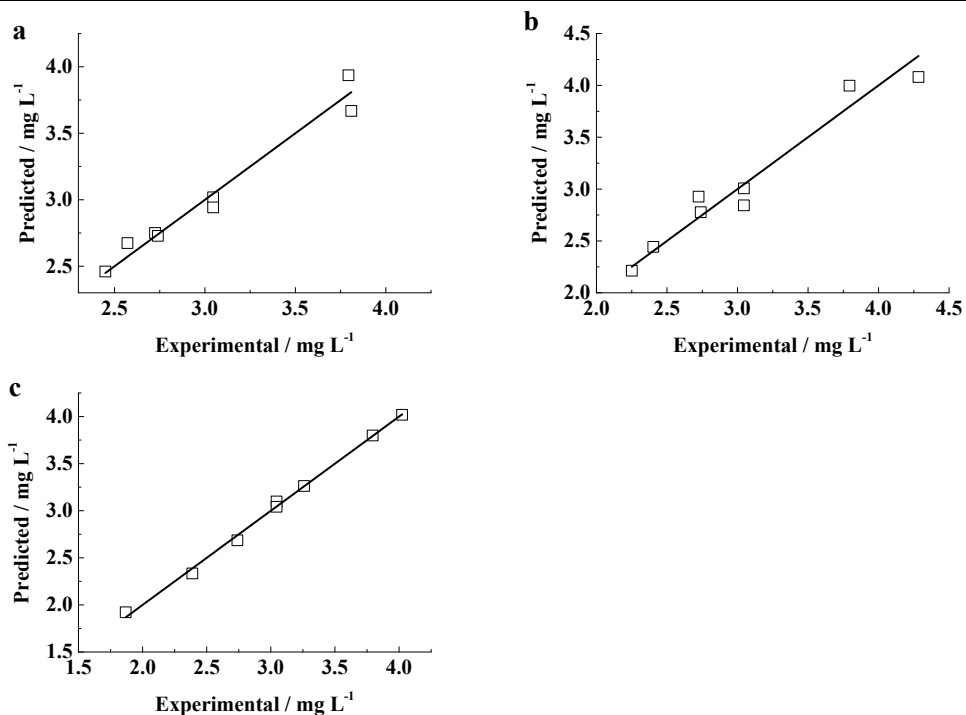


Fig. 5.10 Comparison of experimental (data in table 5.2) and predicted (calculated data according to Eqs. 5.8 to 5.10)  $\Gamma^-$  concentrations (present metal: a: Fe(III); b:  $\text{Zn}^{2+}$ ; c:  $\text{Ca}^{2+}$ ).

## 5.5 Conclusions

The results of the photocatalytic experiments showed an effective removal of DA and the formation of  $\Gamma^-$ . The experimental design results revealed that the degradation of DA was strongly affected by the amount of DO present and by the presence of metal ions, increasing the DO concentration and decreasing the metal ions concentration led to the highest reaction rate constant of the photocatalytic degradation of DA. The DO concentration as well as NOM had the most intense influence on  $\Gamma^-$  formation, and the simultaneous increase of both led to the highest  $\Gamma^-$  formation. The empirical models were developed for DA elimination and  $\Gamma^-$  formation, and the high  $R^2$  values signify that the models obtained are well suited to describe the response of the system in the range studied. Investigating major water constituents in competitive application under well defined reaction conditions opens the door for the identification of the drivers of the reactions useful for the basic understanding of aquatic systems and for water treatment as well.

## **6 Aggregation behavior of TiO<sub>2</sub> nanoparticles in aqueous solution: influence of different types of DOM under different pH values and electrolytes**

The increasing application of TiO<sub>2</sub> NPs by consumer and industrial has led to increased concerns about potential environmental and human health impacts (Gottschalk et al. 2009, Ju-Nam and Lead 2008). The first step in NPs assessment is to show their transport, fate, and behavior in the environment. The environmental transportation and transformation, as well as the toxicity against organism, of TiO<sub>2</sub> NPs in the aquatic environment might be strongly dependent on their sizes, surface properties and interactions with other substances in water (Battin et al. 2009). The aggregation of TiO<sub>2</sub> NPs seems to be a critical factor affecting most of the other NP properties in the aquatic environment.

The work presented in this Chapter consists to investigate the characteristics, dispersions and stabilities of TiO<sub>2</sub> NPs as a function of pH value and ionic strength of NaCl and CaCl<sub>2</sub> solutions in the presence of five various DOM sources: Hohloh Lake 10 fulvic acid (HO10FA), alginate, bovine serum albumin (BSA),  $\alpha$ -amylase and SDS at realistic DOM environmental concentrations.

### **6.1 Determination of aggregation kinetics**

Kinetic size measurement was carried out immediately after the suspensions were prepared. Each measurement lasted for 100 s. Each sample was measured continuously for 30 runs. The aggregation rates ( $k$ ) are expressed as the slope  $\Delta D/\Delta t$  (nm s<sup>-1</sup>), where  $\Delta D$  means the increase in the TiO<sub>2</sub> NPs diameters (nm) and  $\Delta t$  denotes the time range (s). All the size data were number mean value according to the literature to avoid overestimate the particle size (Domingos et al. 2009a, Li and Sun 2011, Romanello and de Cortalezzi 2013). Final hydrodynamic diameter was estimated as an average of the

last 6 measurements taken.

The particle attachment efficiency ( $\alpha$ ) is used to quantify the aggregation kinetics of TiO<sub>2</sub> NPs. It is defined as normalizing the measured aggregation rate by the aggregation rate constant ( $k_{fast}$ ) under diffusion-limited conditions, where the aggregation is independent of the electrolyte concentration. The TiO<sub>2</sub> NPs concentration in all aggregation experiments is kept constant, thus the  $\alpha$  value is calculated by the initial slope of the aggregation profile at a given electrolyte concentration normalized by the initial slope under favorable (fast) aggregation conditions:

$$\alpha = \frac{k}{k_{fast}} = \frac{\left(\frac{dD}{dt}\right)_{t \rightarrow 0}}{\left(\frac{dD}{dt}\right)_{t \rightarrow 0, fast}} \quad (6.1)$$

To calculate  $\alpha$  in the presence of DOM,  $\left(\frac{dD}{dt}\right)_{t \rightarrow 0, fast}$  is obtained from the average values of  $\left(\frac{dD}{dt}\right)_{fast}$  in the diffusion-limited regime in the presence of either NaCl or CaCl<sub>2</sub>.

## 6.2 Adsorption of DOM onto the surface of TiO<sub>2</sub> NPs

The adsorption properties of different DOM onto the TiO<sub>2</sub> NPs' surface were shown in Fig. 6.1. With the increase of DOC concentration, the adsorption of DOM increased except SDS. As a linear hydrophobic compound, SDS can not interact with the -OH located on the TiO<sub>2</sub> surface efficiently. Hence, no obvious adsorption of SDS on the TiO<sub>2</sub> NPs' surface was observed. BSA showed the strongest adsorption capacity, followed by  $\alpha$ -amylase, HO10FA and alginate. The TiO<sub>2</sub> NPs and all the DOM samples exhibited negative zeta potential at the given pH (8.6). However, the relative abundance of the positively charged molecular regions (Arg, Lys) of BSA is higher than the one of the negatively charged regions (Glu, Asp) (Watanabe et al. 1988) by which enhanced the adsorption of BSA to negative TiO<sub>2</sub> surface. Compared to alginate, the more abundant aromatic components in HO10FA facilitate their adsorption onto the surface of TiO<sub>2</sub> NPs

due to a bridging interaction (Domingos et al. 2009b).

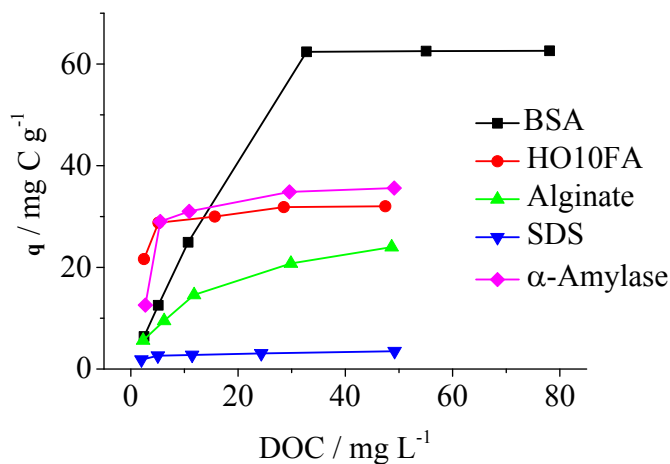


Fig. 6.1 Adsorption isotherm of DOM onto the surface of TiO<sub>2</sub> NPs

## 6.3 Material characterization

### 6.3.1 DOM characterization

The zeta potential of various DOM solutions was determined by adjusting the pH from 2 to 11 with the HCl or NaOH (Fig. 6.2a). The zeta potential of all DOM models decreased with the increase of the pH value in the domain investigated here. As shown in Fig. 6.2a, the zeta potential of SDS and alginate decreased from  $0 \pm 2.5$  mV to  $-35 \pm 1.1$  mV with the increase of pH value. HO10FA exhibited negative zeta potentials in all selected pH values due to the presence of carboxylic acid and phenolic functional groups (Loosli et al. 2013). In case of BSA, a zeta potential plateau of about  $-25 \pm 2$  mV was found between pH 5.5 and 11. At lower pH value, the zeta potential increased dramatically due to the continuous protonation to reach a value of  $15 \pm 1.5$  mV at pH 3.5, and the PZC is observed at pH 4.5 approximately, which is in good agreement with previous works (Salgin et al. 2012). A wide range of PZC of  $\alpha$ -amylase was observed between pH 3 and 7. At higher pH, the zeta potential significantly dropped to reach a value of  $-31 \pm 1.2$  mV.

### 6.3.2 TiO<sub>2</sub> NPs

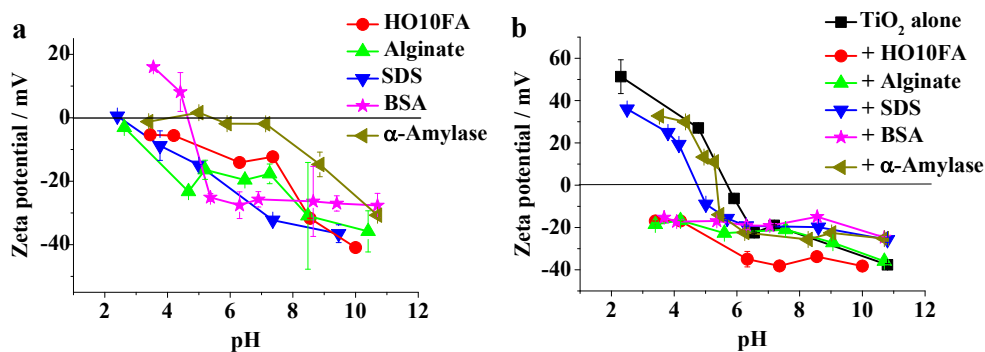


Fig. 6.2 (a) Zeta potential of different types of DOM ( $\rho(\text{DOC}) = 1 \text{ mg L}^{-1}$ ) as a function of pH values; (b) Zeta potential of TiO<sub>2</sub> NPs ( $\rho(\text{TiO}_2) = 20 \text{ mg L}^{-1}$ ) as a function of pH values in the absence and presence of different types of DOM.

The zeta potential of TiO<sub>2</sub> NPs in the absence and presence of different types of DOM resources is shown in Fig. 6.2b. TiO<sub>2</sub> NPs exhibit a strong positive zeta potential of  $52 \pm 5.2 \text{ mV}$  at pH 2.5 in the absence of DOM. Then the zeta potential decreased to the PZC at  $\text{pH } 5.5 \pm 0.1$ . By increasing the pH, the zeta potential became negative and reached  $-38 \pm 0.6 \text{ mV}$  at pH 10.7. The addition of BSA caused more negative surface charge of TiO<sub>2</sub> NPs at  $\text{pH} < 6$ , a stable and negative zeta potential ( $-20 \pm 3.5 \text{ mV}$ ) of TiO<sub>2</sub> NPs was observed in the pH range 2 to 11. It might result from the structure rearrangements in the BSA molecule in the adsorption process. The  $\alpha$ -helix content of BSA decreases and the  $\beta$ -turn content increases upon adsorption (Lynch and Dawson 2008). TiO<sub>2</sub> NPs showed more negative surface charge in the pH range 2 to 11 in the presence of HO10FA and alginate as well. By increasing the pH value, the zeta potential decreased from  $-17 \pm 0.5 \text{ mV}$  to  $-38 \pm 0.7 \text{ mV}$  and to  $-35 \pm 0.5 \text{ mV}$  in the presence of HO10FA and alginate, respectively. It is suggested that the adsorption of HO10FA and alginate introduce more negative charge to the TiO<sub>2</sub> surface. In the presence of the nearly neutral  $\alpha$ -amylase, no significant change of surface charge was observed. The presence of SDS on the surface of TiO<sub>2</sub> NPs did not contribute much on the change of zeta potential due to its low adsorptivity.

## 6.4 Aggregation and stability of TiO<sub>2</sub> NPs as a function of pH value

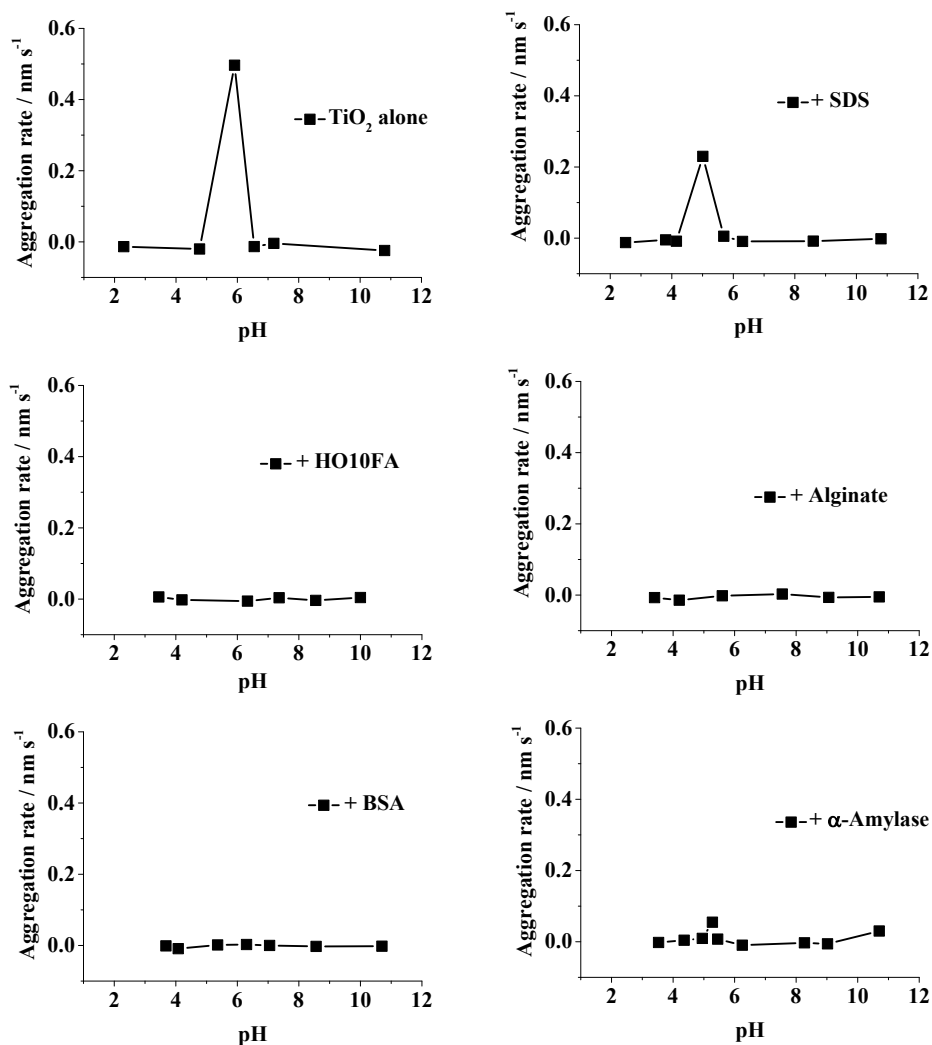


Fig. 6.3 Aggregation rates of TiO<sub>2</sub> NPs as a function of pH values in the absence and presence of different types of DOM.

The determination of TiO<sub>2</sub> NPs aggregation and stability as a function of pH values in the presence of different types of DOM were carried out in the pH range 2 to 11. As shown in Fig. 6.3 and 6.4, both aggregation rates and final hydrodynamic diameters of the TiO<sub>2</sub> NPs are at their peak around pH 6 in the absence of DOM. The final hydrodynamic diameter is larger than 1200 nm, which is about 8 times compared to that under the stable situations. Another significant aggregation was detected in the presence of SDS at pH 5. However, the aggregation rate decreased for ca. 50% in the presence of



6 Aggregation behavior of TiO<sub>2</sub> nanoparticles in aqueous solution: influence of different types of DOM under different pH values and electrolytes

SDS compared to that of pure TiO<sub>2</sub> NPs suspension, and the final hydrodynamic diameter decreased for ca. 35% accordingly. At other pH values, the final hydrodynamic diameter was in good agreement with the case where no SDS was added. In the presence of  $\alpha$ -amylase, a minor aggregation rate was identified at pH 5. However, the aggregation was negligible at every pH assessed in cases where HO10FA, alginate and BSA were added to the suspension. And no significant change of the final hydrodynamic diameter was detected.

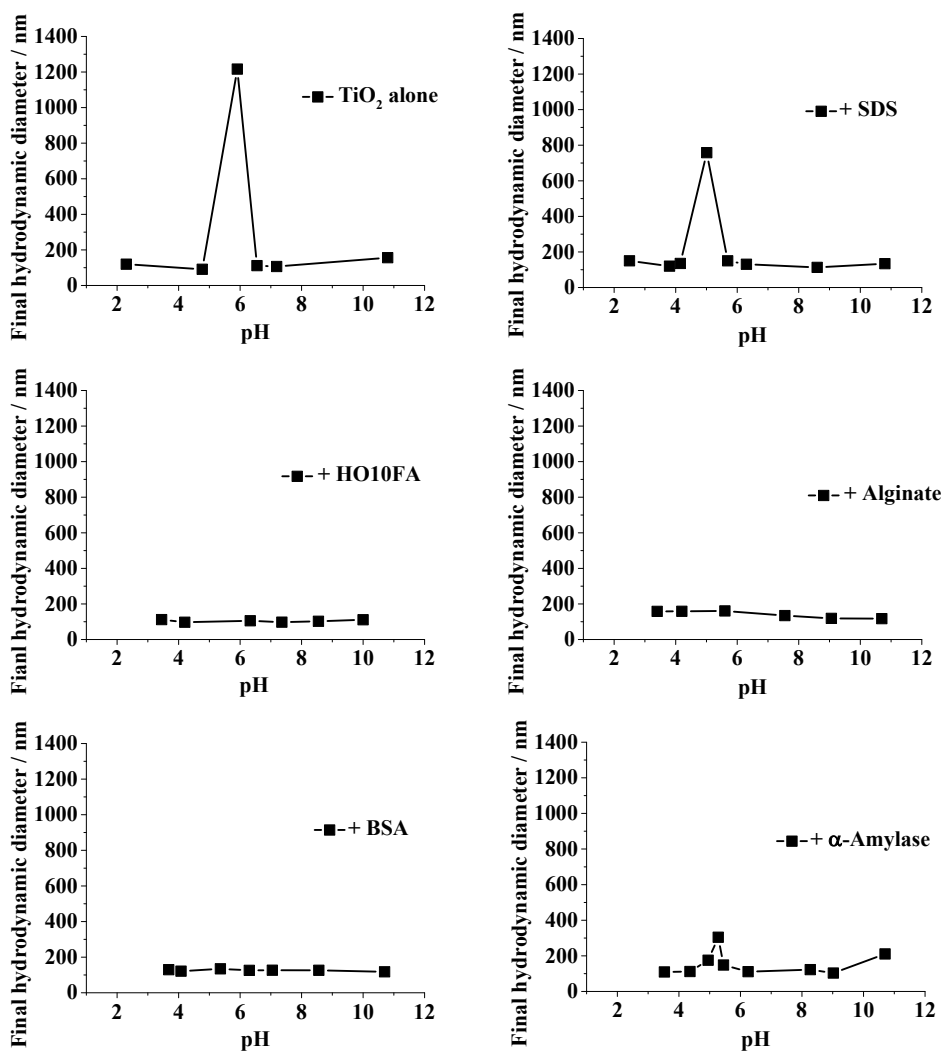


Fig. 6.4 Final hydrodynamic diameters of TiO<sub>2</sub> NPs as a function of pH values in the absence and presence of different types of DOM.

The peak aggregation rate and hydrodynamic diameter were observed at pH values near the PZC, but at pH values far from the PZC, no aggregation was observed. Overall,

the presence of the DOM stabilized the TiO<sub>2</sub> NPs distribution in different extent. The inefficient stabilization effect of SDS is probably due to its weak adsorption property onto the surface of TiO<sub>2</sub> NPs. The results of aggregation rate and final hydrodynamic diameter fit well to the zeta potential of the TiO<sub>2</sub> NPs in the presence of different types of DOM, which indicates that the electrostatic effect was the predominate mechanism of stabilization of TiO<sub>2</sub> NPs.

## **6.5 TiO<sub>2</sub> NPs aggregation kinetics in the presence of monovalent cations**

The TiO<sub>2</sub> NPs stability curve, i.e., the variation of the attachment efficiency ( $\alpha$ ) and zeta potential with the molar concentration of Na<sup>+</sup>, is presented in Fig. 6.6. The pH of all the samples was controlled at  $8.6 \pm 0.1$ . The TiO<sub>2</sub> NPs and all the DOM samples exhibited negative zeta potential at that pH. The aggregation behavior of TiO<sub>2</sub> NPs clearly showed a DLVO-type interaction in the absence of DOM (Fig. 6.5). The increase of the electrolyte concentration led to a significant increase in the aggregation rate at relatively low concentration regime (i.e., < 10 mM), which was defined as slow aggregation regime. At this regime, the increase of electrolyte concentration provided more Na<sup>+</sup> ions to neutralize the negative surface charge, and thus decreased the electrostatic energy barrier between the negatively charged particles and increased the aggregation rate. At the higher concentration regime (> 100 mM), the electrolyte concentration was high enough to eliminate the energy barrier, and no significant change of the attachment efficiency was observed. This regime was comparatively defined as fast aggregation regime. The critical coagulation concentration (CCC) of NaCl for the TiO<sub>2</sub> NPs in this study was ca. 100 mM NaCl (Fig. 6.6a).

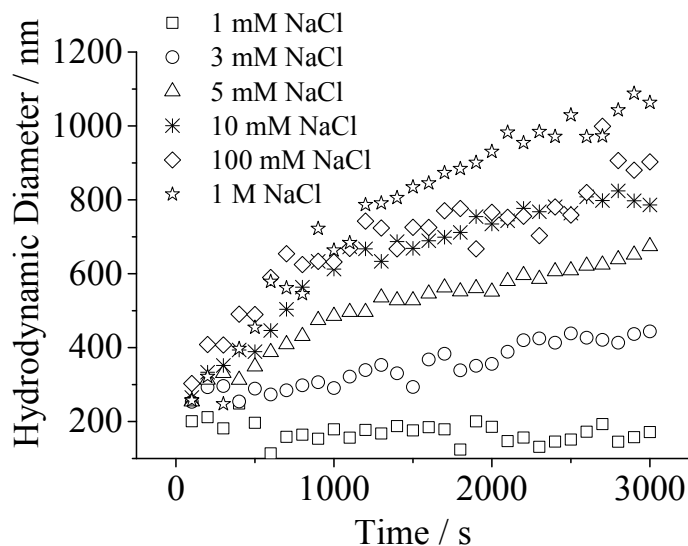


**Fig. 6.5** Aggregation profiles of TiO<sub>2</sub> NPs in the NaCl solution.

To explore the effects of different types of DOM on the TiO<sub>2</sub> NPs aggregation behavior, the attachment efficiencies and zeta potentials in the presence of HO10FA, SDS, BSA,  $\alpha$ -amylase and alginate as a function of NaCl concentrations was also examined (Fig. 6.6). Overall, the presence of DOM retards the aggregation rate of TiO<sub>2</sub> NPs. Among the model organic matter, BSA has the strongest effect with respect to slowing the TiO<sub>2</sub> NPs aggregation rate in the presence of monovalent electrolytes, followed by HO10FA, alginate, SDS and  $\alpha$ -amylase. Notably, no obvious aggregation was observed at the selected concentration range when BSA was added. Another protein model  $\alpha$ -amylase showed a slight stabilization effect on the aggregation behavior of TiO<sub>2</sub> NPs. When the NaCl concentration is lower than 100 mM, all the attachment efficiencies exhibited a negative value, which indicates that the presence of DOM lead to a partial fragmentation of TiO<sub>2</sub> NPs aggregation at low electrolyte concentration.

The zeta potential of TiO<sub>2</sub> NPs was more negative in the presence of BSA, suggesting that adsorbed BSA promoted abundant negative charges to balance the positive charge of Na<sup>+</sup>, and consequently increase the EDL repulsive energy. Similarly, the adsorption of HO10FA and alginate decreased the zeta potential of TiO<sub>2</sub> NPs, which is consistent with the results from previous work (Erhayem and Sohn 2014, Furman et al. 2013, Huangfu et al. 2013). The TiO<sub>2</sub> NPs also exhibited the negative charge and the zeta

potential decreased when SDS was added. A zeta potential plateau of  $-18 \pm 2.3$  mV was found at the low concentration regime of NaCl. By further increasing the Na<sup>+</sup> concentration, the zeta potential increased accordingly. Compared to BSA, the surface charge of TiO<sub>2</sub> NPs changed only slightly in the presence of  $\alpha$ -amylase. At the low concentration regime, the zeta potential exhibited a little less negative charge than that of the pure TiO<sub>2</sub> NPs suspension. With increase of the NaCl concentration, however, the zeta potential jumped and reached the PZC ultimately. Ahmad et al. reported that the stabilization effect of  $\alpha$ -amylase was observed at high protein concentration (protein concentration  $> 2$  mg mL<sup>-1</sup>) (Ahmad et al. 2015). Apparently, the concentration used for the paper was too low to reach the stabilization effect of  $\alpha$ -amylase. The same as natural organic compounds, the stabilization effect of HO10FA and alginate can't distinguish obviously due to the similar properties and same interaction mechanisms, which is in agreement with the previous research (Loosli et al. 2013).

Besides the electrostatic effect, it was previously reported that the steric repulsive force resulting from the adsorption of NOM on the NPs should be responsible for the increase of engineered NPs stability (Loosli et al. 2013, Saleh et al. 2010). BSA molecules, the most efficient model for TiO<sub>2</sub> NPs stabilization, are globular proteins with a tendency to spontaneously accumulate on surfaces (Saleh et al. 2010). The globular architecture of adsorbed BSA on the TiO<sub>2</sub> NPs surfaces induces longer-range steric repulsive forces compared to the relatively linear SDS, HO10FA and alginate macromolecules, thereby having a greater impact on retarding the NPs aggregation rate (Saleh et al. 2010). When a protein molecule is adsorbed to a surface, its parent structure is altered because of the surface attachment. It has been shown that attachment of BSA molecules on NPs surfaces provide enough dehydration of the amino acids within the protein structure and thereby provide a more compact globular structure after attachment (Norde and Anusiem 1992, Norde and Giacomelli 2000).

In addition, the adsorption properties of different DOM contributed the stabilization effect as well. The higher adsorption dosage of BSA onto the surface of TiO<sub>2</sub> NPs provided more negative charge to neutralize the positive charge of electrolyte. On the

6 Aggregation behavior of TiO<sub>2</sub> nanoparticles in aqueous solution: influence of different types of DOM under different pH values and electrolytes

contrary, same as the negative compound, SDS nearly lost this effect due to the weak adsorption.

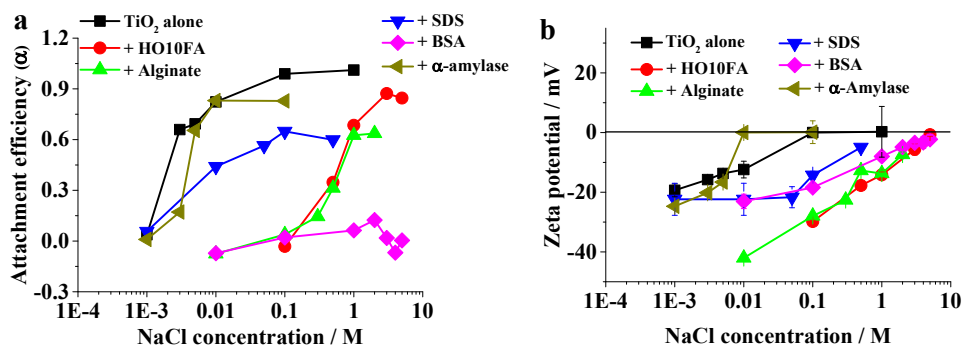


Fig. 6.6 Attachment efficiencies (a) and zeta potentials (b) of TiO<sub>2</sub> NPs as a function of NaCl concentrations in the absence and presence of different types of DOM ( $p(\text{DOC}) = 1 \text{ mg L}^{-1}$ ).

### 6.6 TiO<sub>2</sub> NPs aggregation kinetics in the presence of divalent cations

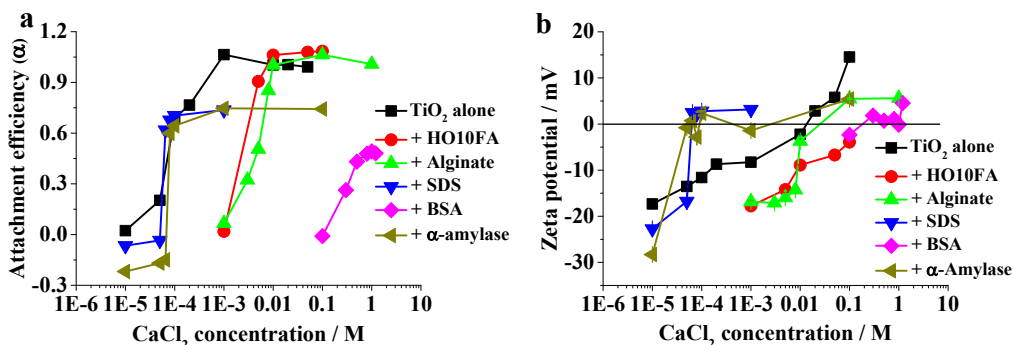


Fig.6.7 Attachment efficiencies (a) and zeta potentials (b) of TiO<sub>2</sub> NPs as a function of CaCl<sub>2</sub> concentrations in the absence and presence of different types of DOM ( $p(\text{DOC}) = 1 \text{ mg L}^{-1}$ ).

The attachment efficiencies and zeta potentials of TiO<sub>2</sub> NPs as a function of Ca<sup>2+</sup> concentration are presented in Fig. 6.7. In the absence of DOM, a DLVO type behavior is similar to that observed in the case of NaCl, with distinct slow and fast aggregation regimes. The estimated CCC value is ca. 1 mM CaCl<sub>2</sub>, 2 orders of magnitude lower than that of NaCl. The CCC values of TiO<sub>2</sub> NPs have a weak dependence on counterion valence. This dependence reflects the Schulze-Hardy rule, which states that the CCC varies as the inverse sixth power of the counter ion charge. The effects of different types

of DOM were also investigated and the data are shown in Fig. 6.7. Overall, the aggregation behavior in the presence of Ca<sup>2+</sup> ions with DOM is analogous to that observed with Na<sup>+</sup> ions. BSA exhibited the strongest retarding effect followed by alginate and HO10FA. The stability profiles in the presence of BSA, alginate, and HO10FA show similar trends compared to that of NaCl. One notable exception, however, is the enhanced aggregation of TiO<sub>2</sub> NPs in the presence of alginate and HO10FA at the fast regime. The recent studies suggested that the Ca<sup>2+</sup> were more effective in enhancing the aggregation of more hydrophobic and aromatic NOM fractions like humic substance (Tamamura et al. 2013, Wang et al. 2013b). It might result from the bridging effect of alginate and HO10FA on the enhanced aggregation behavior of TiO<sub>2</sub> NPs with Ca<sup>2+</sup>. It has been previously shown that Ca<sup>2+</sup> ions can bridge alginate molecules and cause the formation of alginate gel which results in improved aggregation (Chen and Elimelech 2006, 2007). This calcium bridging has also been observed for fullerene nanoparticles in the presence of humic substances and high Ca<sup>2+</sup> concentrations (Chen and Elimelech 2007). SDS and  $\alpha$ -amylase had the weakest impact on TiO<sub>2</sub> NPs aggregation, and the CCC values shifted to the lower CaCl<sub>2</sub> concentration and the favorable attachment efficiencies were lower than 1 in the presence of both SDS and  $\alpha$ -amylase. In the presence of SDS, the zeta potential jumped significantly in the low concentration regime and kept a stable and positive value of  $4 \pm 1.1$  mV when the Ca<sup>2+</sup> concentration was higher than 100  $\mu$ M. The tendency of the zeta potential indicates the primary electrostatic effect.

## 6.7 Image analysis

TEM images were taken as tool to prove the existence of calcium-alginate bridge between TiO<sub>2</sub> NPs. The samples were prepared under the given conditions and stewed on the table after the preparation. The image was taken after different stewing time. It is apparent that in the presence of alginate and CaCl<sub>2</sub>, the TiO<sub>2</sub> aggregations were covered by alginate (Fig. 6.8a to d) compared to the sample in the presence of Ca<sup>2+</sup> alone (Fig. 6.8e), and some obvious calcium-alginate bridges were observed after 15 min of

## 6 Aggregation behavior of TiO<sub>2</sub> nanoparticles in aqueous solution: influence of different types of DOM under different pH values and electrolytes

preparation (Fig. 6.8b). The images revealed that calcium-alginate bridge promotes the formation of aggregation. After 5 min of preparation (Fig. 6.8a), some small aggregations with the size about 100 nm were connected by the alginate. With the increase of stewing time, the small aggregations closed gradually to form large and compact aggregations (Fig. 6.8c and d), and the large eye-catching aggregations were formed ultimately (Fig. 6.9a left bottle). While, in the case of only alginate was added, the TiO<sub>2</sub> aggregations were covered by alginate and dispersed with the size of 100 nm (Fig. 6.8f).

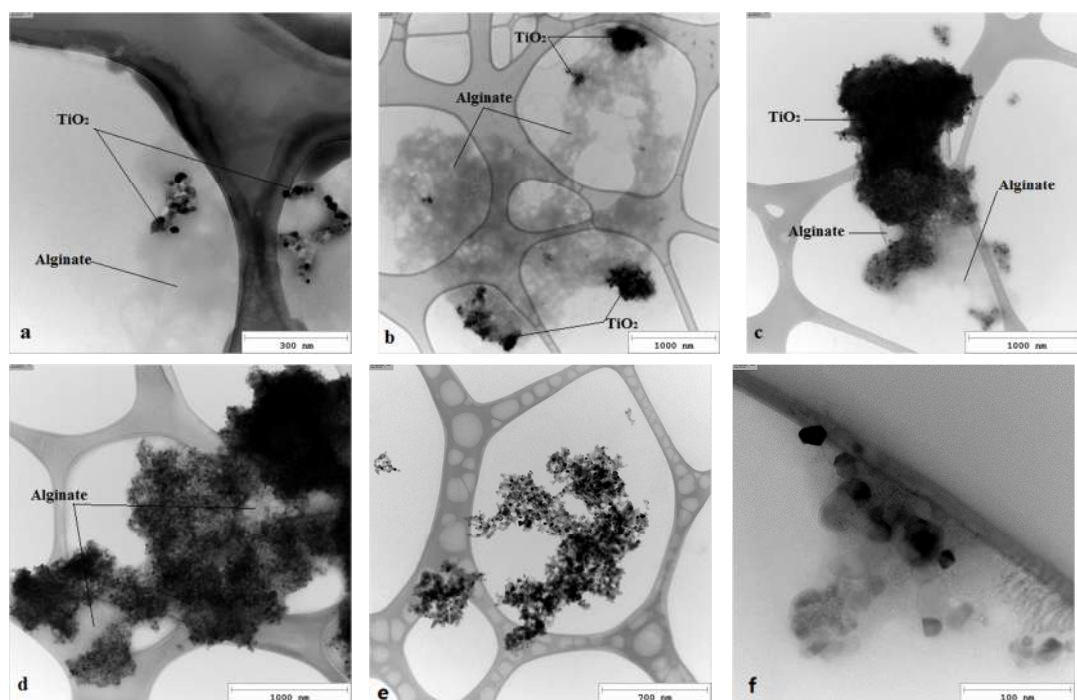


**Fig. 6.8 (a) to (d): TEM images of TiO<sub>2</sub> (20 mg L<sup>-1</sup>) aggregates in the presence of alginate ( $\rho(\text{DOC}) = 1 \text{ mg L}^{-1}$ ) + CaCl<sub>2</sub> (0.1 M) after different stewing time (a: 5 min; b: a 15 min; c: 30 min; d: 60 min); (e): TEM images of TiO<sub>2</sub> (20 mg L<sup>-1</sup>) aggregates in the presence of CaCl<sub>2</sub> (0.1 M), 30 min after preparation. (f): TEM images of TiO<sub>2</sub> (20 mg L<sup>-1</sup>) aggregates in the presence of alginate ( $\rho(\text{DOC}) = 1 \text{ mg L}^{-1}$ ), 30 min after preparation.**

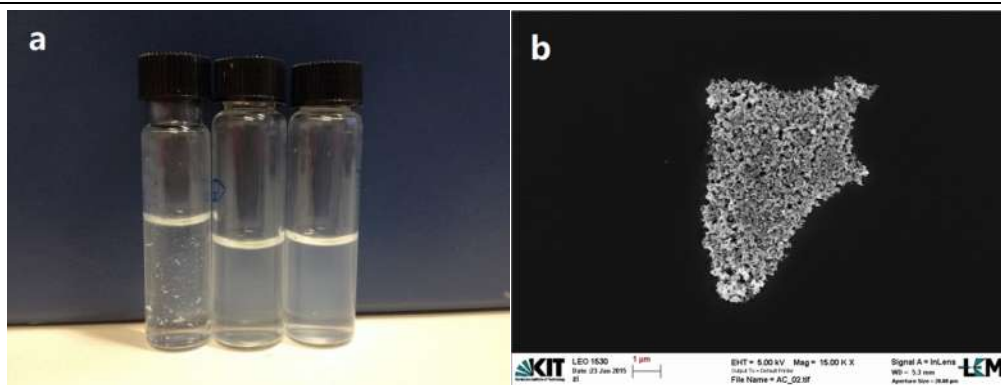


**Fig. 6.9 (a):** photographs of TiO<sub>2</sub> (20 mg L<sup>-1</sup>) aggregates, 1 h after preparation (Left: in the presence of alginate ( $\rho(\text{DOC}) = 1 \text{ mg L}^{-1}$ ) + CaCl<sub>2</sub> (0.1 M); Middle: in the presence of CaCl<sub>2</sub> (0.1 M); Right: in the presence of alginate ( $\rho(\text{DOC}) = 1 \text{ mg L}^{-1}$ )); (b): SEM image of TiO<sub>2</sub> (20 mg L<sup>-1</sup>) aggregates, in the presence of alginate ( $\rho(\text{DOC}) = 1 \text{ mg L}^{-1}$ ) + CaCl<sub>2</sub> (0.1 M), 1 h after preparation.

## 6.8 Conclusions

Results from this study suggest that TiO<sub>2</sub> NPs can be relatively stable in the aquatic environment. The TiO<sub>2</sub> NPs aggregation rate was significantly decreased in the presence of NOM (BSA, HO10FA and alginate) under the selected pH range, which is ubiquitous in aquatic environments including wastewater, therefore enhancing their transport and mobility upon release. BSA had the strongest effect with respect to slowing the TiO<sub>2</sub> aggregation rate in the presence of both monovalent and divalent electrolytes owing to the synergistic electrostatic effect, steric repulsive effect and high adsorption property. On the contrary, no stabilization effects of SDS and  $\alpha$ -amylase were obvious. Calcium bridges were found in the presence of alginate and CaCl<sub>2</sub> at the fast aggregation regime, which promoted to form large eye-catching and compact aggregations. The results demonstrate that the presence of biopolymers (alginate and BSA) and HO10FA can enhance the stability of TiO<sub>2</sub> NPs even at high salt concentrations, thereby having significant environmental and biological implications. Furthermore, TiO<sub>2</sub> NPs will most likely interact with suspended and colloidal particles and mineral surfaces in aquatic environments. For a profound understanding, further aggregation studies of TiO<sub>2</sub> NPs in



6 Aggregation behavior of TiO<sub>2</sub> nanoparticles in aqueous solution: influence of different types of DOM under different pH values and electrolytes

---

the presence of environmentally relevant particles are need.

## 7 Multi-cycle photocatalytic degradation of bezafibrate (BZF) by polyvinyl alcohol/TiO<sub>2</sub> (PVA/TiO<sub>2</sub>) film

In wastewater treatment processes, TiO<sub>2</sub> NPs have been mostly used in heterogeneous suspension which led to an increased release of TiO<sub>2</sub> NPs into the environment (Irawaty et al. 2011). The work presented in Chapter 6 has indicated the high electrophoretic mobility of TiO<sub>2</sub> NPs under the aquatic environmental conditions and the potential environmental and health impacts of TiO<sub>2</sub> NPs have been proven (Gottschalk et al. 2009, Ju-Nam and Lead 2008). Here we reported an easy and efficient method for the immobilization of TiO<sub>2</sub> in PVA films to decrease the release of TiO<sub>2</sub> NPs and increase the multi-cycle use of the TiO<sub>2</sub> photocatalyst.

Bezafibrate (BZF), a lipid-lowering agent, was chosen as the target. It is recalcitrant to biological wastewater treatment (< 10%) or to membrane bioreactor treatment (< 20%) (Choi et al. 2012, Maeng et al. 2013, Tang et al. 2014). As a result of its wide use, unmetabolized BZF is released into the environment with potential toxic effects for aquatic living organisms (Calamari et al. 2003, Contardo-Jara et al. 2011). Hence elimination of BZF by means of physical chemical process has become a ubiquitous topic.

### 7.1 Characteristics

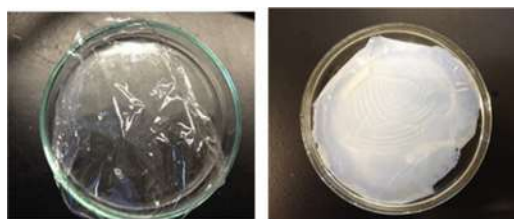
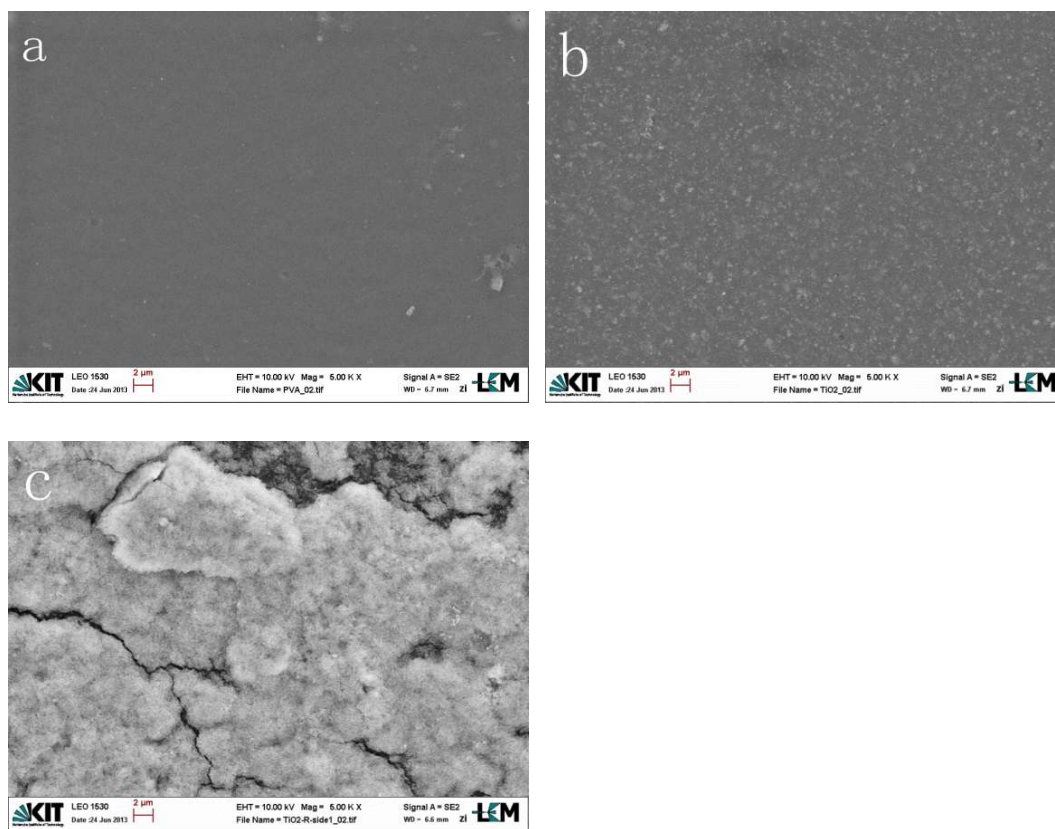


Fig. 7.1 Photographs of the PAV film (left) and the PVA/TiO<sub>2</sub> film (right)

Typical photographs of the PVA film and the PVA/TiO<sub>2</sub> hybrid film are shown in Fig. 7.1. Visual observation proposed that TiO<sub>2</sub> nanoparticles were uniformly distribute

## 7 Multi-cycle photocatalytic degradation of bezafibrate (BZF) by polyvinyl alcohol /TiO<sub>2</sub> (PVA/TiO<sub>2</sub>) film

in the PVA film, and reduced the transmission of the film significantly. The further morphologies of the pure PVA film and of the PVA/TiO<sub>2</sub> hybrid film (before and after irradiation) are shown in Fig. 7.2. In addition to the low resolution of the photograph, the SEM image of the PVA/TiO<sub>2</sub> hybrid film (Fig. 7.2b) displays the even distribution of the individual TiO<sub>2</sub> aggregates in the film. It is evident that the irradiated PVA/TiO<sub>2</sub> film (Fig. 7.3c) has a fairly rough surface and microporous structure, which may be due to the partly degradation of PVA by the exposure of TiO<sub>2</sub> particles to irradiation.



**Fig. 7.2 SEM images of the surface of the PVA film (a), the unirradiated PVA/TiO<sub>2</sub> film (b) and the irradiated PVA/TiO<sub>2</sub> film (c)**

To confirm the immobilization of TiO<sub>2</sub> nanoparticle in the PVA matrix, ATR-FTIR spectra were used. Fig. 7.3 shows the infrared spectra of the pure PVA film and the hybrid films. Expectedly the spectra of PVA/TiO<sub>2</sub> and that of PVA are quite similar, suggesting the typical characteristics of a simple physical solution-blending between the two components (Lei et al. 2012). In the spectra, the -CH<sub>2</sub> group at 1417 cm<sup>-1</sup>, O-H bending vibration at 1325 cm<sup>-1</sup> and C-O-C stretching vibration at 1087 and 916 cm<sup>-1</sup> are

clearly observed. Obviously, the band at 821 cm<sup>-1</sup>, which is assigned to skeletal vibrations of -C-C- bonds, appear only as a shoulder in the PVA/TiO<sub>2</sub> spectra, due to the change in the chemical environment caused by the formation of Ti-O-C bonds (Lei et al. 2012, Sakthivel and Kisch 2003). However, No band characteristic for Ti-O-C (at 450 to 800 cm<sup>-1</sup> (Abd El-kader et al. 2013)) can be assigned in the PVA/TiO<sub>2</sub> film. It might have shifted to lower wave number and is part of the strong band there. In addition, it can be expected that the contribution to that band is relatively weak due to low percentage of TiO<sub>2</sub> in the total film. The interpretation of the spectra and the relative intensities of the bands support the formation of covalent Ti-O-C bonds between PVA and TiO<sub>2</sub> nanoparticles, which results to the immobilization of TiO<sub>2</sub> nanoparticles in the PVA matrix.

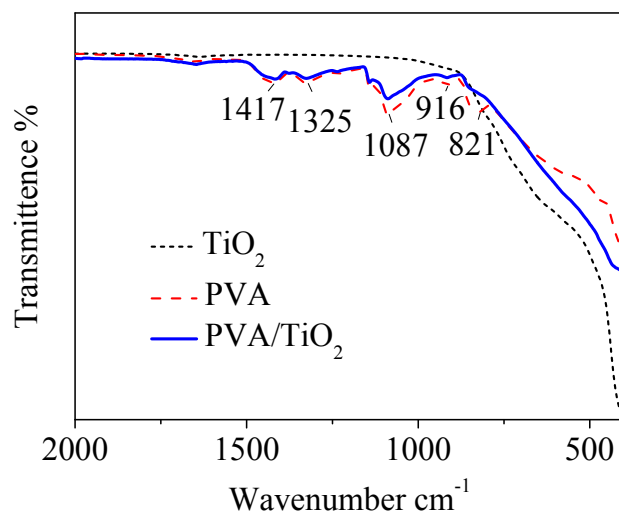


**Fig. 7.3 ATR-FTIR spectra of TiO<sub>2</sub>, the pure PVA film and the PVA/TiO<sub>2</sub> hybrid film.**

Fig. 7.4 shows DSC curves of the PVA and PVA/TiO<sub>2</sub> films. The DSC curve of the PVA film has shown an endotherm with an onset at 218°C and the melting point around 229°C. The decrease of the melting point for the PVA/TiO<sub>2</sub> hybrid film suggests that the crystallinity and perfection of the crystal structure of PVA/TiO<sub>2</sub> film were increased in the presence of TiO<sub>2</sub>.

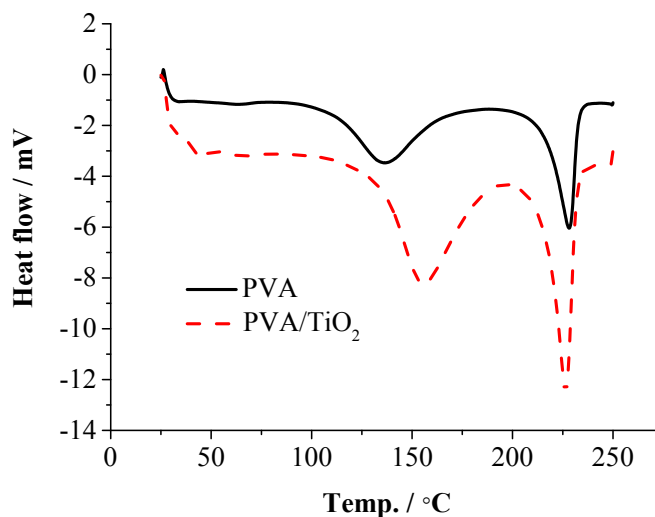


Fig. 7.4 DSC thermograms of the PVA and hybrid PVA/TiO<sub>2</sub> films.

The swelling ability of the PVA and PVA/TiO<sub>2</sub> hybrid film is shown in Table 7.1. It is obvious that the PVA/TiO<sub>2</sub> hybrid film showed a higher swelling ability than the pure PVA film at different pH conditions. It might result from the increase of the cross-linking in the hybrid PVA/TiO<sub>2</sub> film (Sairam et al. 2006). PVA contains large number of -OH groups. At high temperature, Ti-OH groups on the surface of TiO<sub>2</sub> can react with the -OH groups linking to the PVA chains. Dehydration and condensation reactions occur between both the -OH groups. A strong interfacial bond Ti-O-C can be formed on the surface of TiO<sub>2</sub>, leading to form ordered and denser crystalline regions in the PVA/TiO<sub>2</sub> film (Hassan and Peppas 2000, Liu et al. 2010b). The crystalline regions and Ti-O-C bonds serve as physical and chemical crosslinking points, respectively. The highly crosslinked structure cannot be expanded and it holds a large quantity of water (Hosseinzadeh 2013).

Table 7.1 Swelling degree (DS %) for the PVA and PVA/TiO<sub>2</sub> film

pH	DS / %	
	PVA	PVA/TiO <sub>2</sub>
4.2	77	106
6.9	183	204
9.2	71	82

(b) Effect of film thickness (pH = 6.9)

Film	Thickness / $\mu\text{m}$	DS/%
PAV/TiO <sub>2</sub>	40~50	197
	60	157
	80	154
	>80	204

## 7.2 Stability of the PVA/TiO<sub>2</sub> film

Table 7.2 Weight loss and TiO<sub>2</sub> release under different irradiation conditions

Sample	pH	Weight loss (%)		$\rho(\text{Ti}^{4+}) / \mu\text{g L}^{-1}$	
		24 h	48 h	24 h	48 h
PAV/TiO <sub>2</sub>	4.2	13.3	15.1	62	77
	6.9	10.1	10.9	< 5	< 5
	9.2	< 1	< 1	< 5	< 5

All the samples were irradiated under a 1000-W Xe short-arc lamp for 48 h. The initial weight for each sample was 0.05 g, which contains 10 wt.% TiO<sub>2</sub>. The volume of solution was 40 mL.

The remobilization of TiO<sub>2</sub> nanoparticles from the PVA/TiO<sub>2</sub> film during the reaction time is of great importance to the photocatalytic efficiency. For the evaluation of the effective immobilization of TiO<sub>2</sub>, UV irradiation was applied for 48 h (Table 7.2). The initial total weight of the film was 100 mg, containing 10 mg TiO<sub>2</sub> and 90 mg PVA. The solution volume was 40 mL. After 24 h of irradiation, the total weight decreased for 13.3% and 10.1% at pH of 4.2 and 6.9 respectively. With increase further irradiation time, the total weight decreased for 15.1% and 10.9% at pH of 4.2 and 6.9 respectively after 48 h of irradiation. Apparently, the weight loss rate decreased with the increase of irradiation time. Compared to the total weight loss, the weight loss of TiO<sub>2</sub> is negligible. Furthermore the relatively small weight loss in alkaline solution reveals a protective effect on the PVA film under irradiation. The results support the conclusion by Hsu et al. (Hsu et al. 2011) who reported that the photocatalytic degradation rate of PVA decreased

with the increase of pH value. For neutral and alkaline condition no significant concentrations of mobilized Ti were determined, which can be explained by the strong Ti-O-C chemical bonds. However, acidic conditions decreased the stability of the Ti-O-C bonds. They can be destroyed in the presence of H<sup>+</sup> which results in a TiO<sub>2</sub> release into the solution.

### 7.3 Photocatalytic activity of the PVA/TiO<sub>2</sub> film

#### 7.3.1 Effect of thickness

Table 7.1b shows that the thickness of the PVA/TiO<sub>2</sub> film affected its swelling degree which was also expected to influence the photocatalytic activity. The thickness can also affect the TiO<sub>2</sub> distribution and the surface area of the hybrid film. The photocatalysis of BZF using 40 μm, 60 μm, 80 μm and > 80 μm films were carried out (Fig. 7.5). No significant influence of thickness was observed with the exception of the > 80 μm film showed a slightly higher activity. This might result from that a higher and relative constant swelling degree contributes to a higher photocatalytic activity due to the better enwrapping of TiO<sub>2</sub> in the matrix (Lei et al. 2012).

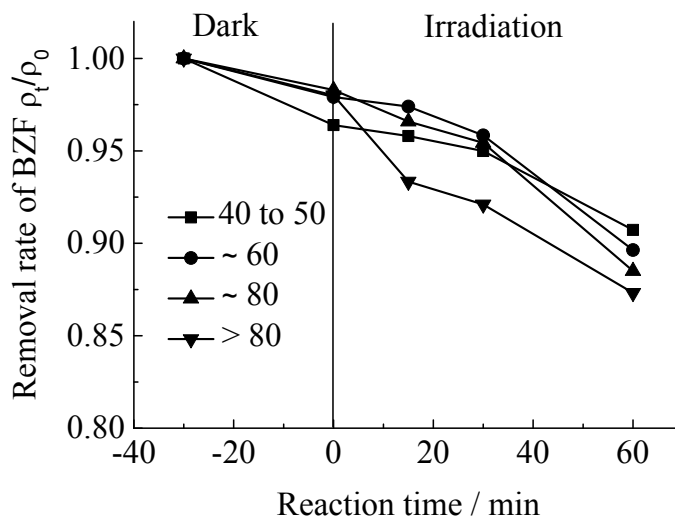


Fig. 7.5 Effect of film thickness (μm) on the photocatalytic degradation of BZF ( $\rho$  (TiO<sub>2</sub>) = 1 g L<sup>-1</sup>,  $\rho_0$  (BZF) = 10 mg L<sup>-1</sup>, pH = 6.3)

However, all the new hybrid films showed a quite low photocatalytic activity. Despite a relatively large amount of TiO<sub>2</sub> can be clearly observed by SEM, only less than 10% of BZF was eliminated after 1 h of irradiation, which suggested that most of TiO<sub>2</sub> nanoparticles were inlaid in the inner PVA film. It is reasonable to assume that the outside of the PVA film functioned as an electron acceptor and by this resists to the electron transfer from TiO<sub>2</sub> to the BZF molecules.

### 7.3.2 Effect of film age

In spite of the low photocatalytic efficiency of the virgin PVA/TiO<sub>2</sub> film, the SEM results pointed towards the possibility for multi-use of the hybrid film. As was mentioned in Section 7.1, the hidden TiO<sub>2</sub> particles were exposed after irradiation, which was expected to promote the photocatalytic activity of the hybrid film with increased irradiation time.

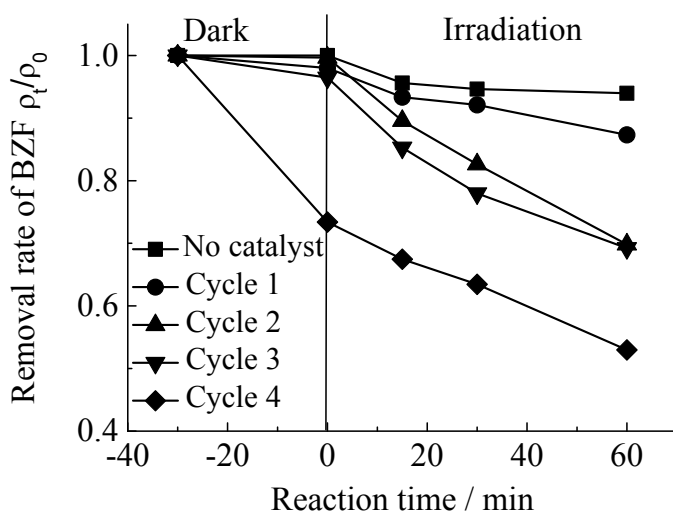


Fig. 7.6 Effect of usage age of the PVA/TiO<sub>2</sub> film on the photocatalytic degradation of BZF ( $\rho$  (TiO<sub>2</sub>) = 1 g L<sup>-1</sup>,  $\rho_0$  (BZF) = 10 mg L<sup>-1</sup>, pH = 6.3)

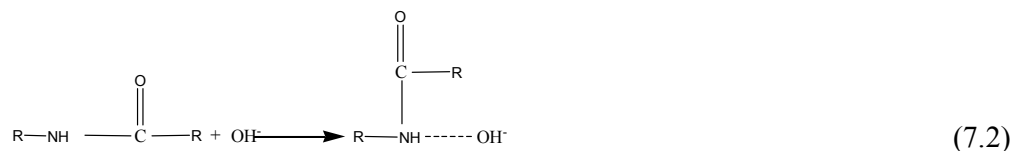
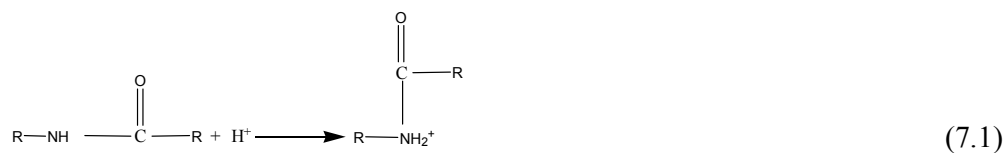
The degradation rates of BZF for the increased reuse cycle of the PVA/TiO<sub>2</sub> film are given in Fig. 7.6. After each cycle, the used film was washed with ultrapure water until no BZF was detected in the rinse solution. A significantly increased degradation rate of BZF was obvious with increase of recycle number of the PVA/TiO<sub>2</sub> film. For the 4<sup>th</sup>



cycle, a higher preadsorption capacity of the PVA/TiO<sub>2</sub> film was observed as well. These results exhibited a strong evidence for our hypothesis. For the new PVA/TiO<sub>2</sub> film, the inlaid TiO<sub>2</sub> can't receive UV irradiation efficiently which led to the lower photocatalytic activity. With the initiation of irradiation, the surface PVA film was degraded by the photolysis and TiO<sub>2</sub> exposed to the surface and generated electron/hole pairs. The contact of TiO<sub>2</sub> with water also applied a plenty of opportunities to form •OH radicals which can oxidize organic matter in the solution efficiently. With the increase of irradiation time, the photocatalytic activity of the PVA/TiO<sub>2</sub> hybrid film increased owing to the continuous exposed TiO<sub>2</sub>.

### 7.3.3 Effect of pH

BZF photocatalytic elimination rates at the pH values of 4.2, 6.9 and 9.2 are given in Fig. 7.7. Before the experiments, the PVA/TiO<sub>2</sub> films had been irradiated with a 1000 W Xe short-arc lamp (detail in Section 3.3.1.2) for 4 h to achieve a higher photocatalytic activity. The results showed that both of the acid and alkaline pH values enhanced the preadsorption capacity of the PVA/TiO<sub>2</sub> film. At lower pH condition, TiO<sub>2</sub> displayed a positive surface by adsorbing H<sup>+</sup>, which can easily react with the -NHCOR group of BZF to form an organic cation according to Eq. 7.1 (Wang et al. 2014b). At higher pH value, OH<sup>-</sup> ions can reaction on the surface of the PVA film with the -NHCOR group via hydrogen bonds according to Eq. 7.2 (Jin and Bai 2002).



The PVA/TiO<sub>2</sub> film exhibited higher photocatalytic efficiency under acid conditions compared to the one under neutral condition (pH of 6.9). No degradation of BZF after adsorption was observed under alkaline solution. The results can be explained by two

synergistic reasons showed by many researchers: (a) the photocatalytic degradation rate of organic matter by TiO<sub>2</sub> decrease with the increase of pH, owing to the increase of the band gap (Molea et al. 2014) and weak electrostatic interactions (Chu et al. 2007, Haroune et al. 2014, Ke et al. 2010); (b) the degradation of PVA decrease with the increase of pH (Hsu et al. 2011), which causes the decrease of the amount of exposed TiO<sub>2</sub> accordingly.

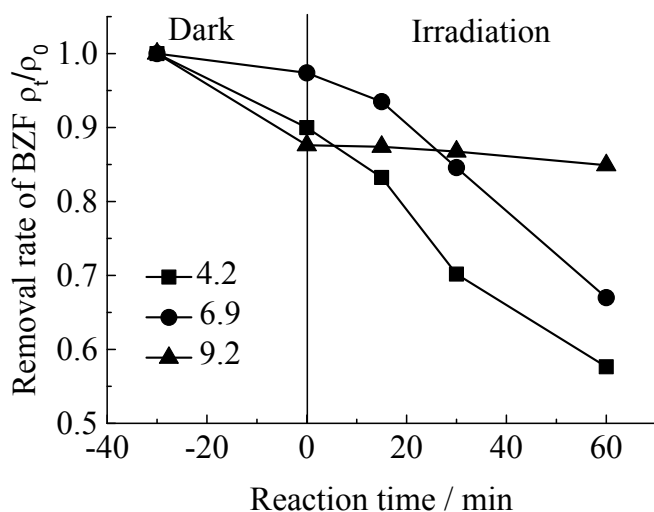


Fig. 7.7 Effect of pH value on the photocatalytic degradation of BZF ( $\rho(\text{TiO}_2) = 1 \text{ g L}^{-1}$ ,  $\rho_0(\text{BZF}) = 10 \text{ mg L}^{-1}$ )

#### 7.4 Comparison study of the immobilized TiO<sub>2</sub> for long term use

The multi-cycling of PVA/TiO<sub>2</sub> hybrid films, pumice/TiO<sub>2</sub>, porous glass bead/TiO<sub>2</sub> and P25 suspension was evaluated by means of the final removal rate (after 1 h of irradiation) of BZF degradation during continuous cycle use, and the results are presented in Fig. 7.8. An increased photocatalytic efficiency of the PVA/TiO<sub>2</sub> film during 8 cycles was clearly observed, probably to the sufficient TiO<sub>2</sub> amount of exposed with irradiation time. After 8 cycles, the photocatalytic efficiency remains constant which is in agreement with the decreased weight loss rate. The results indicate that the surface PVA film was degraded completely within 8 cycles, and no increased amount of TiO<sub>2</sub> was exposed in the latter cycles. The P25 suspension exhibited the highest efficiency at the

first cycle, but the efficiency decreased with the increase of reuse cycle owing to the hydrodynamic loss of TiO<sub>2</sub> during the reuse. The pumice/TiO<sub>2</sub> and porous glass bead/TiO<sub>2</sub> composition displayed the much lower photocatalytic activity. The decreased tendency of the efficiency of pumice/TiO<sub>2</sub> and porous glass bead/TiO<sub>2</sub> was also observed with increased number of reuse cycle.

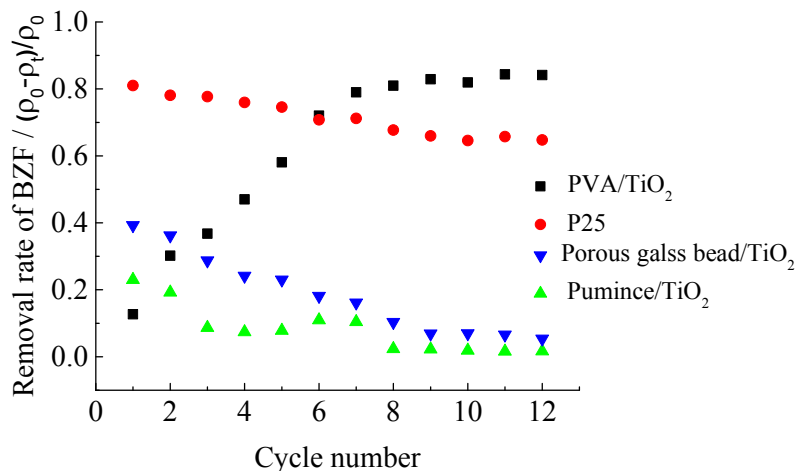


Fig. 7.8 Comparison of the photocatalytic activity of the PVA/TiO<sub>2</sub> film with P25 suspension, pumice/TiO<sub>2</sub> and porous glass bead/TiO<sub>2</sub> for the photocatalytic degradation of BZF ( $\rho$  (TiO<sub>2</sub>) = 1 g L<sup>-1</sup>,  $\rho_0$  (BZF) = 10 mg L<sup>-1</sup>, pH = 6.3)

## 7.5 Application prospect of hybrid PVA/TiO<sub>2</sub> film

Although the photocatalysis by using TiO<sub>2</sub> suspension is a so called green advanced oxidation process, it is difficult to avoid it releases into the environment even by using powder activity carbon as sorbent and subsequent ultrafiltration process (Ziegmann et al. 2010). The risk of released TiO<sub>2</sub> nanoparticles is already reported (Dankovic et al. 2007) which made this catalyst is not absolutely green. In addition, the high operation cost of membrane filtration and the damage of the membrane material caused by the abrasion of TiO<sub>2</sub> nanoparticles (Ziegmann et al. 2010) become an enormous resistance of the widely application of heterogeneous photocatalysis based on the TiO<sub>2</sub> suspension.

As discussed above, PVA/TiO<sub>2</sub> hybrid film not only retains higher efficiency for

BZF degradation compared to other immobilized composition but also possesses high stability and sufficient recyclability. In addition, the main advantages of PVA/TiO<sub>2</sub> hybrid film are its simplicity of separation and striking possibility of long-term use which reduces operation cost extremely. It suggested that the PVA/TiO<sub>2</sub> hybrid film is more suitable for long-term use in the degradation of pollutants e.g. in wastewater. Concerning about the operation of the real wastewater plant, more detail work about the influence of environmental relative conditions (ions and natural organic matter content in the solution) and design of continued operation should be studied in the further. In addition, new synthesis methods to achieve PVA/TiO<sub>2</sub> film with higher photocatalytic activity under visible light irradiation are worthy to be studied.

## 7.6 Conclusions

An easy and efficient method for the immobilization of TiO<sub>2</sub> in PVA films (Ti-O-C bond formation) provided a highly active and recyclable photocatalyst for water purification without depth filtration demand. The photocatalytic tests for the degradation of BZF underlined the good photocatalytic activity of the PVA/TiO<sub>2</sub> film. Since the photocatalytic degradation efficiency increased with increase of reuse cycles, this points towards an economically and ecologically attractive application of this hybrid photocatalyst. Technically the hybrid PVA/TiO<sub>2</sub> film was fairly stable under long-term irradiation of the work: weight loss rate of the hybrid film decreased with the increase of irradiation time and no major release of TiO<sub>2</sub> was observed. Comparing the photocatalytic activity with P25 suspension and other immobilized TiO<sub>2</sub> composites (pumice/TiO<sub>2</sub> and porous glass bead/TiO<sub>2</sub>), the PVA/TiO<sub>2</sub> hybrid film opens the door of a promising application of photocatalysis in wastewater treatment.

## 8 Summary and outlook

The work described here adds to a better understanding of the application of TiO<sub>2</sub> based NPs in photocatalytic processes under environmentally relevant conditions and its aggregation behavior in the aquatic environment. The development of a novel immobilization method of TiO<sub>2</sub> serves the aim of a decreasing release of TiO<sub>2</sub> NPs into the environment by increasing the multi-cycle use of TiO<sub>2</sub> as photocatalyst.

### 8.1 Photocatalytic degradation of pharmaceutically active compounds by Pt/TiO<sub>2</sub> under environmentally relevant conditions

First, the photocatalytic degradation of two pharmaceutically active compounds (PhACs): carbamazepine (CBZ) and clofibric acid (CA) by Pt/TiO<sub>2</sub> nanoparticles was investigated. The basic effects such as pH, metal ions, and natural organic matter (NOM) content on the reaction rate constants were used to imitate the aquatic environmental conditions and the requirements of water and wastewater treatment.

Photocatalytic degradation of PhACs was strongly affected by the environmentally relevant conditions (e.g. pH, NOM, metal ions and etc.) and the character of the targeted compounds. The studied parameters may have different, even opposite, effects on the efficiency and kinetics of the photocatalytic degradation when comparing CBZ with CA. For instance, the increase of pH values exhibited enhanced photocatalytic degradation for the neutral CBZ molecules, but didn't contribute significantly on the photocatalytic degradation of the anionic compound CA.

Results demonstrate that the presence of NOM is the most restrictive parameter for the application of photocatalysis in wastewater treatment plants and in environment. Some attempts were done to eliminate this inhibitory NOM effect in this work. In the case of lower DOC concentration (from NOM), the addition of metal ions (Fe(III), Zn<sup>2+</sup>

and  $\text{Ca}^{2+}$ ) showed an enhancement of the photocatalytic degradation rate constant for both CBZ and CA in relation to what was observed with NOM and no cations. However, in the presence of higher DOC concentrations (from NOM,  $> 1.6 \text{ mg L}^{-1}$ ), the added metal ions did not show a significant enhancement effect to balance the inhibition effect of NOM.

Furthermore, the effect of dissolved oxygen (DO) on the elimination of the inhibitory NOM effect was investigated. For these experiments, different gases ( $\text{N}_2$ , air and  $\text{O}_2$ ) were purged into the photocatalytic system. The results indicate that DO in the photocatalytic system was an efficient parameter to eliminate the inhibitory NOM effect. With increase of the DO concentration, the inhibitory effect of NOM decreased significantly. An increased effect of NOM was even observed in the case of low DOC concentrations (from NOM) at air purging. The SEC-DOC results suggested that larger molecular sized fractions are predominant during the whole process in the absence of DO, while lower molecular sized fractions predominate after the first few minutes of air and  $\text{O}_2$  purging owing to the oxidation of higher molecular sized fractions. The inhibitory effect of NOM is more dependent on the molecular size of NOM than on its concentration. High molecular sized NOM fractions with high aromaticity are more easily adsorbed onto the catalyst particles and act as an electron-hole scavenger and a light filter, reducing the photocatalytic degradation rate. In contrast, the lower molecular sized NOM fractions cause less inhibition of the degradation reaction.

An example study was given to evaluate the relationship among DO, metal ions and NOM in the photocatalytic process. A full factorial design was used for photocatalytic degradation of diatrizoate (DA) and  $\text{I}^-$  formation in the presence of different concentration of DO, NOM and metal ions. The experimental design results showed that the degradation of DA was strongly affected by the amount of DO present and by the presence of metal ions. Increasing the DO concentration and decreasing the metal ions concentration leads to the highest reaction rate constant of the photocatalytic degradation of DA. The DO concentration and NOM had the most intense influence on  $\text{I}^-$  formation, and the simultaneous increase of both factors lead to the highest  $\text{I}^-$  formation. The

empirical models were developed for DA elimination and  $I^-$  formation, and the high  $R^2$  values signify that the model obtained is able to give a reasonably good estimate of response for the system in the range studied.

## **8.2 Aggregation behavior of $TiO_2$ nanoparticles in aquatic solution: influence of different types of DOM under different pH values and electrolytes**

The increasing application of  $TiO_2$  NPs in consumer goods and industrial production has led to an increase of research about their aggregation behavior in the aquatic system. Aggregation of  $TiO_2$  NPs was evaluated in the presence of different types of dissolved organic matter (DOM) — Hohloh Lake 10 fulvic acid (HO10FA), alginate, bovine serum albumin (BSA),  $\alpha$ -amylase and sodium dodecylbenzene sulfonate (SDS) under different pH and electrolytes.

The results suggest that  $TiO_2$  NPs can be relatively stable in aquatic environments, and their aggregation behavior exhibited a DLVO-type interaction in the absence of DOM. Under the selected pH range ( $2.5 < \text{pH} < 11$ ), the  $TiO_2$  NPs aggregation rate was significantly decreased in the presence of NOM (BSA, HO10FA and alginate), which are ubiquitous in aquatic environments. Enhancement of transport and mobility of  $TiO_2$  is a consequence. BSA had the strongest effect with respect to slowing down the  $TiO_2$  aggregation rate in the presence of both monovalent and divalent electrolytes owing to the synergistic electrostatic effect and steric repulsive effect. On the contrary, the stabilization effects of SDS and  $\alpha$ -amylase were not observed. Calcium bridges were found in the presence of alginate and  $CaCl_2$  at the fast aggregation regime, which promoted to form large eye-catching and compact aggregations. The finding demonstrates that the presence of biopolymer (alginate and BSA) and HO10FA can enhance the stability of  $TiO_2$  NPs even at high salt concentrations, thereby having significant environmental and biological implications.

### **8.3 Multi-cycle photocatalytic degradation of bezafibrate by polyvinyl alcohol/TiO<sub>2</sub> (PVA/TiO<sub>2</sub>) film**

In this work an easy and efficient method for the immobilization of TiO<sub>2</sub> in PVA films (Ti-O-C bond formation) was developed. The PVA/TiO<sub>2</sub> hybrid film provided a highly active and recyclable photocatalyst for water purification without depth filtration demand. The photocatalytic tests for the degradation of bezafibrate (BZF) underlined the good photocatalytic activity of the PVA/TiO<sub>2</sub> film. The photocatalytic degradation efficiency increased with increase of the number of reuse cycles (7 times increase after 8 reuse cycles), this points towards an economically and ecologically attractive application of hybrid photocatalysts. Technically the hybrid PVA/TiO<sub>2</sub> film was fairly stable under long-term irradiation: weight loss rate of the hybrid film decreased with the increase of irradiation time and no release of TiO<sub>2</sub> was observed. Comparing the photocatalytic activity with the one for P25 suspension and other immobilized TiO<sub>2</sub> composition (pumice/TiO<sub>2</sub> and porous glass bead/TiO<sub>2</sub>), the PVA/TiO<sub>2</sub> hybrid film is the most promising and opens the door for a broad application of photocatalysis in wastewater treatment.

### **8.4 Outlook**

The present study demonstrates that the degradation rate in heterogeneous photocatalysis is strongly affected by the environmentally relevant conditions (e.g. pH, NOM content and inorganic ions content). NOM showed the greatest deactivation effect caused by adsorption, which is critical for the design of practical treatment systems. To obtain widespread application of TiO<sub>2</sub> in photocatalysis for real wastewater treatment, a novel approach of TiO<sub>2</sub> modification has to be developed to modify and improve the surface properties of the photocatalyst and to resist the deactivation effect of NOM. In this study, the inhibitory effect of NOM significantly decreased with the increase of DO concentration, and an increased photocatalytic degradation rate was observed in the presence of low DOC concentrations (from NOM, < 1.6 mg L<sup>-1</sup>), which applies a new



direction for the design of wastewater treatment plant operation to optimize the technologies and reaction conditions. Additionally, to separate and reuse the TiO<sub>2</sub> catalyst, novel immobilization technique could be developed.

The particular aggregation and stability behavior of TiO<sub>2</sub> NPs in the presence of different types of DOM were shown. Further aggregation studies of TiO<sub>2</sub> NPs in the presence of environmentally relevant particles (colloidal, minerals and etc.) are highly recommended.

## 9 References

Abbt-Braun, G., Frimmel, F.H. and Lipp, P. (1991) Isolation of Organic Substance from Aquatic and Terrestrial Systems- Comparison of some Methods. *Z. Wasser-Abwasser-Forsch* 24, 285-292.

Abd El-kader, F., Hakeem, N.A., Elashmawi, I.S. and Ismail, A.M. (2013) Enhancement of structural and thermal properties of PEO/PVA blend embedded with TiO<sub>2</sub> nanoparticles. *In. J. Phys.* 87(10), 983-990.

Abd El-Rehim, H.A., Hegazy, E.-S.A. and Diaa, D.A. (2012) Photo-catalytic degradation of Metanil Yellow dye using TiO<sub>2</sub> immobilized into polyvinyl alcohol/acrylic acid microgels prepared by ionizing radiation. *React. Funct. Polym.* 72(11), 823-831.

Abe, T., Kobayashi, S. and Kobayashi, M. (2011) Aggregation of colloidal silica particles in the presence of fulvic acid, humic acid, or alginate: Effects of ionic composition. *Coll. Surf. A* 379(1-3), 21-26.

Ahmad, R., Mohsin, M., Ahmad, T. and Sardar, M. (2015) Alpha amylase assisted synthesis of TiO<sub>2</sub> nanoparticles: Structural characterization and application as antibacterial agents. *J. Hazard. Mater.* 283, 171-177.

Ahmadpoor, P., Nateri, A.S. and Motaghitalab, V. (2013) The optical properties of PVA/TiO<sub>2</sub> composite nanofibers. *J. Appl. Polym. Sci.* 130(1), 78-85.

Antonopoulou, M. and Konstantinou, I. (2015) TiO<sub>2</sub> photocatalysis of 2-isopropyl-3-methoxy pyrazine taste and odor compound in aqueous phase: Kinetics, degradation pathways and toxicity evaluation. *Catal. Today* 240, 22-29.

Asahi, R. (2001) Visible-Light Photocatalysis in Nitrogen-Doped Titanium Oxides. *Science* 293(5528), 269-271.

Augugliaro, V., García-López, E., Loddo, V., Malato-Rodríguez, S., Maldonado, I., Marci, G., Molinari, R. and Palmisano, L. (2005) Degradation of lincomycin in aqueous medium: Coupling of solar photocatalysis and membrane separation. *Sol. Energy* 79(4), 402-408.

Axelsson, A.K. and Dunne, L.J. (2001) Mechanism of photocatalytic oxidation of 3,4-dichlorophenol on TiO<sub>2</sub> semiconductor surfaces. *J. Photochem. Photobio. A* 144(2-3), 205-213.

Azrague, K., Aimar, P., Benoit-Marquié, F. and Maurette, M.T. (2007) A new combination of a membrane and a photocatalytic reactor for the depollution of turbid water. *Appl. Catal. B* 72(3-4), 197-204.

- Battin, T.J., Kammer, F.V.D., Weilhartner, A., Ottofuelling, S. and Hofmann, T. (2009) Nanostructured TiO<sub>2</sub>: Transport Behavior and Effects on Aquatic Microbial Communities under Environmental Conditions. *Environ. Sci. Technol.* 43(21), 8098-8104.
- Bazzo, A. and Urakawa, A. (2013) Origin of Photocatalytic Activity in Continuous Gas Phase CO<sub>2</sub> Reduction over Pt/TiO<sub>2</sub>. *ChemSuschem* 6(11), 2095-2102.
- Benotti, M.J., Stanford, B.D., Wert, E.C. and Snyder, S.A. (2009) Evaluation of a photocatalytic reactor membrane pilot system for the removal of pharmaceuticals and endocrine disrupting compounds from water. *Water Res.* 43(6), 1513-1522.
- Bessekhouad, Y., Brahim, R., Hamdini, F. and Trari, M. (2012) Cu<sub>2</sub>S/TiO<sub>2</sub> heterojunction applied to visible light Orange II degradation. *J. Photochem. Photobio. A* 248, 15-23.
- Bolyard, S.C., Reinhart, D.R. and Santra, S. (2013) Behavior of Engineered Nanoparticles in Landfill Leachate. *Environ. Sci. Technol.* 47(15), 8114-8122.
- Boreen, A.L., Arnold, W.A. and McNeill, K. (2003) Photodegradation of pharmaceuticals in the aquatic environment: A review. *Aquat. Sci.* 65(4), 320-341.
- Borisover, M., Sela, M. and Chefetz, B. (2011) Enhancement effect of water associated with natural organic matter (NOM) on organic compound–NOM interactions: A case study with carbamazepine. *Chemosphere* 82(10), 1454-1460.
- Borrok, D., Aumend, K. and Fein, J.B. (2007) Significance of ternary bacteria-metal-natural organic matter complexes determined through experimentation and chemical equilibrium modeling. *Chem. Geol.* 238(1-2), 44-62.
- Box, G.E.P., Hunter, J.S. and Hunter, W.G. (2005) *Statistics for experimenters : design, innovation, and discovery*, Wiley-Interscience, Hoboken, N.J.
- Brezova, V., Blazkova, A., Borosova, E., Ceppan, M. and Fiala, R. (1995) The Influence of Dissolved Metal-Ions on the Photocatalytic Degradation of Phenol in Aqueous TiO<sub>2</sub> Suspensions. *J. Mol. Catal. A* 98(2), 109-116.
- Brinkmann, T., Horsch, P., Sartorius, D. and Frimmel, F.H. (2003) Photoformation of low-molecular-weight organic acids from brown water dissolved organic matter. *Environ. Sci. Technol.* 37(18), 4190-4198.
- Bumajdad, A., Madkour, M., Abdel-Moneam, Y. and El-Kemary, M. (2014) Nanostructured mesoporous Au/TiO<sub>2</sub> for photocatalytic degradation of a textile dye: the effect of size similarity of the deposited Au with that of TiO<sub>2</sub> pores. *J. Mater. Sci.* 49(4), 1743-1754.
- Calamari, D., Zuccato, E., Castiglioni, S., Bagnati, R. and Fanelli, R. (2003) Strategic survey of therapeutic drugs in the rivers Po and Lambro in northern Italy. *Environ. Sci.*

Technol. 37(7), 1241-1248.

Canario, A.R., Guillemot, L., Diaz-Valdes, J., Valdes, J.E., Vargas, P. and Esaulov, V.A. (2013) Electron transfer and energy loss processes in fluorine scattering on oxygen covered Ag(110) - Crystal azimuthal dependence. Nucl. Instr. Met. Phys. Res. Section B 315, 36-41.

Carp, O., Huisman, C.L. and Reller, A. (2004) Photoinduced reactivity of titanium dioxide. Prog. Solid State Chem. 32(1-2), 33-177.

Chen, C.C., Li, X.Z., Ma, W.H., Zhao, J.C., Hidaka, H. and Serpone, N. (2002) Effect of transition metal ions on the TiO<sub>2</sub>-assisted photodegradation of dyes under visible irradiation: A probe for the interfacial electron transfer process and reaction mechanism. J. Phys. Chem. B 106(2), 318-324.

Chen, C.Y., Kuo, J.T., Yang, H.A. and Chung, Y.C. (2013) A coupled biological and photocatalysis pretreatment system for the removal of crystal violet from wastewater. Chemosphere 92(6), 695-701.

Chen, K.L. and Elimelech, M. (2006) Aggregation and deposition kinetics of fullerene (C-60) nanoparticles. Langmuir 22(26), 10994-11001.

Chen, K.L. and Elimelech, M. (2007) Influence of humic acid on the aggregation kinetics of fullerene (C-60) nanoparticles in monovalent and divalent electrolyte solutions. J. Colloid Interface Sci. 309(1), 126-134.

Chen, S.H., Lv, B.L. and Xu, Y. (2012) Fe-quinoline complexes sensitized Si-doped TiO<sub>2</sub> with enhanced visible light photocatalytic activity. Mater. Lett. 77, 32-34.

Chen, Y.J. and Dionysiou, D.D. (2005) Immobilization of transparent NaNO<sub>2</sub>-TiO<sub>2</sub> photocatalytic films on stainless steel for water purification. Abs. Ameri. Chem. Socie. 229, U922-U922.

Chiang, K., Lim, T.M., Tsen, L. and Lee, C.C. (2004) Photocatalytic degradation and mineralization of bisphenol A by TiO<sub>2</sub> and platinumized TiO<sub>2</sub>. Appl. Catal. A 261(2), 225-237.

Choi, M., Choi, D.W., Lee, J.Y., Kim, Y.S., Kim, B.S. and Lee, B.H. (2012) Removal of pharmaceutical residue in municipal wastewater by DAF (dissolved air flotation)-MBR (membrane bioreactor) and ozone oxidation. Water Sci. Technol. 66(12), 2546-2555.

Chong, M.N. and Jin, B. (2012) Photocatalytic treatment of high concentration carbamazepine in synthetic hospital wastewater. J. Hazard. Mater. 199, 135-142.

Chong, M.N., Jin, B., Chow, C.W.K. and Saint, C. (2010) Recent developments in photocatalytic water treatment technology: A review. Water Res. 44(10), 2997-3027.

- Chu, W., Choy, W.K. and So, T.Y. (2007) The effect of solution pH and peroxide in the TiO<sub>2</sub>-induced photocatalysis of chlorinated aniline. *J. Hazard. Mater.* 141(1), 86-91.
- Clara, M., Strenn, B. and Kreuzinger, N. (2004) Carbamazepine as a possible anthropogenic marker in the aquatic environment: investigations on the behaviour of Carbamazepine in wastewater treatment and during groundwater infiltration. *Water Res.* 38(4), 947-954.
- Clevers, M. (2003) Aquatic ecotoxicity of pharmaceuticals including the assessment of combination effects. *Toxicol. Lett.* 142(3), 185-194.
- Comoretto, L. and Chiron, S. (2005) Comparing pharmaceutical and pesticide loads into a small Mediterranean river. *Sci. Total Environ.* 349(1-3), 201-210.
- Contardo-Jara, V., Lorenz, C., Pflugmacher, S., Nutzmann, G., Kloas, W. and Wiegand, C. (2011) Exposure to human pharmaceuticals Carbamazepine, Ibuprofen and Bezafibrate causes molecular effects in *Dreissena polymorpha*. *Aquat. Toxicol.* 105(3-4), 428-437.
- Crey-Desbiolles, C., Cavalli, S., Polesello, S. and Valsecchi, S. (2009) Automated Determination of Linear Alkylbenzene Sulphonate (LAS) in Wastewater Treatment Plants Effluents Using on Line Solid-phase Extraction Followed by HPLC with Fluorescence Detection. *Tenside Surfact Det* 46(6), 346-351.
- Crittenden, J.C., Suri, R.P.S., Perram, D.L. and Hand, D.W. (1997) Decontamination of water using adsorption and photocatalysis. *Water Res.* 31(3), 411-418.
- Cui, E.T. and Lu, G.X. (2013) Modulating Photogenerated Electron Transfer and Hydrogen Production Rate by Controlling Surface Potential Energy on a Selectively Exposed Pt Facet on Pt/TiO<sub>2</sub> for Enhancing Hydrogen Production. *J. Phys. Chem. C* 117(50), 26415-26425.
- Cui, L., Wang, Y., Niu, M., Chen, G. and Cheng, Y. (2009) Synthesis and visible light photocatalysis of Fe-doped TiO<sub>2</sub> mesoporous layers deposited on hollow glass microbeads. *J. Solid State Chem.* 182(10), 2785-2790.
- Cunningham, V.L., Perino, C., D'Aco, V.J., Hartmann, A. and Bechter, R. (2010) Human health risk assessment of carbamazepine in surface waters of North America and Europe. *Regul. Toxicol. Pharm.* 56(3), 343-351.
- Daimon, T. and Nosaka, Y. (2007) Formation and behavior of singlet molecular oxygen in TiO<sub>2</sub> photocatalysis studied by detection of near-infrared phosphorescence. *J. Phys. Chem. C* 111(11), 4420-4424.
- Daneshvar, N., Salari, D., Niaei, A., Rasoulifard, M.H. and Khataee, A.R. (2005) Immobilization of TiO<sub>2</sub> nanopowder on glass beads for the photocatalytic decolorization of an azo dye CI Direct Red 23. *J. Environ. Health Part A* 40(8), 1605-1617.

- Dankovic, D., Kuempel, E. and Wheeler, M. (2007) An approach to risk assessment for TiO<sub>2</sub>. *Inhalation Toxicol.* 19, 205-212.
- Denny, F., Scott, J., Chiang, K., Teoh, W.Y. and Amal, R. (2007) Insight towards the role of platinum in the photocatalytic mineralisation of organic compounds. *J. Mol. Catal. A* 263(1-2), 93-102.
- Diebold, U. (2003a) Structure and properties of TiO<sub>2</sub> surfaces: a brief review. *Appl. Phys. A* 76(5), 681-687.
- Diebold, U. (2003b) The surface science of titanium dioxide. *Surf. Sci. Rep.* 48(5-8), 53-229.
- Dionysiou, D.D., Antoniou, M.G., Pelaez, M., Choi, H., de la Cruz, A.A. and Shoemaker, J.A. (2008) ANYL 267-Application of UV and visible-light activated nanostructured TiO<sub>2</sub> catalysts for the destruction of emerging organic contaminants in water. *Abs. Ameri. Chem. Socie.* 236.
- Doll, T.E. and Frimmel, F.H. (2004a) Development of easy and reproducible immobilization techniques using TiO<sub>2</sub> for photocatalytic degradation of aquatic pollutants. *Acta Hydroch. Hydrob.* 32(3), 201-213.
- Doll, T.E. and Frimmel, F.H. (2003a) Fate of pharmaceuticals-photodegradation by simulated solar UV-light. *Chemosphere* 52(10), 1757-1769.
- Doll, T.E. and Frimmel, F.H. (2003b) Fate of pharmaceuticals—photodegradation by simulated solar UV-light. *Chemosphere* 52(10), 1757-1769.
- Doll, T.E. and Frimmel, F.H. (2004b) Kinetic study of photocatalytic degradation of carbamazepine, clofibrac acid, iomeprol and iopromide assisted by different TiO<sub>2</sub> materials--determination of intermediates and reaction pathways. *Water Res.* 38(4), 955-964.
- Doll, T.E. and Frimmel, F.H. (2005) Photocatalytic degradation of carbamazepine, clofibrac acid and iomeprol with P25 and Hombikat UV100 in the presence of natural organic matter (NOM) and other organic water constituents. *Water Res.* 39(2-3), 403-411.
- Domingos, R.F., Baalousha, M.A., Ju-Nam, Y., Reid, M.M., Tufenkji, N., Lead, J.R., Leppard, G.G. and Wilkinson, K.J. (2009a) Characterizing Manufactured Nanoparticles in the Environment: Multimethod Determination of Particle Sizes. *Environ. Sci. Technol.* 43(19), 7277-7284.
- Domingos, R.F., Tufenkji, N. and Wilkinson, K.J. (2009b) Aggregation of Titanium Dioxide Nanoparticles: Role of a Fulvic Acid. *Environ. Sci. Technol.* 43(5), 1282-1286.
- Drosos, M., Ren, M. and Frimmel, F.H. (2015) The effect of NOM to TiO<sub>2</sub>: interactions

- and photocatalytic behavior. *Appl. Catal. B* 165, 328-334.
- Du, E.D., Zhang, Y.X. and Zheng, L. (2009) Photocatalytic degradation of dimethyl phthalate in aqueous TiO<sub>2</sub> suspension: a modified Langmuir-Hinshelwood model. *React. Kinet. Catal. Lett.* 97(1), 83-90.
- Egerton, T.A. and Mattinson, J.A. (2010) Effects of particle dispersion on photocatalysis probed by the effect of platinum on dichloroacetic acid oxidation by P25 and nanoparticulate rutile. *Appl. Catal. B* 99(3-4), 407-412.
- Einaga, H., Ogata, A., Futamura, S. and Ibusuki, T. (2001) The stabilization of active oxygen species by Pt supported on TiO<sub>2</sub>. *Chem. Phys. Lett.* 338(4-6), 303-307.
- Emeline, A.V., Ryabchuk, V. and Serpone, N. (2000) Factors affecting the efficiency of a photocatalyzed process in aqueous metal-oxide dispersions - Prospect of distinguishing between two kinetic models. *J. Photochem. Photobio. A* 133(1-2), 89-97.
- Erhayem, M. and Sohn, M. (2014) Stability studies for titanium dioxide nanoparticles upon adsorption of Suwannee River humic and fulvic acids and natural organic matter. *Sci. Total Environ.* 468, 249-257.
- Espinoza, L.A.T., Rembor, M., Matesanz, C.A., Heidt, A. and Frimmel, F.H. (2009) Formation of bromoform in irradiated titanium dioxide suspensions with varying photocatalyst, dissolved organic carbon and bromide concentrations. *Water Res.* 43(17), 4143-4148.
- Falch, A. and Kriek, R.J. (2013) Laser induced H<sub>2</sub> production employing Pt-TiO<sub>2</sub> photocatalysts. *J. Photochem. Photobio. A* 271, 117-123.
- Fang, D., Luo, Z., Huang, K. and Lagoudas, D.C. (2011) Effect of heat treatment on morphology, crystalline structure and photocatalysis properties of TiO<sub>2</sub> nanotubes on Ti substrate and freestanding membrane. *Appl. Surf. Sci.* 257(15), 6451-6461.
- Fatta-Kassinos, D., Vasquez, M.I. and Kummerer, K. (2011) Transformation products of pharmaceuticals in surface waters and wastewater formed during photolysis and advanced oxidation processes - Degradation, elucidation of byproducts and assessment of their biological potency. *Chemosphere* 85(5), 693-709.
- Fogler, H.S. (1999) *Elements of chemical reaction engineering*, Prentice Hall PTR, Upper Saddle River, N.J.
- French, R.A., Jacobson, A.R., Kim, B., Isley, S.L., Penn, R.L. and Baveye, P.C. (2009) Influence of Ionic Strength, pH, and Cation Valence on Aggregation Kinetics of Titanium Dioxide Nanoparticles. *Environ. Sci. Technol.* 43(5), 1354-1359.
- Frimmel, F.H. (2002) *Refractory organic substances in the environment*, Wiley-VCH, Weinheim Cambridge.

- Frimmel, F.H., Bauer, H., Putzien, J., Murasecco, P. and Braun, A.M. (1987) Laser Flash-Photolysis of Dissolved Aquatic Humic Material and the Sensitized Production of Singlet Oxygen. *Environ. Sci. Technol.* 21(6), 541-545.
- Frimmel, F.H. and Niessner, R. (2010) *Nanoparticles in the water cycle : properties, analysis and environmental relevance*, Springer, Heidelberg ; New York.
- Fujishima, A. (1999) Photoelectrochemistry and photofunctional materials. *Electrochem. Commun.* 67(7), 800-800.
- Furman, O., Usenko, S. and Lau, B.L.T. (2013) Relative Importance of the Humic and Fulvic Fractions of Natural Organic Matter in the Aggregation and Deposition of Silver Nanoparticles. *Environ. Sci. Technol.* 47(3), 1349-1356.
- Gaya, U.I. and Abdullah, A.H. (2008) Heterogeneous photocatalytic degradation of organic contaminants over titanium dioxide: A review of fundamentals, progress and problems. *J. Photochem. Photobio. C* 9(1), 1-12.
- Gerischer, H. and Heller, A. (1991) The Role of Oxygen in Photooxidation of Organic-Molecules on Semiconductor Particles. *J. Phys. Chem.* 95(13), 5261-5267.
- Gogniat, G., Thyssen, M., Denis, M., Pulgarin, C. and Dukan, S. (2006) The bactericidal effect of TiO<sub>2</sub> photocatalysis involves adsorption onto catalyst and the loss of membrane integrity. *FEMS Microbiol. Lett.* 258(1), 18-24.
- Gottschalk, F., Sonderer, T., Scholz, R.W. and Nowack, B. (2009) Modeled Environmental Concentrations of Engineered Nanomaterials (TiO<sub>2</sub>, ZnO, Ag, CNT, Fullerenes) for Different Regions. *Environ. Sci. Technol.* 43(24), 9216-9222.
- Guo, Y., Cheng, C., Wang, J., Wang, Z., Jin, X., Li, K., Kang, P. and Gao, J. (2011) Detection of reactive oxygen species (ROS) generated by TiO<sub>2</sub>(R), TiO<sub>2</sub>(R/A) and TiO<sub>2</sub>(A) under ultrasonic and solar light irradiation and application in degradation of organic dyes. *J. Hazard. Mater.* 192(2), 786-793.
- Gutmann, S., Wolak, M.A., Conrad, M., Beerbom, M.M. and Schlaf, R. (2010) Effect of ultraviolet and x-ray radiation on the work function of TiO<sub>2</sub> surfaces. *J. Appl. Phys.* 107(10).
- Habibi, M.H., Hassanzadeh, A. and Mahdavi, S. (2005) The effect of operational parameters on the photocatalytic degradation of three textile azo dyes in aqueous TiO<sub>2</sub> suspensions. *J. Photochem. Photobio. A* 172(1), 89-96.
- Hajdu, A., Illes, E., Tombacz, E. and Borbath, I. (2009) Surface charging, polyanionic coating and colloid stability of magnetite nanoparticles. *Coll. Surf. A* 347(1-3), 104-108.
- Hamadani, M., Reisi-Vanani, A., Razi, P., Hoseinifard, S. and Jabbari, V. (2013) Photodeposition-assisted synthesis of novel nanoparticulate In, S-codoped TiO<sub>2</sub> powders



- with high visible light-driven photocatalytic activity. *Appl. Surf. Sci.* 285, 121-129.
- Haroune, L., Salaun, M., Menard, A., Legault, C.Y. and Bellenger, J.P. (2014) Photocatalytic degradation of carbamazepine and three derivatives using TiO<sub>2</sub> and ZnO: Effect of pH, ionic strength, and natural organic matter. *Sci. Total Environ.* 475, 16-22.
- Hassan, C.M. and Peppas, N.A. (2000) Structure and applications of poly(vinyl alcohol) hydrogels produced by conventional crosslinking or by freezing/thawing methods. *Biopol. Hydro. Pol. Nanocom.* 153, 37-65.
- He, C.-H. and Gong, J. (2003) The preparation of PVA–Pt/TiO<sub>2</sub> composite nanofiber aggregate and the photocatalytic degradation of solid-phase polyvinyl alcohol. *Polym. Degrad. Stab.* 81(1), 117-124.
- Heberer, T. (2002) Tracking persistent pharmaceutical residues from municipal sewage to drinking water. *J. Hydrol.* 266(3-4), 175-189.
- Herrmann, J.M., Tahiri, H., Guillard, C. and Pichat, P. (1999) Photocatalytic degradation of aqueous hydroxy-butandioic acid (malic acid) in contact with powdered and supported titania in water. *Catal. Today* 54(1), 131-141.
- Hoffmann, M.R., Martin, S.T., Choi, W.Y. and Bahnemann, D.W. (1995) Environmental Applications of Semiconductor Photocatalysis. *Chem. Rev.* 95(1), 69-96.
- Hosseini, S.N., Borghei, S.M., Vossoughi, M. and Taghavinia, N. (2007) Immobilization of TiO<sub>2</sub> on perlite granules for photocatalytic degradation of phenol. *Appl. Catal. B* 74(1-2), 53-62.
- Hosseinzadeh, H. (2013) Synthesis and swelling properties of a poly(vinyl alcohol)-based superabsorbing hydrogel. *Curr. Chem. Lett.* 2(3), 153-158.
- Hou, J.W., Dong, G.X., Ye, Y. and Chen, V. (2014) Laccase immobilization on titania nanoparticles and titania-functionalized membranes. *J. Membr. Sci.* 452, 229-240.
- Hsu, L.J., Lee, L.T. and Lin, C.C. (2011) Adsorption and photocatalytic degradation of polyvinyl alcohol in aqueous solutions using P-25 TiO<sub>2</sub>. *Chem. Eng. J.* 173(3), 698-705.
- Hu, C., Tang, Y.H., Jiang, Z., Hao, Z.P., Tang, H.X. and Wong, P.K. (2003) Characterization and photocatalytic activity of noble-metal-supported surface TiO<sub>2</sub>/SiO<sub>2</sub>. *Appl. Catal. A* 253(2), 389-396.
- Huang, H.C., Huang, G.L., Chen, H.L. and Lee, Y.D. (2006) Immobilization of TiO<sub>2</sub> nanoparticles on carbon nanocapsules for photovoltaic applications. *Thin Solid Films* 511, 203-207.
- Huangfu, X.L., Jiang, J., Ma, J., Liu, Y.Z. and Yang, J. (2013) Aggregation Kinetics of Manganese Dioxide Colloids in Aqueous Solution: Influence of Humic Substances and

- Biomacromolecules. Environ. Sci. Technol. 47(18), 10285-10292.
- Huber, S.A. and Frimmel, F.H. (1991) Flow-Injection Analysis of Organic and Inorganic Carbon in the Low-Ppb Range. Anal. Chem. 63(19), 2122-2130.
- Hwang, S., Lee, M.C. and Choi, W. (2003) Highly enhanced photocatalytic oxidation of CO on titania deposited with Pt nanoparticles: kinetics and mechanism. Appl. Catal. B 46(1), 49-63.
- Ibragimov, K.I. and Korol'kov, V.A. (2001) Temperature dependence of the work function of metals and binary alloys. Inorg. Mater. 37(6), 567-572.
- Iliev, V., Tomova, D., Rakovsky, S., Eliyas, A. and Puma, G.L. (2010) Enhancement of photocatalytic oxidation of oxalic acid by gold modified WO<sub>3</sub>/TiO<sub>2</sub> photocatalysts under UV and visible light irradiation. J. Mol. Catal. A 327(1-2), 51-57.
- Imai, A., Fukushima, T., Matsushige, K., Kim, Y.H. and Choi, K. (2002) Characterization of dissolved organic matter in effluents from wastewater treatment plants. Water Res. 36(4), 859-870.
- Imanishi, A., Tsuji, E. and Nakato, Y. (2007) Dependence of the work function of TiO<sub>2</sub> (Rutile) on crystal faces, studied by a scanning auger microprobe. J. Phys. Chem. C 111(5), 2128-2132.
- Inturi, S.N.R., Boningari, T., Suidan, M. and Smirniotis, P.G. (2014) Visible-light-induced photodegradation of gas phase acetonitrile using aerosol-made transition metal (V, Cr, Fe, Co, Mn, Mo, Ni, Cu, Y, Ce, and Zr) doped TiO<sub>2</sub>. Appl. Catal. B 144, 333-342.
- Irawaty, W., Friedmann, D., Scott, J., Pichat, P. and Amal, R. (2011) Photocatalysis in TiO<sub>2</sub> aqueous suspension: Effects of mono- or di-hydroxyl substitution of butanedioic acid on the disappearance and mineralisation rates. Catal. Today 178(1), 51-57.
- Ishibashi, K., Fujishima, A., Watanabe, T. and Hashimoto, K. (2000) Quantum yields of active oxidative species formed on TiO<sub>2</sub> photocatalyst. J. Photochem. Photobio. A 134(1-2), 139-142.
- IUPAC (2012) Electron work function. . <http://goldbook.iupac.org/>.
- Ji, Y.F., Zhou, L., Ferronato, C., Salvador, A., Yang, X. and Chovelon, J.M. (2013) Degradation of sunscreen agent 2-phenylbenzimidazole-5-sulfonic acid by TiO<sub>2</sub> photocatalysis: Kinetics, photoproducts and comparison to structurally related compounds. Appl. Catal. B 140, 457-467.
- Jiang, H., Zhang, G., Huang, T., Chen, J., Wang, Q. and Meng, Q. (2010) Photocatalytic membrane reactor for degradation of acid red B wastewater. Chem. Eng. J. 156(3), 571-577.

- Jin, L. and Bai, R.B. (2002) Mechanisms of lead adsorption on chitosan/PVA hydrogel beads. *Langmuir* 18(25), 9765-9770.
- Joss, A., Keller, E., Alder, A.C., Gobel, A., McArdell, C.S., Ternes, T. and Siegrist, H. (2005) Removal of pharmaceuticals and fragrances in biological wastewater treatment. *Water Res.* 39(14), 3139-3152.
- Ju-Nam, Y. and Lead, J.R. (2008) Manufactured nanoparticles: An overview of their chemistry, interactions and potential environmental implications. *Sci. Total Environ.* 400(1-3), 396-414.
- Jung, J.T., Kim, J.O. and Choi, W.Y. (2008) Treatment Performance of Photocatalysis/H<sub>2</sub>O<sub>2</sub>/Metal Membrane Process for Organics Removal. *Mater. Sci. Forum* 569, 5-8.
- Kabra, K., Chaudhary, R. and Sawhney, R.L. (2004) Treatment of hazardous organic and inorganic compounds through aqueous-phase photocatalysis: A review. *Ind. Eng. Chem. Res.* 43(24), 7683-7696.
- Kamegawa, T., Matsuura, S., Seto, H. and Yamashita, H. (2013) A Visible-Light-Harvesting Assembly with a Sulfocalixarene Linker between Dyes and a Pt-TiO<sub>2</sub> Photocatalyst. *Angew. Chem. Int. Ed.* 52(3), 916-919.
- Kampen, T.U., Das, A., Park, S., Hoyer, W. and Zahn, D.R.T. (2004) Relation between morphology and work function of metals deposited on organic substrates. *Appl. Surf. Sci.* 234(1-4), 333-340.
- Kandiel, T.A., Feldhoff, A., Robben, L., Dillert, R. and Bahnemann, D.W. (2010) Tailored Titanium Dioxide Nanomaterials: Anatase Nanoparticles and Brookite Nanorods as Highly Active Photocatalysts. *Chem. Mater.* 22(6), 2050-2060.
- Katsumata, H., Sada, M., Nakaoka, Y., Kaneco, S., Suzuki, T. and Ohta, K. (2009) Photocatalytic degradation of diuron in aqueous solution by platinumized TiO<sub>2</sub>. *J. Hazard. Mater.* 171(1-3), 1081-1087.
- Ke, T.Y., Lee, C.Y. and Chiu, H.T. (2010) Photocatalysis by Electron Transfer between Different-sized Anatases. *Appl. Catal. A* 381(1-2), 109-113.
- Khataee, A.R., Fathinia, M. and Joo, S.W. (2013) Simultaneous monitoring of photocatalysis of three pharmaceuticals by immobilized TiO<sub>2</sub> nanoparticles: Chemometric assessment, intermediates identification and ecotoxicological evaluation. *Spectro. Acta Part A* 112, 33-45.
- Kiatkittipong, K., Scott, J. and Amal, R. (2011) Hydrothermally Synthesized Titanate Nanostructures: Impact of Heat Treatment on Particle Characteristics and Photocatalytic Properties. *Appl. Mater. Interf.* 3(10), 3988-3996.

Kiejna, A. and Wojciechowski, K.F. (1981) Work Function of Metals - Relation between Theory and Experiment. *Prog. Surf. Sci.* 11(4), 293-338.

Kim, J., Qin, S.Y., Yao, W., Niu, Q., Chou, M.Y. and Shih, C.K. (2010) Quantum size effects on the work function of metallic thin film nanostructures. *Proc. Natl. Acad. Sci. U. S. A.* 107(29), 12761-12765.

Kim, S., Song, K., Kim, M., Jang, I. and Oh, S.G. (2013) Preparation of Pt-TiO<sub>2</sub> composite particles by alcohol reduction method and their photocatalytic activities. *J. Phys. Chem. Solids* 74(3), 524-529.

Kim, Y., Choi, K., Jung, J.Y., Park, S., Kim, P.G. and Park, J. (2007) Aquatic toxicity of acetaminophen, carbamazepine, cimetidine, diltiazem and six major sulfonamides, and their potential ecological risks in Korea. *Environ. Int.* 33(3), 370-375.

Kivrak, H., Mastalir, A., Kiraly, Z. and Uner, D. (2009) Determination of the dispersion of supported Pt particles by gas-phase and liquid-phase measurements. *Catal. Commun.* 10(6), 1002-1005.

Kohler, C., Venditti, S., Igos, E., Klepiszewski, K., Benetto, E. and Cornelissen, A. (2012) Elimination of pharmaceutical residues in biologically pre-treated hospital wastewater using advanced UV irradiation technology: a comparative assessment. *J. Hazard. Mater.* 239-240, 70-77.

Kondrakov, A.O., Ignatev, A.N., Frimmel, F.H., Brase, S., Horn, H. and Revelsky, A.I. (2014) Formation of genotoxic quinones during bisphenol A degradation by TiO<sub>2</sub> photocatalysis and UV photolysis: A comparative study. *Appl. Catal. B* 160, 106-114.

Kozlov, V.M. and Bicelli, L.P. (2000) Influence of temperature and of structure of antimony substrate on gallium diffusion into the GaSb semiconductor compound. *J. Alloys Compd.* 313, 161-167.

Kozlova, E.A., Lyubina, T.P., Nasalevich, M.A., Vorontsov, A.V., Miller, A.V., Kaichev, V.V. and Parmon, V.N. (2011) Influence of the method of platinum deposition on activity and stability of Pt/TiO<sub>2</sub> photocatalysts in the photocatalytic oxidation of dimethyl methylphosphonate. *Catal. Commun.* 12(7), 597-601.

Kozlova, E.A. and Vorontsov, A.V. (2010) Photocatalytic hydrogen evolution from aqueous solutions of organophosphorous compounds. *Int. J. Hydrogen Energy* 35(14), 7337-7343.

Kuemmere, K., Erbe, T., Gartiser, S. and Brinker, L. (1998) AOX -Emissions from Howitals into Municipal Waste Water. *Chemosphere* 36(11), 2437-2445.

Kusior, A., Klich-Kafel, J., Trenczek-Zajac, A., Swierczek, K., Radecka, M. and Zakrzewska, K. (2013) TiO<sub>2</sub>-SnO<sub>2</sub> nanomaterials for gas sensing and photocatalysis. *J. Eur. Ceram. Soc.* 33(12), 2285-2290.

- Kutty, T.R.N. and Avudathai, M. (1989) Photocatalytic Activity of Tin-Substituted TiO<sub>2</sub> in Visible-Light. *Chem. Phys. Lett.* 163(1), 93-97.
- Kwon, J.M., Kim, Y.H., Song, B.K., Yeom, S.H., Kim, B.S. and Bin Im, J. (2006) Novel immobilization of titanium dioxide (TiO<sub>2</sub>) on the fluidizing carrier and its application to the degradation of azo-dye. *J. Hazard. Mater.* 134(1-3), 230-236.
- Lacey, C., McMahon, G., Bones, J., Barron, L., Morrissey, A. and Tobin, J.M. (2008) An LC-MS method for the determination of pharmaceutical compounds in wastewater treatment plant influent and effluent samples. *Talanta* 75(4), 1089-1097.
- Laera, G., Chong, M.N., Jin, B. and Lopez, A. (2011) An integrated MBR-TiO<sub>2</sub> photocatalysis process for the removal of Carbamazepine from simulated pharmaceutical industrial effluent. *Bioresour. Technol.* 102(13), 7012-7015.
- Lakshminarasimhan, N., Bae, E. and Choi, W. (2007) Enhanced photocatalytic production of H<sub>2</sub> on mesoporous TiO<sub>2</sub> prepared by template-free method: Role of interparticle charge transfer. *J. Phys. Chem. C* 111(42), 15244-15250.
- Lee, J.S. and Choi, W.Y. (2004) Effect of platinum deposits on TiO<sub>2</sub> on the anoxic photocatalytic degradation pathways of alkylamines in water: Dealkylation and N-alkylation. *Environ. Sci. Technol.* 38(14), 4026-4033.
- Lei, P., Wang, F., Gao, X.W., Ding, Y.F., Zhang, S.M., Zhao, J.C., Liu, S.R. and Yang, M.S. (2012) Immobilization of TiO<sub>2</sub> nanoparticles in polymeric substrates by chemical bonding for multi-cycle photodegradation of organic pollutants. *J. Hazard. Mater.* 227, 185-194.
- Leng, W.H., Liu, H., Cheng, S.A., Zhang, J.Q. and Cao, C.N. (2000) Kinetics of photocatalytic degradation of aniline in water over TiO<sub>2</sub> supported on porous nickel. *J. Photochem. Photobio. A* 131(1-3), 125-132.
- Li, C.H., Hsieh, Y.H., Chiu, W.T., Liu, C.C. and Kao, C.L. (2007) Study on preparation and photocatalytic performance of Ag/TiO<sub>2</sub> and Pt/TiO<sub>2</sub> photocatalysts. *Sep. Purif. Technol.* 58(1), 148-151.
- Li, S. and Sun, W.L. (2011) A comparative study on aggregation/sedimentation of TiO<sub>2</sub> nanoparticles in mono- and binary systems of fulvic acids and Fe(III). *J. Hazard. Mater.* 197, 70-79.
- Li, W.T., Chen, S.Y., Xu, Z.X., Li, Y., Shuang, C.D. and Li, A.M. (2014) Characterization of Dissolved Organic Matter in Municipal Wastewater Using Fluorescence PARAFAC Analysis and Chromatography Multi-Excitation/Emission Scan: A Comparative Study. *Environ. Sci. Technol.* 48(5), 2603-2609.
- Li, Z., Schram, T., Stesmans, A., Franquet, A., Witters, T., Pantisano, L., Yamada, N., Tsunoda, T., Hooker, J., De Gendt, S. and De Meyer, K. (2008) Influence of metal

capping layer on the work function of Mo gated metal-oxide semiconductor stacks. *Appl. Phys. Lett.* 93(8).

Liang, P., Wang, L., Xiong, S.Y., Dong, Q.M. and Li, X.Y. (2012) Research on the photocatalysis synergistic effect of Mo-X(B, C, N, O, F) codoped TiO<sub>2</sub>. *Acta Phys. Sin.* 61(5).

Lin, C.J. and Yang, W.T. (2014) Ordered mesostructured Cu-doped TiO<sub>2</sub> spheres as active visible-light-driven photocatalysts for degradation of paracetamol. *Chem. Eng. J.* 237, 131-137.

Linsebigler, A.L., Lu, G.Q. and Yates, J.T. (1995) Photocatalysis on TiO<sub>2</sub> Surfaces - Principles, Mechanisms, and Selected Results. *Chem. Rev.* 95(3), 735-758.

Liu, G.J., Zhang, X.R., Talley, J.W., Neal, C.R. and Wang, H.Y. (2008) Effect of NOM on arsenic adsorption by TiO<sub>2</sub> in simulated As(III)-contaminated raw waters. *Water Res.* 42(8-9), 2309-2319.

Liu, J.H., Guo, Q., Yu, M. and Li, S.M. (2014a) Effect of TiO<sub>2</sub> nanostructures on specific capacitance of Al<sub>2</sub>O<sub>3</sub>-TiO<sub>2</sub> composite film on etched aluminum foil formed by the sol-gel and anodizing. *Ceram. Int.* 40(2), 3687-3692.

Liu, J.J., Zuo, S.L., Yu, L.M., Yu, Y.C., Li, B.S. and Chen, P.W. (2013) Visible light photodegradation of methylene blue by AgBr-TiO<sub>2</sub>/SiO<sub>2</sub>@Fe<sub>3</sub>O<sub>4</sub> magnetic photocatalysts. *Particuology* 11(6), 728-731.

Liu, L., Zhao, C. and Yang, F. (2012) TiO<sub>2</sub> and polyvinyl alcohol (PVA) coated polyester filter in bioreactor for wastewater treatment. *Water Res.* 46(6), 1969-1978.

Liu, S., Lim, M. and Amal, R. (2014b) TiO<sub>2</sub>-coated natural zeolite: Rapid humic acid adsorption and effective photocatalytic regeneration. *Chem. Eng. Sci.* 105, 46-52.

Liu, Y.H., Chang, M.C., Liu, P.I., Chung, L.C., Shao, H., Huang, M.S., Horng, R.Y. and Yang, A.C.M. (2010a) Innovative one-step immobilization of TiO<sub>2</sub> on polymer material by the sol-gel method under IL/MW conditions. *J. Mater. Sci.* 45(22), 6212-6217.

Liu, Y.R., Geever, L.M., Kennedy, J.E., Higginbotham, C.L., Cahill, P.A. and McGuinness, G.B. (2010b) Thermal behavior and mechanical properties of physically crosslinked PVA/Gelatin hydrogels. *J. Mech. Behav. Biomed. Mater.* 3(2), 203-209.

Loosli, F., Le Coustumer, P. and Stoll, S. (2013) TiO<sub>2</sub> nanoparticles aggregation and disaggregation in presence of alginate and Suwannee River humic acids. pH and concentration effects on nanoparticle stability. *Water Res.* 47(16), 6052-6063.

Lynch, I. and Dawson, K.A. (2008) Protein-nanoparticle interactions. *Nano Today* 3(1-2), 40-47.

- Ma, N., Zhang, Y., Quan, X., Fan, X. and Zhao, H. (2010) Performing a microfiltration integrated with photocatalysis using an Ag-TiO<sub>2</sub>/HAP/Al<sub>2</sub>O<sub>3</sub> composite membrane for water treatment: Evaluating effectiveness for humic acid removal and anti-fouling properties. *Water Res.* 44(20), 6104-6114.
- Ma, Y.S., Chang, C.N., Chiang, Y.P., Sung, H.F. and Chao, A.C. (2008) Photocatalytic degradation of lignin using Pt/TiO<sub>2</sub> as the catalyst. *Chemosphere* 71(5), 998-1004.
- Maeda, K. (2011) Photocatalytic water splitting using semiconductor particles: History and recent developments. *J. Photochem. Photobio. C* 12(4), 237-268.
- Maeng, S.K., Choi, B.G., Lee, K.T. and Song, K.G. (2013) Influences of solid retention time, nitrification and microbial activity on the attenuation of pharmaceuticals and estrogens in membrane bioreactors. *Water Res.* 47(9), 3151-3162.
- Mateos-Pedrero, C., Gonzalez-Carrazan, S.R., Soria, M.A. and Ruiz, P. (2013) Effect of the nature of TiO<sub>2</sub> support over the performances of Rh/TiO<sub>2</sub> catalysts in the partial oxidation of methane. *Catal. Today* 203, 158-162.
- Matsuzawa, S., Maneerat, C., Hayata, Y., Hirakawa, T., Negishi, N. and Sano, T. (2008) Immobilization of TiO<sub>2</sub> nanoparticles on polymeric substrates by using electrostatic interaction in the aqueous phase. *Appl. Catal. B* 83(1-2), 39-45.
- Mehinto, A.C. (2010) Uptake and Biological Effects of Environmentally Relevant Concentrations of the Nonsteroidal Anti-inflammatory Pharmaceutical Diclofenac in Rainbow Trout (*Oncorhynchus mykiss*). *Environ. Sci. Technol.* 44, 2176-2182.
- Miao, X.S. and Metcalfe, C.D. (2003) Determination of cholesterol-lowering statin drugs in aqueous samples using liquid chromatography-electrospray ionization tandem mass spectrometry. *J. Chromatogr. A* 998(1-2), 133-141.
- Miller, K.L., Lee, C.W., Falconer, J.L. and Medlin, J.W. (2010) Effect of water on formic acid photocatalytic decomposition on TiO<sub>2</sub> and Pt/TiO<sub>2</sub>. *J. Catal.* 275(2), 294-299.
- Miranda-García, N., Suárez, S., Sánchez, B., Coronado, J.M., Malato, S. and Maldonado, M.I. (2011) Photocatalytic degradation of emerging contaminants in municipal wastewater treatment plant effluents using immobilized TiO<sub>2</sub> in a solar pilot plant. *Appl. Catal. B* 103(3-4), 294-301.
- Mohamed, R.M. and Aazam, E. (2013) Synthesis and characterization of Pt-ZnO-hydroxyapatite nanoparticles for photocatalytic degradation of benzene under visible light. *Desal. Water Treat.* 51(31-33), 6082-6090.
- Molea, A., Popescu, V., Rowson, N.A. and Dinescu, A.M. (2014) Influence of pH on the formulation of TiO<sub>2</sub> nano-crystalline powders with high photocatalytic activity. *Powder Technol.* 253, 22-28.

- Moon, J., Takagi, H., Fujishiro, Y. and Awano, M. (2001) Preparation and characterization of the Sb-doped TiO<sub>2</sub> photocatalysts. *J. Mater. Sci.* 36(4), 949-955.
- Mozia, S. (2010) Photocatalytic membrane reactors (PMRs) in water and wastewater treatment. A review. *Sep. Purif. Technol.* 73(2), 71-91.
- Mozia, S., Morawski, A.W., Toyoda, M. and Tsumura, T. (2010) Integration of photocatalysis and membrane distillation for removal of mono- and poly-azo dyes from water. *Desalination* 250(2), 666-672.
- Mozia, S., Tomaszewska, M. and Morawski, A.W. (2005) A new photocatalytic membrane reactor (PMR) for removal of azo-dye Acid Red 18 from water. *Appl. Catal. B* 59(1-2), 131-137.
- Mulyukov, R.R. (2006) Influence of nanocrystalline structure on work function of tungsten. *J. Vac. Sci. Technol., B* 24(2), 1061-1066.
- Munoz-Batista, M.J., Gomez-Cerezo, M.N., Kubacka, A., Tudela, D. and Fernandez-Garcia, M. (2014) Role of Interface Contact in CeO<sub>2</sub>-TiO<sub>2</sub> Photocatalytic Composite Materials. *Catalysis* 4(1), 63-72.
- Musumeci, F. and Pollack, G.H. (2012) Influence of water on the work function of certain metals. *Chem. Phys. Lett.* 536, 65-67.
- Muzyka, J.L. and Fox, M.A. (1991) Oxidative Photocatalysis in the Absence of Oxygen - Methyl Viologen as an Electron Trap in the TiO<sub>2</sub>-Mediated Photocatalysis of the Diels-Alder Dimerization of 2,4-Dimethyl-1,3-Pentadiene. *J. Photochem. Photobio. A* 57(1-3), 27-39.
- Nakata, K. and Fujishima, A. (2012) TiO<sub>2</sub> photocatalysis: Design and applications. *J. Photochem. Photobio. C* 13(3), 169-189.
- Nishimoto, S. and Bhushan, B. (2013) Bioinspired self-cleaning surfaces with superhydrophobicity, superoleophobicity, and superhydrophilicity. *Rsc Advances* 3(3), 671-690.
- Nomikos, G.N., Panagiotopoulou, P., Kondarides, D.I. and Verykios, X.E. (2014) Kinetic and mechanistic study of the photocatalytic reforming of methanol over Pt/TiO<sub>2</sub> catalyst. *Appl. Catal. B* 146, 249-257.
- Norde, W. and Anusiem, A.C.I. (1992) Adsorption, Desorption and Readsorption of Proteins on Solid-Surfaces. *Coll. Surf.* 66(1), 73-80.
- Norde, W. and Giacomelli, C.E. (2000) BSA structural changes during homomolecular exchange between the adsorbed and the dissolved states. *J. Biotechnol.* 79(3), 259-268.
- Obiefuna, G.I. and Orazulike, D.M. (2010) Chemical Speciation of Some metal ions in



- Groundwaters of Yola Area Using Geochemical Model. *J. Appl. Sci. Environ. Manag.* 14(2), 65-70.
- Ollis, D.F. (2005) Kinetics of liquid phase photocatalyzed reactions: An illuminating approach. *J. Phys. Chem. B* 109(6), 2439-2444.
- Ostermeyer, A.K., Mumuper, C.K., Semprini, L. and Radniecki, T. (2013) Influence of Bovine Serum Albumin and Alginate on Silver Nanoparticle Dissolution and Toxicity to *Nitrosomonas europaea*. *Environ. Sci. Technol.* 47(24), 14403-14410.
- Ozkan, A., Ozkan, M.H., Gurkan, R., Akcay, M. and Sokmen, M. (2004) Photocatalytic degradation of a textile azo dye, Sirius Gelb GC on TiO<sub>2</sub> or Ag-TiO<sub>2</sub> particles in the absence and presence of UV irradiation: the effects of some inorganic anions on the photocatalysis. *J. Photochem. Photobio. A* 163(1-2), 29-35.
- Pastrana-Martinez, L.M., Morales-Torres, S., Papageorgiou, S.K., Katsaros, F.K., Romanos, G.E., Figueiredo, J.L., Faria, J.L., Falaras, P. and Silva, A.M.T. (2013) Photocatalytic behaviour of nanocarbon-TiO<sub>2</sub> composites and immobilization into hollow fibres. *Appl. Catal. B* 142, 101-111.
- Pelaez, M., de la Cruz, A.A., O'Shea, K., Falaras, P. and Dionysiou, D.D. (2011) Effects of water parameters on the degradation of microcystin-LR under visible light-activated TiO<sub>2</sub> photocatalyst. *Water Res.* 45(12), 3787-3796.
- Peral, J., Domenech, X. and Ollis, D.F. (1997) Heterogeneous photocatalysis for purification, decontamination and deodorization of air. *J. Chem. Technol. Biotechnol.* 70(2), 117-140.
- Petkovich, N.D., Rudisill, S.G., Wilson, B.E., Mukherjee, A. and Stein, A. (2014) Control of TiO<sub>2</sub> Grain Size and Positioning in Three-Dimensionally Ordered Macroporous TiO<sub>2</sub>/C Composite Anodes for Lithium Ion Batteries. *Inorg. Chem.* 53(2), 1100-1112.
- Pettibone, J.M., Cwiertny, D.M., Scherer, M. and Grassian, V.H. (2008) Adsorption of organic acids on TiO<sub>2</sub> nanoparticles: Effects of pH, nanoparticle size, and nanoparticle aggregation. *Langmuir* 24(13), 6659-6667.
- Philippe, A. and Schaumann, G.E. (2014) Interactions of Dissolved Organic Matter with Natural and Engineered Inorganic Colloids: A Review. *Environ. Sci. Technol.* 48(16), 8946-8962.
- Phillips, P.J., Smith, S.G., Kolpin, D.W., Zaugg, S.D., Buxton, H.T., Furlong, E.T., Esposito, K. and Stinson, B. (2010) Pharmaceutical Formulation Facilities as Sources of Opioids and Other Pharmaceuticals to Wastewater Treatment Plant Effluents. *Environ. Sci. Technol.* 44(13), 4910-4916.
- Piscopo, A., Robert, D. and Weber, J.V. (2001) Influence of pH and chloride anion on the

photocatalytic degradation of organic compounds - Part I. Effect on the benzamide and para-hydroxybenzoic acid in TiO<sub>2</sub> aqueous solution. *Appl. Catal. B* 35(2), 117-124.

Prasse, C., Schlusener, M.P., Schulz, R. and Ternes, T.A. (2010) Antiviral Drugs in Wastewater and Surface Waters: A New Pharmaceutical Class of Environmental Relevance? *Environ. Sci. Technol.* 44(5), 1728-1735.

Putschew, A., Wischnack, S. and Jekel, M. (2000) Occurrence of triiodinated X-ray contrast agents in the aquatic environment. *Sci. Total Environ.* (255), 129-134.

Qu, Y.Q. and Duan, X.F. (2013) Progress, challenge and perspective of heterogeneous photocatalysts. *Chem. Soc. Rev.* 42(7), 2568-2580.

Radjenovic, J., Petrovic, M. and Barcelo, D. (2007) Advanced mass, spectrometric methods applied to the study of fate and removal of pharmaceuticals in wastewater treatment. *Trac. Tren. Anal. Chem.* 26(11), 1132-1144.

Rammohan, G. and Nadagouda, M.N. (2013) Green Photocatalysis for Degradation of Organic Contaminants: A Review. *Curr. Org. Chem.* 17(20), 2338-2348.

Rao, K.V.S., Rachel, A., Subrahmanyam, M. and Boule, P. (2003) Immobilization of TiO<sub>2</sub> on pumice stone for the photocatalytic degradation of dyes and dye industry pollutants. *Appl. Catal. B* 46(1), 77-85.

Reemtsma, T., These, A., Springer, A. and Linscheid, M. (2008) Differences in the molecular composition of fulvic acid size fractions detected by size-exclusion chromatography-on line Fourier transform ion cyclotron resonance (FTICR-) mass spectrometry. *Water Res.* 42(1-2), 63-72.

Rincon, A.G. and Pulgarin, C. (2004) Effect of pH, inorganic ions, organic matter and H<sub>2</sub>O<sub>2</sub> on E-coli K12 photocatalytic inactivation by TiO<sub>2</sub> - Implications in solar water disinfection. *Appl. Catal. B* 51(4), 283-302.

Romanello, M.B. and de Cortalezzi, M.M.F. (2013) An experimental study on the aggregation of TiO<sub>2</sub> nanoparticles under environmentally relevant conditions. *Water Res.* 47(12), 3887-3898.

Rothenberger, G., Moser, J., Gratzel, M., Serpone, N. and Sharma, D.K. (1985) Charge Carrier Trapping and Recombination Dynamics in Small Semiconductor Particles. *J. Am. Chem. Soc.* 107(26), 8054-8059.

Rupp, F., Haupt, M., Klostermann, H., Kim, H.S., Eichler, M., Peetsch, A., Scheideler, L., Doering, C., Oehr, C., Wendel, H.P., Sinn, S., Decker, E., von Ohle, C. and Geis-Gerstorfer, J. (2010) Multifunctional nature of UV-irradiated nanocrystalline anatase thin films for biomedical applications. *Acta Biomater.* 6(12), 4566-4577.

Sacher, F., Lange, F.T., Brauch, H.-J. and Blankenhorn, I. (2001) Pharmaceuticals in

- groundwaters Analytical methods and results of a monitoring program in Baden-Wurttemberg, Germany. *J. Chromatogr. A*, 199-210.
- Sairam, M., Patil, M., Veerapur, R., Patil, S. and Aminabhavi, T. (2006) Novel dense poly(vinyl alcohol)-TiO<sub>2</sub> mixed matrix membranes for pervaporation separation of water-isopropanol mixtures at 30°C. *J. Membr. Sci.* 281(1-2), 95-102.
- Sajjadi, H., Modaresi, A., Magri, P., Domanska, U., Sindt, M., Mieloszynski, J.L., Mutelet, F. and Rogalski, M. (2013) Aggregation of nanoparticles in aqueous solutions of ionic liquids. *J. Mol. Liq.* 186, 1-6.
- Sakthivel, S. and Kisch, H. (2003) Daylight photocatalysis by carbon-modified titanium dioxide. *Angew. Chem. Int. Ed.* 42(40), 4908-4911.
- Saleh, N.B., Pfefferle, L.D. and Elimelech, M. (2010) Influence of Biomacromolecules and Humic Acid on the Aggregation Kinetics of Single-Walled Carbon Nanotubes. *Environ. Sci. Technol.* 44(7), 2412-2418.
- Salgin, S., Salgin, U. and Bahadir, S. (2012) Zeta Potentials and Isoelectric Points of Biomolecules: The Effects of Ion Types and Ionic Strengths. *Int. J. Electrochem. Sci.* 7(12), 12404-12414.
- Sanderson, H., Brain, R.A., Johnson, D.J., Wilson, C.J. and Solomon, K.R. (2004) Toxicity classification and evaluation of four pharmaceutical classes: antibiotics, antineoplastics, cardiovascular, and sex hormones. *Toxicology* 203(1-3), 27-40.
- Sarria, V., Parra, S., Invernizzi, M., Peringer, P. and Pulgarin, C. (2001) Photochemical-biological treatment of a real industrial biorecalcitrant wastewater containing 5-amino-6-methyl-2-benzimidazolone. *Water Sci. Technol.* 44(5), 93-101.
- Sasahara, A., Pang, C.L. and Onishi, H. (2006) Local work function of Pt clusters vacuum-deposited on a TiO<sub>2</sub> surface. *J. Phys. Chem. B* 110(35), 17584-17588.
- Schmelling, D.C., Gray, K.A. and Kamat, P.V. (1997) The influence of solution matrix on the photocatalytic degradation of TNT in TiO<sub>2</sub> slurries. *Water Res.* 31(6), 1439-1447.
- Schwegmann, H., Ruppert, J. and Frimmel, F.H. (2013) Influence of the pH-value on the photocatalytic disinfection of bacteria with TiO<sub>2</sub> - Explanation by DLVO and XDLVO theory. *Water Res.* 47(4), 1503-1511.
- Seitz, W., Weber, W.H., Jiang, J.Q., Lloyd, B.J., Maier, M., Maier, D. and Schulz, W. (2006) Monitoring of iodinated X-ray contrast media in surface water. *Chemosphere* 64(8), 1318-1324.
- Shibuya, S., Aoki, S., Sekine, Y. and Mikami, I. (2013) Influence of oxygen addition on photocatalytic oxidation of aqueous ammonia over platinum-loaded TiO<sub>2</sub>. *Appl. Catal. B* 138, 294-298.

- Shifu, C., Xuqiang, L., Yunzhang, L. and Gengyu, C. (2007) The preparation of nitrogen-doped TiO<sub>2</sub>-xNx photocatalyst coated on hollow glass microbeads. *Appl. Surf. Sci.* 253(6), 3077-3082.
- Skriver, H.L. and Rosengaard, N.M. (1992) Surface-Energy and Work Function of Elemental Metals. *Phys. Rev. B* 46(11), 7157-7168.
- Song, G.H., Shi, M.Q., Chu, Y.Q. and Ma, C.A. (2013) Synthesis and characterization of highly dispersed Pt-TiO<sub>2</sub> vertical bar WC/BC as anode catalyst for methanol oxidation. *Electrochim. Acta* 112, 53-58.
- Song, Y.Q., Zhang, J.L., Yang, H.G., Xu, S.B., Jiang, L. and Dan, Y. (2014) Preparation and visible light-induced photo-catalytic activity of H-PVA/TiO<sub>2</sub> composite loaded on glass via sol-gel method. *Appl. Surf. Sci.* 292, 978-985.
- Stumm, W., Sigg, L. and Sulzberger, B. (1992) Chemistry of the solid-water interface : processes at the mineral-water and particle-water interface in natural systems, Wiley, New York.
- Sugihara, M.N., Moeller, D., Paul, T. and Strathmann, T.J. (2013) TiO<sub>2</sub>-photocatalyzed transformation of the recalcitrant X-ray contrast agent diatrizoate. *Appl. Catal. B* 129, 114-122.
- Sun, L.Z. and Bolton, J.R. (1996) Determination of the quantum yield for the photochemical generation of hydroxyl radicals in TiO<sub>2</sub> suspensions. *J. Phys. Chem.* 100(10), 4127-4134.
- Tachikawa, T., Tojo, S., Fujitsuka, M. and Majima, T. (2004) Influence of metal ions on the charge recombination processes during TiO<sub>2</sub> photocatalytic one-electron oxidation reactions. *J. Phys. Chem. B* 108(30), 11054-11061.
- Tamamura, S., Ohashi, R., Nagao, S., Yamamoto, M. and Mizuno, M. (2013) Molecular-size-distribution-dependent aggregation of humic substances by Na(I), Ag(I), Ca(II), and Eu(III). *Coll. Surf. A* 434, 9-15.
- Tan, S.S., Zou, L. and Hu, E. (2006) Photocatalytic reduction of carbon dioxide into gaseous hydrocarbon using TiO<sub>2</sub> pellets. *Catal. Today* 115(1-4), 269-273.
- Tanaka, K., Capule, M.F.V. and Hisanaga, T. (1991) Effect of Crystallinity of TiO<sub>2</sub> on Its Photocatalytic Action. *Chem. Phys. Lett.* 187(1-2), 73-76.
- Tang, Y., Li, X.M., Xu, Z.C., Guo, Q.W., Hong, C.Y. and Bing, Y.X. (2014) Removal of naproxen and bezafibrate by activated sludge under aerobic conditions: Kinetics and effect of substrates. *Biotechnol. Appl. Biochem.* 61(3), 333-341.
- Tapin, B., Epron, F., Especel, C., Ly, B.K., Pinel, C. and Besson, M. (2013) Study of Monometallic Pd/TiO<sub>2</sub> Catalysts for the Hydrogenation of Succinic Acid in Aqueous

Phase. *Catalysis* 3(10), 2327-2335.

Ternes, T.A., Bonerz, M., Herrmann, N., Teiser, B. and Andersen, H.R. (2007) Irrigation of treated wastewater in Braunschweig, Germany: an option to remove pharmaceuticals and musk fragrances. *Chemosphere* 66(5), 894-904.

Thio, B.J.R., Lee, J.H., Meredith, J.C. and Keller, A.A. (2010) Measuring the Influence of Solution Chemistry on the Adhesion of Au Nanoparticles to Mica Using Colloid Probe Atomic Force Microscopy. *Langmuir* 26(17), 13995-14003.

Thio, B.J.R., Zhou, D.X. and Keller, A.A. (2011) Influence of natural organic matter on the aggregation and deposition of titanium dioxide nanoparticles. *J. Hazard. Mater.* 189(1-2), 556-563.

Tran, T.H., Nosaka, A.Y. and Nosaka, Y. (2006) Adsorption and photocatalytic decomposition of amino acids in TiO<sub>2</sub> photocatalytic systems. *J. Phys. Chem. B* 110(50), 25525-25531.

Trasatti, S. (1971) Work Function, Electronegativity, and Electrochemical Behaviour of Metals. *Chim. Ind.* 53(4), 364-368.

Trovo, A.G., Nogueira, R.F.P., Aguera, A., Fernandez-Alba, A.R., Sirtori, C. and Malato, S. (2009) Degradation of sulfamethoxazole in water by solar photo-Fenton. Chemical and toxicological evaluation. *Water Res.* 43(16), 3922-3931.

Tsuru, T., Kan-no, T., Yoshioka, T. and Asaeda, M. (2006) A photocatalytic membrane reactor for VOC decomposition using Pt-modified titanium oxide porous membranes. *J. Membr. Sci.* 280(1-2), 156-162.

Tsuruta, T., Okuda, M. and Katayama, K. (2008) Detection of active oxygen species dynamics in TiO<sub>2</sub> sol solutions using single-shot near-field heterodyne transient grating method. *Chem. Phys. Lett.* 456(1-3), 47-50.

Turchi, C.S. and Ollis, D.F. (1990) Photocatalytic Degradation of Organic-Water Contaminants - Mechanisms Involving Hydroxyl Radical Attack. *J. Catal.* 122(1), 178-192.

Valencia, S., Marín, J., Velásquez, J., Restrepo, G. and Frimmel, F.H. (2012) Study of pH effects on the evolution of properties of brown-water natural organic matter as revealed by size-exclusion chromatography during photocatalytic degradation. *Water Res.* 46(4), 1198-1206.

Vamathevan, V., Tse, H., Amal, R., Low, G. and McEvoy, S. (2001) Effects of Fe<sup>3+</sup> and Ag<sup>+</sup> ions on the photocatalytic degradation of sucrose in water. *Catal. Today* 68(1-3), 201-208.

Wan, L.H., Sheng, J.Y., Chen, H.H. and Xu, Y.M. (2013) Different recycle behavior of

Cu<sup>2+</sup> and Fe<sup>3+</sup> ions for phenol photodegradation over TiO<sub>2</sub> and WO<sub>3</sub>. *J. Hazard. Mater.* 262, 114-120.

Wang, J., Guo, Y., Gao, J., Jin, X., Wang, Z., Wang, B., Li, K. and Li, Y. (2011) Detection and comparison of reactive oxygen species (ROS) generated by chlorophyllin metal (Fe, Mg and Cu) complexes under ultrasonic and visible-light irradiation. *Ultrason. Sonochem.* 18(5), 1028-1034.

Wang, L., Wang, X., Cui, S.F., Fan, X.Y., Zu, B.Y. and Wang, C.Y. (2013a) TiO<sub>2</sub> supported on silica nanolayers derived from vermiculite for efficient photocatalysis. *Catal. Today* 216, 95-103.

Wang, L.F., Wang, L.L., Ye, X.D., Li, W.W., Ren, X.M., Sheng, G.P., Yu, H.Q. and Wang, X.K. (2013b) Coagulation Kinetics of Humic Aggregates in Mono- and Di-Valent Electrolyte Solutions. *Environ. Sci. Technol.* 47(10), 5042-5049.

Wang, Q.Y., Jiang, H.Q., Zang, S.Y., Li, J.S. and Wang, Q.F. (2014a) Gd, C, N and P quaternary doped anatase-TiO<sub>2</sub> nano-photocatalyst for enhanced photocatalytic degradation of 4-chlorophenol under simulated sunlight irradiation. *J. Alloys Compd.* 586, 411-419.

Wang, S., Bai, L.N., Sun, H.M., Jiang, Q. and Lian, J.S. (2013c) Structure and photocatalytic property of Mo-doped TiO<sub>2</sub> nanoparticles. *Powder Technol.* 244, 9-15.

Wang, X.H., Sun, R.Z. and Wang, C.Y. (2014b) pH dependence and thermodynamics of Hg(II) adsorption onto chitosan-poly(vinyl alcohol) hydrogel adsorbent. *Coll. Surf. A* 441, 51-58.

Wang, Y., Zhong, M., Chen, F. and Yang, J. (2009) Visible light photocatalytic activity of TiO<sub>2</sub>/D-PVA for MO degradation. *Appl. Catal. B* 90(1-2), 249-254.

Wantala, K., Sthiannopkao, S., Srinameb, B.O., Grisdanurak, N. and Kim, K.W. (2010) Synthesis and characterization of Fe-MCM-41 from rice husk silica by hydrothermal technique for arsenate adsorption. *Environ. Geochem. Health* 32(4), 261-266.

Watanabe, N., Shirakawa, T., Iwahashi, M. and Seimiya, T. (1988) Effect of Surface-Charge on Adsorption of Bovine Serum-Albumin .2. Interaction of Protein Molecules with an Anionic Monolayer, as Studied by Ellipsometry, Radiotracer and Surface-Tension Measurements. *Colloid. Polym. Sci.* 266(3), 254-260.

Weston, A., Caminada, D., Galicia, H. and Fent, K. (2009) Effects of Lipid-Lowering Pharmaceuticals Bezafibrate and Clofibrac Acid on Lipid Metabolism in Fathead Minnow (*Pimephales Promelas*). *Environ. Toxicol. Chem.* 28(12), 2648-2655.

Wong, C.C. and Chu, W. (2003) The direct photolysis and photocatalytic degradation ofalachlor at different TiO<sub>2</sub> and UV sources. *Chemosphere* 50(8), 981-987.

- Wu, R.-J., Chen, C.-Y., Chen, M.-H. and Sun, Y.-L. (2007) Photoreduction measurement of ozone using Pt/TiO<sub>2</sub>-SnO<sub>2</sub> material at room temperature. *Sensors Actuators B: Chem.* 123(2), 1077-1082.
- Yang, C.-C., Chiu, S.-J., Lee, K.-T., Chien, W.-C., Lin, C.-T. and Huang, C.-A. (2008) Study of poly(vinyl alcohol)/titanium oxide composite polymer membranes and their application on alkaline direct alcohol fuel cell. *J. Power Sources* 184(1), 44-51.
- Yang, H., An, T., Li, G., Song, W., Cooper, W.J., Luo, H. and Guo, X. (2010) Photocatalytic degradation kinetics and mechanism of environmental pharmaceuticals in aqueous suspension of TiO<sub>2</sub>: A case of  $\beta$ -blockers. *J. Hazard. Mater.* 179(1-3), 834-839.
- Yang, K., Lin, D.H. and Xing, B.S. (2009) Interactions of Humic Acid with Nanosized Inorganic Oxides. *Langmuir* 25(6), 3571-3576.
- Youn, N.K., Heo, J.E., Joo, O.S., Lee, H., Kim, J. and Min, B.K. (2010) The effect of dissolved oxygen on the 1,4-dioxane degradation with TiO<sub>2</sub> and Au-TiO<sub>2</sub> photocatalysts. *J. Hazard. Mater.* 177(1-3), 216-221.
- Zhang, D.R., Liu, H.L., Han, S.Y. and Piao, W.X. (2013a) Synthesis of Sc and V-doped TiO<sub>2</sub> nanoparticles and photodegradation of rhodamine-B. *J. Ind. Eng. Chem.* 19(6), 1838-1844.
- Zhang, J.H., Maurer, F.H.J. and Yang, M.S. (2011) In situ Formation of TiO<sub>2</sub> in Electrospun Poly(methyl methacrylate) Nanohybrids. *J. Phys. Chem. C* 115(21), 10431-10441.
- Zhang, J.L., Song, Y.Q., Yang, H.G., Xu, S.B., Jiang, L. and Dan, Y. (2013b) TiO<sub>2</sub>/T-PVA Composites Immobilized on Cordierite: Structure and Photocatalytic Activity for Degrading RhB Under Visible Light. *Water Air Soil Pollut* 224(7).
- Zhang, Q., Jing, Y.H., Shiue, A., Chang, C.T., Ouyang, T., Lin, C.F. and Chang, Y.M. (2013c) Photocatalytic degradation of malathion by TiO<sub>2</sub> and Pt-TiO<sub>2</sub> nanotube photocatalyst and kinetic study. *J. Environ. Sci. Health Part B* 48(8), 686-692.
- Zhao, X.L., Xiao, G., Zhang, X., Su, H.J. and Tan, T.W. (2012) The Effect of Ni<sup>2+</sup> and Cu<sup>2+</sup> on the Photocatalytic Degradation of Dyes by the Chitosan-TiO<sub>2</sub> Complex. *Appl. Biochem. Biotechnol.* 168(1), 183-197.
- Zhu, M., Wang, H.T., Keller, A.A., Wang, T. and Li, F.T. (2014) The effect of humic acid on the aggregation of titanium dioxide nanoparticles under different pH and ionic strengths. *Sci. Total Environ.* 487, 375-380.
- Ziegmann, M., Saravia, F., Torres, P.A. and Frimmel, F.H. (2010) The hybrid process TiO<sub>2</sub>/PAC: performance of membrane filtration. *Water Sci. Technol.* 62(5), 1205-1212.
- Zielinska-Jurek, A. and Zaleska, A. (2014) Ag/Pt-modified TiO<sub>2</sub> nanoparticles for toluene

## 9 References

---

photooxidation in the gas phase. *Catal. Today* 230, 104-111.



---

**Abbreviation list**

AOI	organically-bound iodine adsorbable onto activated carbon
AOP	advanced oxidation process
AOX	organically-bound halogens adsorbable onto activated carbon
BSA	bovine serum albumin
BZF	bezafibrate
CA	clofibric acid
CB	conductive band
CBZ	carbamazepine
CCC	critical coagulation concentration
DA	diatrizoate
DLS	dynamic light scattering
DO	dissolved oxygen
DOC	dissolved organic carbon
DOM	dissolved organic matter
DSC	differential scanning calorimetry
EDL	electrical double layer
FTIR	fourier transform infrared spectroscopy
g	gram
h	hour
HA	humic acid
HPLC	high pressure liquid chromatograph
HO10FA	Hohloh Lake fulvic acid, 10 <sup>th</sup> sampling
HO24	Hohloh Lake, 24 <sup>th</sup> sampling
IC	ion exchange chromatography
ICM	iodinated contrast media
ICP-OES	inductively coupled plasma optical emission spectrometry

## Abbreviation list

---

L	liter
LAS	linear alkylbenzene sulfonates
L-H kinetics	Langmuir–Hinshelwood kinetics
M	mole per liter
$\mu\text{M}$	micromole per liter
mg	milligram
min	minutes
mL	milliliter
NOM	natural organic matter
NP	nanoparticle
pH	“hydrogen potential”, a measure of acidity and basicity in dilute aqueous solutions
PhAC	pharmaceutically active compound
pKa	the symbol for the acid dissociation constant at logarithmic scale
PSS	pseudo-steady state
PVA	polyvinyl alcohol
PZC	point of zero charge
ROS	radical oxygen species
s	second
SDS	sodium dodecyl sulfate
SEC	size exclusion chromatography
SEC-DOC	size exclusion chromatography with dissolved organic carbon detection
SEC-UV	size exclusion chromatography with ultraviolet detection
SEM	scanning electron microscopy
STEM	scanning transmission electron microscopy
TEM	transmission electron microscopy
TOC	total organic carbon
UV	ultraviolet

VB	valence band
WWTP	wastewater treatment plant
XRD	X-ray diffraction